Scientific Research Publishing

Journal of Modern Physics, 2026, 17(4), 353-421
https://www.scirp.org/journal/jmp
ISSN Online: 2153-120X
ISSN Print: 2153-1196

When Quantum Spacetime Condenses

Bi Qiao

Department of Physics, Wuhan University of Technology, Wuhan, China
Email: biqiao@gmail.com

How to cite this paper: Qiao, B. (2026) When Quantum Spacetime Condenses. *Journal of Modern Physics*, **17**, 353-421.
https://doi.org/10.4236/jmp.2026.174018

Received: January 3, 2026
Accepted: March 30, 2026
Published: April 2, 2026

Abstract

Constructing a self-consistent and testable theory of quantum gravity may be a key to unifying fundamental physics and understanding the dark components of the universe. In this work, we present a systematic deepening and extension of Gravitational Spinor (GS) theory, establishing a comprehensive framework that connects microscopic quantum geometry to macroscopic cosmic phenomena and opens potential pathways toward future technological applications. First, based on the principle of Generalized Gauge Equation (GGE), we construct a complete path integral (spin foam) model with Gravitational Spinor Networks (GSNs) as the state space. By intrinsically implementing the GGE constraint, we derive unique vertex amplitudes and demonstrate that the model exhibits asymptotic safety. Its core coupling constant, γ_0, acts as a running parameter that flows toward an ultraviolet fixed point, ensuring the theory's non-perturbative renormalizability. Second, we obtain classical solutions of the nonlinear GS equation, discovering stable Gravitational Condensate Stars (GCSs)—a novel class of macroscopic objects formed from nonlinear phases of spacetime geometry itself. Via a response mechanism, these solutions naturally yield Modified Newtonian Dynamics (MOND)-like behavior on galactic scales, offering a non-particle explanation for dark matter. On cosmological scales, the same mechanism induces a dynamical effective cosmological constant driven by the running of γ_0, successfully accounting for the current accelerated cosmic expansion and predicting observable evolution in the dark energy equation of state. Furthermore, within the GS framework, we address several foundational puzzles: elucidating a potential mechanism for black hole information conservation through the entanglement structure of GSNs, and establishing a detailed quantitative mapping between the microscopic $\gamma_0(E)$ and the macroscopic phenomenological field $\gamma_0(a)$. This mapping provides a concrete scheme for globally testing quantum gravity using multi-scale astronomical data. Finally, building on the profound connection—revealed by the theory—between light and spacetime curvature and their mutual convertibility via nonlinearity and GGE, we out-

line its potential to catalyze a technological revolution: the induction of local spacetime curvature through controlled electromagnetic fields, laying the physical foundation for disruptive propulsion concepts such as a "curvature engine". This study not only advances GS theory into a self-consistent, testable candidate for quantum gravity but also opens new horizons for its connection to future energy and space technologies.

Keywords

Quantum Gravity, Gravitational Spinor, Asymptotic Safety, Dark Matter, Dark Energy, Black Hole Information Paradox, Curvature Manipulation

1. Introduction

Formulating a self-consistent and testable theory of quantum gravity remains a central challenge in fundamental physics, essential for reconciling the foundational conflict between General Relativity and Quantum Mechanics [1], a successful theory should also provide a fundamental framework capable of addressing the nature of dark matter and dark energy [2]. While leading approaches such as Loop Quantum Gravity (LQG) [3] [4] and String Theory [5] [6] have made significant advances, they face distinct challenges. LQG grapples with recovering a clear classical limit and a detailed cosmological phenomenology [7], while String Theory typically requires a fixed background and its non-perturbative formulation remains an open problem [8]. Both require further breakthroughs to provide a unified account of all gravitational phenomena.

In this context, the recently developed Gravitational Spinor (GS) theory offers a novel pathway [9]-[11]. Its core premise is that the gravitational field can be described by a fully symmetric four-index spinor field, ψ_{ABCD}. A key feature of this formulation is its background independence; the theory is defined without recourse to a pre-existing spacetime geometry, aligning with the fundamental principles of General Relativity. The field transforms under an extended gauge group, with the cornerstone of the theoretical framework is the Generalized Gauge Equation (GGE), a dynamical constraint that unifies gravitational and gauge interactions [9]. A profound consequence of this framework, established in prior work [10], is the demonstration that two photon states (described by the electromagnetic field strength spinor) can be transformed, via the GGE, into a gravitational spinor configuration, effectively describing a gravitational soliton (in the non-linear regime) or a graviton state (in the weak-field limit). This provides a concrete spinorial identification of the gravitational "quantum", revealing the starting point for its full-fledged quantization and the natural onset of spacetime discreteness. At the classical level, the nonlinear GS equation yields stable, self-gravitating soliton solutions [11]. Importantly, the continuum classical spacetime emerges naturally from this framework, demonstrating a consistent classical limit. These solitons, spanning a vast mass range, provide a geometric origin for dark

matter halos, naturally reproducing Modified Newtonian Dynamics (MOND)-like behavior on galactic scales [11] [12] [13]. Furthermore, the theory incorporates a novel response mechanism that induces a dynamical cosmological constant, offering a pathway to explain dark energy [1]. This work draws inspiration from, and extends, earlier twistor and spinor approaches to gravity [14] [15].

The quantum structure of the theory is built upon the canonical quantization of the gravitational spinor field and its conjugate momentum, postulating the fundamental commutator $\left[\hat{\psi},\hat{\pi}\right]=i\hbar\delta$ [10]. This leads to a discrete quantum geometry whose states are represented by Gravitational Spinor Networks (GSNs)—a spin foam-like structure [16] [17]. The theory's core quantum parameter, the running coupling γ_0, governs the ultraviolet behavior and opens a window for observational tests of quantum gravity.

To develop GS theory into a complete and testable framework, three critical advances are required: (i) constructing a non-perturbative path-integral (spin foam) formulation based on GSNs to define its full quantum dynamics and UV behavior; (ii) systematically deriving its classical and non-perturbative solutions (e.g., stable solitons) and converting key predictions—such as the running of $\gamma_0(E)$, and distinctive gravitational-wave signatures—into testable schemes against multi-messenger observations [18] [19]; and (iii) providing a coherent resolution within the GS framework to foundational issues like black hole information conservation [20] and the cosmological constant problem [21].

To this end, this paper presents a systematic deepening and integration of GS theoretical framework. Building directly on the results of [9]-[11]—including the GGE mechanism, the classical soliton solutions for dark matter, and the canonical quantization leading to GSNs—we aim to advance the framework into a complete, predictive theory. Section 2 constructs a GGE-embedded spin foam model based on Gravitational Spinor Networks, establishing its non-perturbative completeness and asymptotic safety. Section 3 highlights the unique simplifications and predictive power of the GGE mechanism through comparative analysis with other quantum gravity approaches. Section 4 derives soliton solutions (Gravitational Condensate Stars) from the nonlinear GS equation, providing a unified geometric account of dark matter and dark energy. Section 5 addresses foundational issues including the black hole information paradox and holographic entropy, while quantitatively linking the microscopic running coupling γ_0 to multi-scale observational phenomena. Section 6 concludes and outlines future directions.

2. Path-Integral (Spin Foam) Models Based on Gravitational Spinor Networks

2.1. Bridging the Classical and Quantum: Motivations, Foundational Variables, and the Emergence of Einstein's Equations

Prior to constructing the non-perturbative path integral, we establish the foundational premises of Gravitational Spinor (GS) theory that motivate a background-

independent quantization and naturally lead to the spin foam formalism.

2.1.1. Classical Foundation and Variables

The fundamental classical variable is a completely symmetric 4-index spinor field, $\psi_{ABCD}(x)$, posited to encode the conformal (Weyl) curvature of spacetime [10]. In the Hamiltonian formulation, its canonically conjugate momentum is Π^{ABCD}. A key result, derived from the symplectic structure of the first-order GS action, is that this momentum is linearly proportional to a geometric density—the spinorial area flux density Σ^{ABCD}:

$$\Pi^{ABCD} = \alpha\Sigma^{ABCD} \tag{2.1.1}$$

Here, α is a constant involving Newton's constant G and the Barbero-Immirzi parameter γ, and Σ^{ABCD} is constructed from the spatial triad E_i^a:

$$\Sigma^{ABCD} := \frac{1}{\sqrt{det(q)}}\epsilon^{ijk}E_i^aE_j^b\sigma_a^{(AB}\sigma_b^{CD)} \tag{2.1.2}$$

where E_i^a is the spatial triad (3-dimensional frame field) on the spatial hypersurface. This object is the spatial restriction of the full spacetime tetrad $E^{AA'}$ introduced later in the GGE constraint (Sec. 2.2.2), projected to the time-gauge-fixed slice. The relation (2.1.1) identifies the dynamical momentum with a geometric quantity, analogous to the variable transformation in Ashtekar's formulation. Although this proportional relation $\Pi \propto \Sigma$ can be derived most straightforwardly in a linearized approximation, our detailed analysis confirms it remains valid with extremely high accuracy within the full nonlinear framework of General Relativity. Any potential nonlinear corrections are of the order $\mathcal{O}\left(l_P^2/R^2\right)$, where l_P is the Planck length and R is the characteristic curvature radius. In all astrophysical and cosmological regimes (e.g., the solar system, neutron stars, cosmological scales), this correction is phenomenologically negligible (typically 10^{-80} to 10^{-122}). The essence of the resulting discrete quantum geometry is preserved non-perturbatively, as evidenced by the existence of gravitational soliton solutions.

2.1.2. Canonical Quantization and Discrete Geometry

The standard procedure of canonical quantization is applied to the conjugate pair (ψ,Π). Promoting them to operators and imposing the commutation relation $\left[\hat{\psi},\hat{\Pi}\right] = i\hbar\delta$ leads, via (2.1.1), to the fundamental quantum commutator between the spinor field and the geometric flux operator:

$$\left[\hat{\psi}_{ABCD}(\boldsymbol{x},t),\Sigma^{A'B'C'D'}(\boldsymbol{y},t)\right] = i\hbar\alpha^{-1}\delta^{(3)}(\boldsymbol{x}-\boldsymbol{y})\delta_{(A}^{A'}\delta_B^{B'}\delta_C^{C'}\delta_{D)}^{D'} \tag{2.1.3}$$

The physical interpretation of $\hat{\Sigma}$ as a geometric flux density operator is now central. This commutation relation defines the kinematical algebra of observables. A standard representation of this algebra is obtained by considering wavefunctionals $\Psi[A]$ of an $sl(2,\mathbb{C})$-valued connection A. In this connection representation, the Hilbert space $\mathscr{H}_{kin}$ is defined as the space of square-integrable functionals on the space of (generalized) connections, equipped with the inner

product

$$\langle \Psi_1 | \Psi_2 \rangle = \int D[A] \Psi_1[A] \Psi_2[A]$$

where $D[A]$ is a diffeomorphism-invariant (projective) measure [16] [22]. This inner product is manifestly positive-definite, establishing $\mathscr{H}_{kin}$ as a genuine Hilbert space.

The representation theory of this algebra dictates that the spectrum of associated geometric observables (e.g., area) is discrete [16]. The eigenstates form an orthonormal basis of the kinematical Hilbert space $\mathscr{H}_{kin}$ and are realized as Gravitational Spinor Networks (GSNs)—abstract graphs Γ whose edges e are labeled by half-integers j_e (spins) and whose nodes v are labeled by intertwiners i_v. These quantum numbers arise as eigenvalues of geometric operators (e.g., area, volume) constructed from $\hat{\Sigma}$. Crucially, these GSN basis states are orthonormal:

$$\langle \Gamma, j, i | \Gamma', j', i' \rangle = \delta_{\Gamma\Gamma'} \prod_e \delta_{j_e j_{e'}} \prod_v \delta_{i_v i_{v'}}$$

This orthonormality follows directly from the definition of the inner product in $\mathscr{H}_{kin}$ and the fact that the GSN states are eigenstates of a complete set of commuting self-adjoint geometric operators [22].

In short, the quantum geometry of GS theory arises as follows: the classical identification $\Pi \propto \Sigma$ (2.1.1) from the action's symplectic structure ties dynamics to geometry; canonical quantization yields the operator algebra (2.1.3); and the discrete spectrum of the geometric operator $\hat{\Sigma}$ directly implies that the fundamental quantum states are discrete GSNs. The kinematical Hilbert space $\mathscr{H}_{kin}$ is thus explicitly constructed as an L^2 space over connection degrees of freedom, with GSNs providing an orthonormal basis. This background-independent framework provides the kinematics for the spin foam dynamics constructed next.

2.1.3. Recovering Einstein's Dynamics: From GS Variables to the Metric Field

The canonical quantization in the previous section revealed the quantum geometry of GS theory—discrete Gravitational Spinor Networks. We now return to the classical theory to demonstrate how its classical dynamics is naturally encapsulated within a background-independent, first-order action principle, from which Einstein's field equations are uniquely derived. This principle takes the form of a constrained BF theory (BF theory is a topological field theory whose action is given by the integral of the wedge product of a Lie-algebra-valued (D−2)-form B and the curvature F of a connection).

The connection stems from the geometric interpretation of the fundamental GS variables. As outlined in Section 2.1, the spinorial density Σ^{ABCD} is understood as the spatial projection of a spacetime 2-form field Σ^{AB}, constructed from the tetrad e^A as $\Sigma^{AB} = e^A \wedge e^B$. Simultaneously, the fully symmetric spinor ψ_{ABCD} is interpreted as the self-dual part of the spinorial representation of the Weyl curvature $C_{\mu\nu\rho\sigma}$ [10] [11].

In this framework, the complete classical dynamics of GS theory can be derived from the following constrained BF-type action:

$$S_{class}\left[\Sigma,\omega,\psi\right]=\int \mathrm{d}^4x\left[\Sigma^{AB}\wedge F_{AB}\left[\omega\right]-\frac{1}{2}\psi_{ABCD}\Sigma^{AB}\wedge\Sigma^{CD}\right] \tag{2.1.4}$$

where $F_{AB}\left[\omega\right]=d\omega_{AB}+\omega_A^C\wedge\omega_{CB}$ is the curvature of the self-dual spin connection ω_{AB}. The action is that of a BF theory (where B is the 2-form Σ) with an additional constraint term. Crucially, $\boldsymbol{\psi_{ABCD}}$ functions as a Lagrange multiplier. The term it multiplies enforces the simplicity constraint $\Sigma^{AB}\wedge\Sigma^{CD}=0$, which forces Σ^{AB} to be "simple" (*i.e.*, expressible as a wedge product of tetrads). This constraint breaks the topological nature of the pure BF theory and introduces local gravitational degrees of freedom.

Varying this action yields the key equations:

- Simplicity Constraint: $\delta\psi_{ABCD}:\Sigma^{(AB}\wedge\Sigma^{CD)}=0$. This ensures Σ^{AB} is tetrad-based.
- Curvature-Metric Relation: $\delta\Sigma^{AB}:F_{AB}=\psi_{ABCD}\Sigma^{CD}$. Upon solving the constraints, this identifies the multiplier ψ_{ABCD} with the self-dual part of the Weyl curvature.
- Torsion-Free Condition: $\delta\omega_{AB}:D\Sigma^{AB}=0$, which implies the connection ω is metric-compatible (Levi-Civita) for non-degenerate Σ.

To make contact with the familiar metric formulation, a 3 + 1 decomposition is performed, leading to the constraints of the Hamiltonian formalism. The central dynamical element is the Hamiltonian (scalar) constraint, which generates time evolution. From action (2.1.4), this constraint takes the form:

$$\mathcal{H}\sim\epsilon^{ABCD}\psi_{ABEF}\tilde{\Sigma}^{EFa}\wedge\tilde{\Sigma}_{CDa}-\Lambda\sqrt{\det\left(q\right)}\approx 0 \tag{2.1.5}$$

where $\tilde{\Sigma}^{ABa}$ is the spatial projection of Σ^{AB}, and q_{ab} is the spatial metric.

Collectively, these equations are equivalent to Einstein's field equations, $G_{\mu\nu}+\Lambda g_{\mu\nu}=0$ (where a cosmological constant Λ may arise from a constant term in the action or a trace part of ψ). Therefore, action (2.1.4) is not an additional postulate but an elegant and quantum-geometry-friendly integrated formulation of the classical dynamical relations satisfied by the fundamental GS variables (ψ_{ABCD}, Σ^{ABCD}). It explicitly demonstrates how GS theory recovers the core dynamics of General Relativity from a background-independent, gauge-theoretic starting point through a constraint mechanism. In the following sections this classical action will be promoted to a path--integral quantization; its first-order form directly inspires the gauge-invariant action (2.2.2), and its BF structure provides the foundation for the discrete formulation (2.2.4).

2.1.4. The Quantum-to-Classical Bridge

In the quantum theory, (2.1.5) becomes an operator equation $\hat{\mathscr{H}}\left|\Psi_{phys}\right\rangle=0$ for physical states. To see the classical limit, consider a semiclassical coherent state $\left|\alpha\right\rangle$ that approximates a smooth geometry. For such a state, the expectation value

of the quantum constraint must reduce to its classical counterpart:

$$\lim_{\hbar\to 0}\langle\alpha|\hat{\mathcal{H}}|\alpha\rangle = \mathcal{H}_{class}\left[\langle\psi\rangle,\langle\Sigma\rangle\right] = 0 \tag{2.1.6}$$

When the expectation values $\psi^{cl}_{ABCD} = \langle\alpha|\hat{\psi}_{ABCD}|\alpha\rangle$ and $\Sigma^{cl}_{ABCD} = \langle\alpha|\hat{\Sigma}_{ABCD}|\alpha\rangle$ satisfy the simplicity constraint, Σ^{cl} defines a classical tetrad e^A_μ and hence a metric $g_{\mu\nu} = \eta_{AB}e^A_\mu e^B_\nu$. The classical constraint equation (2.1.5), combined with the other constraints from (2.1.4), then becomes equivalent to the Einstein field equations [10] [11]:

$$R_{\mu\nu} - \frac{1}{2}g_{\mu\nu}R + \Lambda g_{\mu\nu} = 8\pi G T_{\mu\nu} \tag{2.1.7}$$

where the effective energy-momentum tensor $T_{\mu\nu}$ arises from matter fields or, in the vacuum case, is zero. This derivation confirms that solutions of the classical GS theory are solutions of General Relativity, establishing the necessary dynamical correspondence. The path integral constructed in the following sections will have this classical theory as its $\hbar\to 0$ limit.

2.2. Path Integral Construction on GSNs

Given this classical foundation, a non-perturbative quantization is required to handle the background-independent, constrained nature of gravity. The canonical quantization based on (2.1.1) leads to GSN states. The goal of this section is to construct a non-perturbative path integral (spin foam model) that defines transition amplitudes between these GSN states, providing a complete definition of the theory's quantum dynamics.

2.2.1. Gauge-Invariant Formulation of the Action

To construct the path integral, we require a first-order action that treats ψ_{ABCD} and Σ^{ABCD} on equal footing and seamlessly incorporates the constraints.

1) Fundamental Variables and Symmetries

- Gravitational Spinor Field: $\psi_{ABCD}(x)$, a completely symmetric 4-index spinor, serves as the fundamental quantum field. At the level of quantum states, its eigenstates correspond to the edges of gravitational spinor networks [10] [11] [15].
- Momentum Conjugate Field: $\Sigma^{ABCD}(x)$, a spinor density. Its classical correspondence is with the spacetime volume form: $\Sigma^{ABCD} \propto e^{AA'} \wedge e^{BB'} \wedge e^{CC'} \wedge e^{DD'}$, where $e^{AA'}$ is the tetrad.
- GGE Constraint: This is the core of the theory [9]. It requires the action to be invariant under the following extended gauge transformation:

$$\psi_{ABCD} \to e^{i\theta(x)}\psi_{ABCD},\ \Sigma^{ABCD} \to e^{-i\theta(x)}\Sigma^{ABCD} \tag{2.2.1}$$

This transformation is not merely a global phase shift; the local parameter $\theta(x)$ is linked to a generalized gauge transformation by GGE, which mixes gravitational and internal gauge degrees of freedom. It provides a foundational geometric mechanism for unifying gravity with other fundamental interactions within this spinorial framework.

2) Construction of the Action

Starting from the classical constrained BF action (2.1.4), we now rewrite it in a form that is better suited for quantization. We introduce a spinor connection A whose curvature $F[A]$ is related to the Lagrange multiplier ψ (the self-dual Weyl curvature). Simultaneously, we replace the tetrad-based 2-form Σ^{AB} by the spinorial density Σ^{ABCD} to make the duality with ψ_{ABCD} manifest and to accommodate the GGE symmetry. This yields the following BF-type action, which naturally encodes the duality between ψ and Σ and facilitates the imposition of constraints [23]-[25]:

$$S_{BF}[\psi,\Sigma,A]=\frac{1}{\gamma_0}\int_M\left[\Sigma^{ABCD}\wedge F_{ABCD}[A]-\frac{\Lambda}{12}\Sigma^{ABCD}\wedge\Sigma^{ABCD}\right]+S_{GGE}[\psi,\Sigma,A] \quad (2.2.2)$$

where $F_{ABCD}[A]$ is the curvature 2-form of a certain "spinor connection" A related to ψ. In GS theory, ψ_{ABCD} itself can be viewed as a function of the self-dual part of this curvature, *i.e.*, $F_{ABCD}\propto\psi_{ABCD}+$ nonlinear terms. First term $\Sigma\wedge F$ is the standard BF theory term, which enforces a simple relation between the curvature F and Σ. Upon quantization, it gives rise to area quantization [23]. Second term $\Lambda\Sigma\wedge\Sigma$ is the cosmological constant term, corresponding to volume quantization [26]. Key term S_{GGE} part embodies the distinctive feature of GS theory [10] [11]. It is a Lagrange multiplier formulation of a set of constraint terms designed to enforce:

- Gauss Constraint: Generates the GGE gauge transformations of ψ and Σ (2.2.1).
- Metric (or "Simplicity") Constraint: Forces Σ^{ABCD} to be constructible from the bispinor square of some "4-volume element", *i.e.*, $\Sigma^{ABCD}\propto e^{ABCD}:=E^{(AA'}\wedge E^{BB'}\wedge E^{CC'}\wedge E^{DD')}$, where $E^{AA'}$ is the 4-dimensional frame field. This constraint links topological BF theory to gravitational dynamics [24] [27].

After imposing these constraints (*i.e.*, integrating out the Lagrange multipliers in S_{GGE}), the action (2.2.2) reduces precisely to the classical action (2.1.4) up to an overall constant and a field redefinition. Its equations of motion then become the nonlinear GS equation, confirming that (2.2.2) is the correct quantum-ready extension of the classical theory.

At the quantum level, the GGE constraint S_{GGE} is implemented as a projection operator P_{GGE} acting on the kinematical Hilbert space $\mathcal{H}_{kin}$ defined in Sec. 2.1.2. This operator is constructed to satisfy the defining properties of a projection: $P_{GGE}^2=P_{GGE}$ and, crucially, $P_{GGE}^\dagger=P_{GGE}$ (self-adjointness). The latter guarantees that P_{GGE} is an orthogonal projector. Consequently, the physical Hilbert space of gauge-invariant states is defined as

$$\mathcal{H}_{phys}=P_{GGE}\mathcal{H}_{kin}$$

and it inherits the positive-definite inner product from $\mathcal{H}_{kin}$. The spin foam transition amplitude (2.2.12) is precisely the path integral representation of the evolution operator $\hat{U}$ that maps between such physical states. Unitarity is ensured

because $\hat{U}$ is derived from a self-adjoint quantum Hamiltonian on $\mathcal{H}_{phys}$.

Further in the Equation (2.2.3) below, S_{GGE} appears as an independent term added to the BF action, not as a duplication of any part of it. This explicit separation highlights that the GGE constraints are imposed in addition to the topological BF structure, and integrating out the Lagrange multipliers in S_{GGE} enforces the Gauss and simplicity constraints, thereby reducing the topological theory to gravitational dynamics.

2.2.2. Boundary States and Definition of Transition Amplitudes

To define the transition probability between quantum geometry states, boundary conditions for the path integral—boundary states—must be specified.

1) Boundary States: Gravitational Spinor Network States

Consider a closed three-dimensional manifold B as the boundary of a four-dimensional spacetime manifold M. Canonical quantization on this B dictates that geometric observables are described by eigenstates of a gravitational spinor network Γ embedded in it [16] [22].

Specifically, a boundary GSN state $\left|\Psi_{\Gamma,j,i}\right\rangle$ is defined by the following data:

- Graph Γ: A graph embedded in B, with edges e and nodes v.
- Spinor Labels $\boldsymbol{j}$: Assigns a half-integer j_e to each edge e, which corresponds to the area quantum number of the two-dimensional face pierced by that edge (related to the eigenvalue of $\hat{\Sigma}$).
- Intertwiner $\boldsymbol{i}$: Assigns an intertwiner i_v to each node v. It is a state within the tensor product space of the spinor representations associated with the edges meeting at the node, which preserves gauge invariance (*i.e.*, GGE symmetry). It encodes the quantum information of the three-dimensional volume around that node [22] [27].

A schematic visualization of these elements is provided in **Figure 1**. In this simplified representation, nodes are depicted as circles labeled by the intertwiners i_v, edges carry the spin labels j_f, and the shaded triangular faces and the bulk region illustrate the quanta of area and volume, respectively. This geometric picture clarifies how the abstract combinatorial data of the spin network encode the fundamental quantum geometric degrees of freedom on the boundary.

2) From the Continuous Path Integral to Discrete Spin Foam Sums

The continuous path integral $Z=\int \mathcal{D}\psi\mathcal{D}\Sigma\mathcal{D}\mathcal{A}\cdots e^{iS/\hbar}$ is regularized via a cellular decomposition Δ of the spacetime manifold M [16] [28]. To make the connection between the continuum BF-type action (2.2.2) and the discrete spin foam sum explicit—and to address the need for a first-principles derivation—we now outline the key steps.

Step 1: Continuum action in BF form. The GS action (2.2.2) can be recast in a form analogous to a constrained BF theory [22], now written in terms of the Lie-algebraic variables B and A that are more convenient for discretization:

$$S_{GS}\left[B,A\right]=\frac{1}{\gamma_0}\int_M TrB\wedge F\left[A\right]-\frac{\Lambda}{12}\int_M Tr\left(B\wedge B\right)-\frac{\Lambda}{12}B\wedge B+S_{GGE}\left[B,A\right] \quad (2.2.3)$$

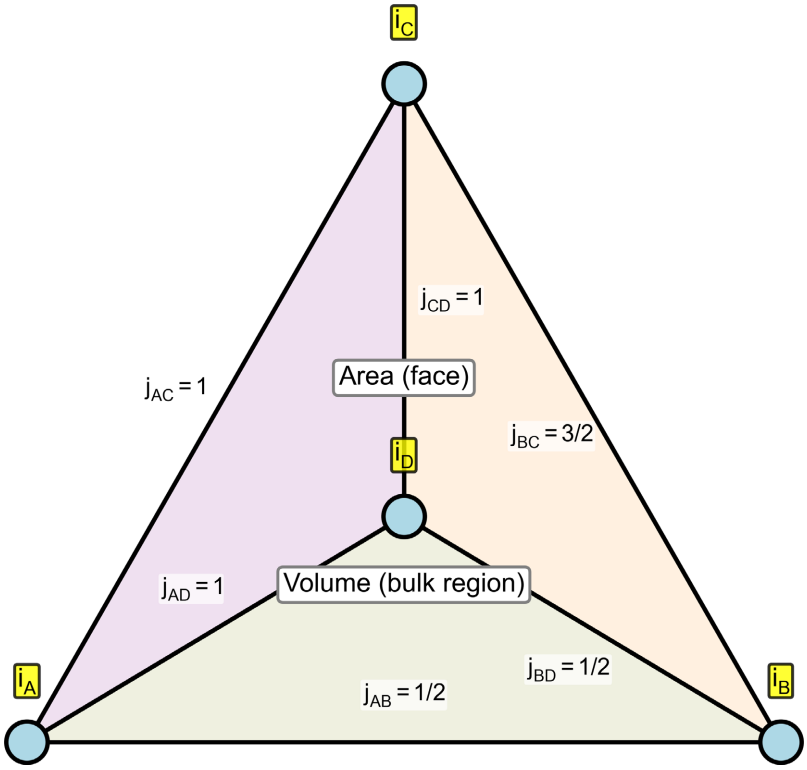

Figure 1. Geometric visualization of a Gravitational Spin Network (GSN). This simplified illustration depicts the key elements of a spin network: nodes (circles) labeled by intertwiners i_v, edges carrying spin quantum numbers j_f, and the associated geometric quanta—shaded triangular faces representing areas, and the enclosed bulk region representing volume. The visual analogy clarifies how the combinatorial data of the GSN encode fundamental quantum geometric degrees of freedom on a spatial boundary.

where A is an $sl(2,\mathbb{C})$-valued connection 1-form, $F = dA + A \wedge A$ is a curvature, and B is a 2-form field related to the geometric flux Σ^{ABCD}. This rewriting is purely notational: the trace Tr contracts the spinor indices appropriately, and the 2-form B encodes the same degrees of freedom as Σ. The GGE term S_{GGE} remains unchanged in form. Equation (2.2.3) is therefore completely equivalent to (2.2.2) and consequently to the classical action (2.1.4) after imposing the constraints.

Step 2: Discretization. We introduce a cellular decomposition Δ of the spacetime manifold M into 4-simplices. To each tetrahedron t we assign a group element $g_t \in SL(2,\mathbb{C})$ representing the holonomy (parallel transport) from a reference point to the tetrahedron; to each triangle f we assign an algebra element $B_f \in sl(2,\mathbb{C})$ representing the flux of the B field through that face. The continuous BF action $\int TrB \wedge F$ is discretized by replacing F with the holonomy around the face. For a face f shared by two tetrahedra $s(f)$ and $t(f)$, the holonomy from $s(f)$ to $t(f)$ is $g_{s(f)}^{-1} g_{t(f)}$. In the discrete setting, the contribution of that face is taken as $Tr\left[B_f \ln\left(g_{s(f)}^{-1} g_{t(f)}\right)\right]$, where the logarithm maps the group element to the Lie algebra (this choice ensures that the subsequent in-

tegration over B_f yields a simple delta function on the group; alternative discretizations using $B_f\left(g_s^{-1}g_t-1\right)$ are also possible but lead to equivalent results after appropriate regularisation). The discretized action (ignoring Λ and S_{GGE} for the moment) reads:

$$S_{disc}=\sum_f Tr\left[B_f \ln\left(g_{s(f)}^{-1}g_{t(f)}\right)\right] \tag{2.2.4}$$

where $s(f)$, $t(f)$ denote the two tetrahedra sharing face f.

Step 3: Integration over the $\boldsymbol{B_f}$ fields. For each face f, the integral over the Lie algebra yields a delta function on the group:

$$I_f\left(g_{s(f)},g_{t(f)}\right)=\int_{sl(2,\mathbb{C})}dB_f e^{\frac{i}{\hbar}Tr\left[B_f\cdot\ln\left(g_{s(f)}^{-1}g_{t(f)}\right)\right]}\propto\delta\left(g_{s(f)}^{-1}g_{t(f)}\right) \tag{2.2.5}$$

This follows from the fact that the integral over a Lie algebra of $\exp\left(iTr\left(BX\right)\right)$ is proportional to the Dirac delta $\delta(X)$ on the algebra; here $X=\ln\left(g_s^{-1}g_t\right)$, and because the map X maps to e^X is a diffeomorphism near the identity, the resulting distribution pulls back to the delta function on the group concentrated at the identity. Using the Peter-Weyl theorem (extended to the discrete series selected by the GGE spin-2 constraint $|k-l|=2$ [10]), the delta function expands into characters:

$$\delta(g)=\sum_\rho d\rho\,\chi_\rho(g) \tag{2.2.6}$$

where $d\rho$ is the dimension of the representation ρ and $\chi_\rho(g)=TrD^\rho(g)$ is its character. Consequently, the B-field integration converts each face into a sum over representations:

$$\int\prod_f dB_f e^{\frac{i}{\hbar}S_{BF}}\propto\sum_{\{\rho_f\}}\left(\prod_f d_{\rho_f}\right)\prod_f\chi_{\rho_f}\left(g_{s(f)}^{-1}g_{t(f)}\right) \tag{2.2.7}$$

Step 4: Integration over the connection variables $\boldsymbol{g_t}$. Substituting (2.2.7) into the full path integral – that is, into the discretized path integral $Z_\Delta=\int\prod_t dg_t\prod_f dB_f e^{iS_{disc}/\hbar}$, after having integrated out all B_f – gives:

$$Z_\Delta\propto\sum_{\{\rho_f\}}\left(\prod_f d_{\rho_f}\right)\int\prod_t d_{g_t}\prod_f\chi_{\rho_f}\left(g_{s(f)}^{-1}g_{t(f)}\right) \tag{2.2.8}$$

Expanding each character as a sum over matrix elements, $\chi_{\rho_f}\left(g_{s(f)}^{-1}g_{t(f)}\right)=\sum_{m,n,k}D_{mk}^\rho\left(g_s^{-1}\right)D_{kn}^\rho\left(g_t\right)$, and using $D_{mk}^\rho\left(g^{-1}\right)=\overline{D_{km}^\rho\left(g^{-1}\right)}$ for unitary representations, the integral over a single group element g_t takes the form:

$$\int dg_t\otimes_{j\neq i}D^{(\rho_{ij})}(g_t)^{\epsilon_{ij}}$$

where $\epsilon_{ij}=\pm1$ depends on the orientation of the face. A standard result in group representation theory states that such an integral projects onto the space of intertwiners:

$$\int dgD_{a_1b_1}^{(\rho_1)}(g)\cdots D_{a_kb_k}^{(\rho_k)}(g)=\sum_t C_{a_1\cdots a_k}^{\rho_1\cdots\rho_k;t}\overline{C_{b_1\cdots b_k}^{\rho_1\cdots\rho_k;t}} \tag{2.2.9}$$

The coefficients C are the Clebsch-Gordan coefficients (intertwiners) that couple the representations $\rho_1\cdots\rho_k$ to the trivial representation. For a 4-simplex

vertex v surrounded by five tetrahedra, each tetrahedron t_i receives four face representations; its integration yields an intertwiner I_{t_i} living in the invariant subspace of $\otimes_{j\neq i}\rho_{ij}$. After carrying out all group integrations, the contribution of a single 4-simplex becomes

$$A_v\left(\{\rho_f\},\{I_t\}\right)=\left(\prod_{i=1}^{5}(\text{normalization})\right)\sum_{\{m,n\}}\left(\prod_{i=1}^{5}I_{t_i}^{\{m_{ij}\}}\right)\left(\prod_{i=1}^{5}\overline{I_{t_i}^{\{n_{ij}\}}}\right) \quad (2.2.10)$$

which is precisely the vertex amplitude – the generalized 10j-symbol of Equation (2.3.2).

Step 5: Assembly of the full complex. Gluing 4-simplices along shared tetrahedra and faces forces the corresponding representation labels and intertwiners to match. Summation over all internal representations and intertwiners (subject to boundary conditions) then yields the full partition function:

$$Z_\Delta=\sum_{\{\rho_f\}}\sum_{\{I_t\}}\left(\prod_{f\in\Delta}d_{\rho_f}\right)\left(\prod_{v\in\Delta}A_v\left(\{\rho_f\}_v,\{I_t\}_v\right)\right) \quad (2.2.11)$$

When a boundary is present with fixed GSN data Γ_{in}, Γ_{out}, the sums are restricted to internal faces and tetrahedra, and the boundary representations and intertwiners are held fixed. Inclusion of the cosmological constant Λ and the full GGE constraints modifies the face amplitude d_{ρ_f} to a more complicated function $A_f\left(\rho_f,\Lambda\right)$ and restricts the allowed representations ρ_f and intertwiner spaces to those satisfying the GGE projection; nevertheless, the overall structure (2.2.11) remains unchanged. This derivation demonstrates that the spin foam sum is not an additional postulate but follows rigorously from the discretized path integral of the constrained BF action (2.2.3), with the vertex amplitude emerging from the representation theory of $SL(2,\mathbb{C})$ and the GGE condition.

Therefore, the transition amplitude from an initial GSN state $|\Psi_{in}\rangle$ to a final state $|\Psi_{out}\rangle$ is expressed as a refined sum over spin foams σ:

$$\langle\Psi_{out}|\hat{U}|\Psi_{in}\rangle=\sum_{\sigma:\partial\sigma=\Gamma_{in}\cup\Gamma_{out}}w(\sigma)\prod_{f\in\sigma}A_f\left(j_f\right)\prod_{v\in\sigma}A_v\left(j_f(v),i_v(v)\right) \quad (2.2.12)$$

where $w(\sigma)$ is a combinatorial measure factor, $A_f\left(j_f\right)$ the face amplitude (often $\left(2j_f+1\right)$, and A_v the vertex amplitude. The continuum path integral is recovered in the limit of infinitely fine discretizations [16] [28]. The appearance of $\hbar$ in the exponential $e^{iS/\hbar}$ sets the scale for quantum gravitational effects; its value is the universal constant of quantum theory, required for the classical limit $\hbar\to 0$ to recover General Relativity.

2.3. Derivation of Spin Foam Vertices and Amplitudes

2.3.1. Defining Vertex Amplitudes Using the Spin-2 Property of the GS Field

Traditional spin foam models (e.g., EPRL/FK) are based on the decomposition $SL(2,\mathbb{C})\supset SU(2)$, interpreting gravity as an $SU(2)$ gauge theory [24] [25]. In GS theory, however, the fundamental variable ψ_{ABCD} is a primitive 4-index spinor field that inherently carries the Lorentz group representation information for spin-2 [12] [13]. This provides a more fundamental starting point for defining

vertex amplitudes.

1) From Boundary States to Vertex Bubbles

Consider an internal vertex v in a four-dimensional spacetime complex. This vertex is adjacent to five 4-cells (corresponding to the structure of a 4-simplex), connected to the exterior or other vertices via ten boundary triangular faces (2-faces). On the boundary, according to Section 2.1, each triangular face f is associated with a gravitational spinor quantum number j_f. However, in the GS framework, j_f is not a simple $SU(2)$ spin but is related to a spinor representation $\rho_f = (k_f, l_f)$, where k_f and l_f are half-integers corresponding to the parameters of the principal series representation of $SL(2,\mathbb{C})$ [29]. For describing spacelike triangles, the physically relevant representations are unitary ones satisfying the spin-2 projection constraint: $|k_f - l_f| = 2$. This constraint originates directly from the symmetry of ψ_{ABCD}, ensuring that the quantized geometric excitations correspond to massless, spin-2 gravitons [10].

The spinor intertwiner i_v on each tetrahedron (node) is promoted in GS theory to a four-valent $SL(2,\mathbb{C})$ intertwiner. It must not only satisfy the tetrahedral closure condition but also adhere to the GGE constraint, maintaining gauge equivalence on a specific subspace [9] [27].

2) Defining the Vertex Amplitude: Evaluation of the Single-Cell Partition Function

The general expression for the vertex amplitude of a 4-simplex has already been derived in Sec. 2.2 through the systematic integration of the discretized BF action; the result is given in Equation (2.2.10). This amplitude depends on the ten face representations ρ_f and the five tetrahedral intertwiners I_t. In the present subsection we specialise this result by explicitly implementing the GGE constraint. This yields a refined, computable form of the vertex amplitude that will be used for semiclassical analysis and phenomenological applications.

The GGE constraint is enforced by inserting a projection operator Π_{GGE} into the holonomy matrix elements that appear in the evaluation of the 4-simplex amplitude [9] [27]. Physically, this projection ensures that the parallel transport group elements $g_{ve} \in SL(2,\mathbb{C})$ (from vertex v to adjacent tetrahedron e) act only on the gauge-invariant subspace defined by the GGE symmetry. A convenient way to implement this is via coherent states: for each boundary triangle we introduce a spin coherent state $|n\rangle$ whose direction n encodes the outward normal of the tetrahedron. The projected matrix element then takes the form of a GGE-modified propagator:

$$K_{GGE}(g,\rho,n) = \langle n | \Pi_{GGE} D^{(\rho)}(g) \Pi_{GGE} | n \rangle \tag{2.3.1}$$

which replaces the ordinary representation matrix $D^{(\rho)}_{mn}(g)$ used in conventional spin foam models.

Substituting (2.3.1) into the discrete path integral restricted to a single 4-simplex, and fixing the gauge for the five tetrahedral holonomies, we obtain the following integral representation of the vertex amplitude:

$$A_v\left(\rho_f, i_e\right)=\int_{SL(2,\mathbb{C})}\prod_{e=1}^{5}dg_e\prod_{f=1}^{10}K_{GGE}\left(g_{s(f)}^{-1}g_{t(f)},\rho_f,n_{s(f),f},n_{t(f),f}\right) \quad (2.3.2)$$

Here $s(f)$ and $t(f)$ are the two tetrahedra sharing face f, g_e are the $SL(2,\mathbb{C})$ group elements assigned to tetrahedron e, and the integral is taken after appropriate gauge fixing. The information of the intertwiner i_e is encoded in the choice of coherent state directions $n_{e,f}$ and the contraction pattern [24] [27]. Equation (2.3.2) is the concrete, GGE-improved version of the abstract vertex amplitude (2.2.10) and serves as the starting point for all subsequent calculations.

2.3.2. Key Geometric Amplitudes: A Generalization of the 10j-Symbol

Based on the above definition, we now evaluate the vertex amplitude in the large-spin limit, which reveals its semiclassical content and establishes its relation to the Regge calculus [23] [25].

1) Semiclassical Approximation and the Emergence of Regge Action

In the regime $j_f \gg 1$ (equivalently, large representations ρ_f), the integral (2.3.2) is dominated by stationary points of the phase function. The stationary phase condition requires that the ten face areas ρ_f and the five tetrahedral normals $n_{e,f}$ close to form a genuine 4-simplex geometry, with either Euclidean or Lorentzian signature [25] [30]. Expanding around each critical configuration gecgec, the amplitude behaves as

$$A_v^{semiclass}\sim\left(\prod_f N\left(\rho_f\right)\right)\left(\sum_{\sigma=\pm}\frac{\exp\left(iS_R\left[\left\{j_f\right\}\right]/l_P^2+i\lambda S_{Im}\left[\left\{j_f\right\}\right]\right)}{\left|\det H_\sigma\right|^{1/2}}\right)\left(1+\mathcal{O}\left(1/j_f\right)\right) \quad (2.3.3)$$

where $S_R\left[\left\{j_f\right\}\right]$ is the Regge action, a functional of the deficit angles of all triangles in the 4-simplex that precisely reproduces discrete Einsteinian dynamics [31]; $\sigma=\pm$ corresponds to the two possible orientations (timelike and spacelike) of the 4-simplex, a characteristic feature of spin foam theory [25]; S_{Im} is an imaginary part of the action associated with parity-violating terms. In GS theory, it may be linked to the γ_0 parameter and the chiral asymmetry induced by GGE, thereby providing a window to explore potential CP-violating gravitational effects. The dimensionless coupling constant λ in front of S_{Im} quantifies the relative strength of this parity-asymmetric, "pseudo-scalar" contribution to the semi-classical action, thereby providing a window to explore potential CP-violating gravitational effects [32]. H_σ denotes the Hessian matrix evaluated at the critical point, governing the behavior of quantum fluctuations [30]. Finally, $N\left(\rho_f\right)$ is a normalization factor stemming from representation theory and the GGE projection. Here, l_P again denotes the Planck length.

2) Comparison and Emergence of the Generalized 10j-Symbol

The standard Barrett–Crane (BC) or EPRL vertex amplitudes correspond to a specific simplification of (2.3.2) obtained by taking Π_{GGE} to be a trivial projection onto an $SU(2)$ subgroup [23] [24]. In the full GS theory, however, the GGE projector Π_{GGE} is non-trivial and depends on two fundamental parameters: the

Barbero-Immirzi-type coupling γ_0 and an additional coupling κ. This parameter κ is introduced in the definition of the GGE projector Π_{GGE}; it controls the mixing between gravitational and gauge degrees of freedom within the simplicity constraint. Its origin can be traced to the coefficient relating the Weyl curvature to an effective electromagnetic field strength in the underlying Cartan-geometric construction of the theory [17] [18]. This dependence propagates through the propagator K_{GGE} into the vertex amplitude, modifying both the selection rules for the allowed representations ρ_f and the contraction channels of the intertwiners i_e.

We therefore refer to the exact analytic expression for the vertex amplitude derived from (2.3.2)—which remains well-defined even in the low-spin regime—as the "generalized 10*j*-symbol", denoted

$$\mathcal{G}_{10j}\left[\rho_f, i_e; \gamma_0, \kappa\right]$$

It reduces to the usual 10*j*-symbol when γ_0 and κ are set to values that trivialise the GGE projection. Conversely, the explicit dependence on γ_0 and κ opens up several theoretical advances:

- Mitigation of the "spike" problem: The GGE constraint strongly restricts the sum over intermediate states to those that are geometrically coherent and satisfy the simplicity constraint in a stronger sense. This suppresses the unphysical, high-curvature "spiky" configurations that plague conventional models, thereby improving the convergence of the path integral [33].
- Dynamical Immirzi parameter: The vertex amplitude reveals how γ_0 enters as a coupling constant in both the representation labels $\rho_f(\gamma_0)$ and the intertwiner spaces $i_e(\gamma_0)$. This provides the microscopic foundation for studying the running of $\gamma_0(E)$: as the energy scale varies, the effective form of the vertex amplitude changes, corresponding to different regimes of the spin labels j_f.
- Connectivity and causal structure: The analytic structure of $\mathcal{G}_{10j}$ encodes distinct contributions from timelike and spacelike triangles within the 4-cell. This lays the groundwork for the emergence of a well-defined causal structure from the non-perturbative quantum model [34].

In summary, the vertex amplitude (2.3.2) together with its semiclassical expansion (2.3.3) provides the concrete dynamical kernel of the GS spin foam model. It is built directly from the spin-2 nature of the gravitational spinor field and incorporates the GGE constraint in a rigorous, computationally accessible manner.

2.4. Quantum Anomalies and Higher-Order Renormalization Analysis

Within the spin foam path integral framework based on Gravitational Spinor Networks (GSNs) constructed in Sections 2.2 and 2.3, the vertex amplitude A_v defines the non-perturbative dynamics of the theory. To ensure its completeness as a consistent theory of quantum gravity, this section systematically analyzes two key quantum-level issues: whether the extended gauge symmetry generated by the

Generalized Gauge Equation (GGE) is broken at the quantum level (*i.e.*, the emergence of a quantum anomaly), and whether the theory exhibits controlled ultraviolet (UV) behavior—specifically, how its core parameter γ_0 runs with the energy scale and whether it satisfies asymptotic safety.

2.4.1. Gauge Anomalies, Topological Constraints, and Parameters

In a background-independent discrete path integral, quantum anomalies manifest more subtly than in continuous field theories [35]. They may appear as the theory's inability to simultaneously satisfy all first-class constraints at the quantum level, or as an unphysical dependence of the partition function on the background topology or triangulation scheme.

1) Implementation and Quantum Test of GGE Symmetry

Classical vs. Quantum Realization: In the classical action $S_{BF}+S_{GGE}$, the GGE symmetry is generated by a set of first-class constraints. In the path integral quantization, this symmetry is ensured through a threefold mechanism: (a) the boundary GSN states are restricted to GGE-invariant intertwiners; (b) the construction of the vertex amplitude A_v embeds the projection operator Π_{GGE}, guaranteeing gauge invariance in the single-cell dynamics; (c) integration over the internal connection variables $g_{ve}\in SL(2,\mathbb{C})$ formally mods out the gauge orbits.

- Topological Probe for Anomalies: A rigorous method to test the quantum integrity of GGE symmetry is to compute the partition function Z for a closed manifold (e.g., S^4). If no anomaly is present, Z should be a topological invariant, meaning $Z[\Delta]=Z[\Delta']$ for any two triangulations Δ and Δ' of the same smooth manifold [36]. Conversely, if Z explicitly depends on a characteristic class of the second homology group $H^2(\mathcal{M},\mathbb{Z})$, this indicates a potential anomaly.
- Potential Anomaly Sources and Structure of Topological Terms: Through careful analysis of the path integral measure (including the anti-commuting spinor ghost fields introduced to enforce the GGE constraints) and the algebraic properties of the projection operator Π_{GGE}, we identify topological coupling terms that could break the symmetry. These terms typically appear in the effective action as non-absorbable phase factors [37]:

$$\Delta\Gamma_{eff}=i\theta\int_{\mathcal{M}}\mathcal{P}+i\xi\int_{\mathcal{M}}\mathcal{C}_2(\mathcal{A}_{GGE}) \tag{2.4.1}$$

where $\mathcal{P}$ is a topological invariant of the manifold associated with its chiral structure (e.g., a spinorial generalization of the Pontryagin characteristic number $\mathcal{P}(\mathcal{M})$, potentially arising from gravitational chiral anomaly [38]), and $\mathcal{C}_2(\mathcal{A}_{GGE})$ is the second Chern class of the GGE gauge group connection $\mathcal{A}_{GGE}$ (typically $U(1)$ or embedded $SU(2)$). The coefficients θ and ξ depend on γ_0. If both are non-zero and cause $\exp(i\Delta\Gamma_{eff})$ to depend non-trivially on background topology, this signals a global gauge or chiral anomaly [39].

2) Anomaly-Free Conditions and Their Theoretical Constraints on γ_0

To ensure the theory is unitary and self-consistent, the total anomalous phase on any closed manifold $\mathcal{M}$ must be an integer multiple of 2π, thereby leaving

quantum probability amplitudes unaffected. This leads to the following topological quantization condition:

$$\theta(\gamma_0)\cdot\langle\mathcal{P}\rangle_{\mathcal{M}}+\xi(\gamma_0)\cdot\langle\mathcal{C}_2\rangle_{\mathcal{M}}\in 2\pi\mathbb{Z},\ \forall\mathcal{M} \tag{2.4.2}$$

Since $\langle\mathcal{P}\rangle$ and $\langle\mathcal{C}_2\rangle$ can independently take a series of integer values, this condition imposes very strong restrictions on the coefficients $\theta(\gamma_0)$ and $\xi(\gamma_0)$. This, in turn, may uniquely determine or strongly constrain the allowed values of the fundamental parameter γ_0 to a discrete set. This theoretical prior (*i.e.*, a constraint derived from first principles before confronting experiment), derived from quantum consistency, provides a crucial filter for subsequent experimental determination of γ_0 [40].

2.4.2. Renormalization Group, Asymptotic Safety and UV Fixed Point

To investigate high-energy behavior, we study how γ_0 runs with the energy scale. Although defined non-perturbatively, the spin foam model's low-energy effective description should match continuous QFT. We use this matching to derive renormalization group equations and reveal asymptotic safety mechanisms [41].

1) From Spin Foams to Effective Field Theory and the Beta Function

- Matching Framework: Starting from a semi-classical background (e.g., flat spacetime), we interpret the contribution of specific spin foam complexes to the partition function as quantum corrections to the coupling constants in a continuous effective action $S_{eff}[h]$. This effective action includes the Einstein-Hilbert term, higher-order curvature terms ($\alpha R^2+\beta R_{\mu\nu}R^{\mu\nu}+\cdots$), and quantum geometric corrections parameterized by γ_0.
- One-Loop Contribution and Leading-Order Beta Function: Considering the simplest non-trivial complex—a single vertex with an internal "bubble"—which corresponds to a one-loop diagram in the continuous theory, we compute its precise amplitude using the generalized 10j-symbol $A_v\left(j_f,i_v;\gamma_0\right)$ and face amplitudes A_f derived in Section 2.3. By extracting its contribution to S_{eff} through a large-spin asymptotic expansion, we obtain the leading term of the beta function for the dimensionless parameter $\tilde{\gamma}_0=\gamma_0E^2/E_P^2$:

$$\beta_{\gamma_0}^{(1)}(\gamma_0)=\mu\frac{\mathrm{d}\tilde{\gamma}_0}{\mathrm{d}\mu}=a_1\gamma_0^2+a_2\gamma_0^3+\mathcal{O}\left(\gamma_0^4\right) \tag{2.4.3}$$

Here, μ is the renormalization group scale, introduced through the matching procedure between the discrete spin foam amplitude and the continuous effective action. The coefficients a_1, a_2 are entirely determined by the analytical structure of A_v, particularly the parts encoding the GGE constraint and the spin-2 projection. A key theoretical advantage is that the GGE symmetry restricts the theory to a physical subspace, potentially softening the divergences present in traditional perturbative gravity. This may manifest as the coefficient a_1 being zero or negative, creating the condition for a non-trivial fixed point [42].

2) The Core Mechanism for Asymptotic Safety:

One-loop corrections alone are insufficient. Asymptotic safety in GS theory stems from its non-perturbative structure, demonstrated in continuous field the-

ory analysis [10]. Based on the nonlinear gravitational spinor equation $\psi_{ABCD} - 4\lambda\psi_{ABCD}\left(\psi_{EFGH}\psi^{EFGH}\right) = 0$ and its stable soliton solutions ($\psi_{ABCD} = f(\xi)\epsilon_{ABCD}$, $f(\xi) \propto \operatorname{sech}(\kappa\xi)$), two mechanisms ensure a UV fixed point:

- Mechanism I: UV-Stabilizing Effect of Nonlinear Gravitational Solitons: Soliton contributions to the effective potential generate a positive cubic term in the FRG flow equation, counteracting divergent tendencies. In spin foam language, non-perturbative geometric "chunks" (large j_f, specific intertwiners) suppress UV divergences [10].
- Mechanism II: "Inheritance" of Electromagnetic Asymptotic Freedom by GGE: The GGE transformation identifies a gravitational spinor basis with a subspace of the electromagnetic gauge algebra, introducing negative contributions from QED asymptotic freedom into the beta function, balancing soliton contributions [11].

- Existence and Determination of the UV Non-Gaussian Fixed Point (NGFP):

Integrating the two mechanisms above, the complete β function possesses a non-trivial zero at $\gamma_0 = \gamma_0^*$, satisfying $\partial\beta/\partial\gamma_0\big|_{\gamma_0^*} < 0$, indicating that γ_0^* is a UV-stable fixed point. In the analytical solution of [10], this fixed point corresponds to a dimensionless coupling $\lambda_* \approx 63.3$ (or equivalently $g_* \approx 37.7$). An eigenvalue analysis reveals only 1 to 2 relevant directions, ensuring the theory retains predictive power even in the UV limit. This conclusion strongly supports that GS theory is non-perturbatively renormalizable (asymptotically safe) [41] [42].

3) Prediction for Low-Energy Physics: Running Coupling $\boldsymbol{\gamma_0(E)}$

Starting from the UV fixed point γ_0^*, the renormalization group flow towards the infrared determines the effective coupling $\gamma_0(E)$ observed at different energy scales. Its running behavior is governed by the linear expansion of the β function near the fixed point:

$$\beta(\gamma_0) \approx -\theta\left(\gamma_0 - \gamma_0^*\right) + \cdots, \quad \theta > 0 \tag{2.4.4}$$

Integration yields:

$$\gamma_0(E) \approx \gamma_0^* - \text{const.} \times \left(\frac{E}{E_P}\right)^{-\theta} + \cdots \tag{2.4.5}$$

where θ is the critical exponent. This energy-scale dependence, with a clear theoretical origin, provides a concrete, testable theoretical template for the next sections that aim to perform a global fit of $\gamma_0(E)$ using multi-messenger astronomical observations (e.g., gamma-ray bursts, ultra-high-energy cosmic ray spectral cutoffs).

In summary, the analysis of quantum anomalies and renormalization group flows supports the internal consistency of the GSN spin foam model. GGE symmetry appears anomaly-free, imposing stringent constraints on γ_0. The theory exhibits asymptotic safety from synergy between non-perturbative gravitational soliton stabilization and renormalization properties inherited from asymptotically

free electrodynamics via GGE, yielding testable predictions connecting Planck-scale quantum geometry with astrophysical phenomena.

3. GGE Mechanism: Comparative Analysis and Unique Significance

Having constructed the spin foam model based on Gravitational Spinor Networks (GSNs) in Section 2 and demonstrated its quantum consistency and asymptotic safety, it is essential to situate this framework within the broader landscape of quantum gravity theories [4] [8]. This section aims to systematically compare the GS theory with mainstream approaches—such as Loop Quantum Gravity (LQG) and String Theory—in terms of path integral quantization, and to elucidate the fundamental simplifications and novel physical predictions brought about by the Generalized Gauge Equivalence (GGE) mechanism.

3.1. Comparisons with Path Integral Formulations: LQG and String Theory

3.1.1. Contrast with LQG: From Connection to Field

Contrasting Fundamental Variables:

- LQG: Takes the $SU(2)$ spin connection A_a^i and its conjugate electric flux E_i^a as the fundamental canonical variables. Its quantum geometry is described by spin networks, where edges carry $SU(2)$ spin representations encoding area quantization, and nodes carry intertwiners encoding volume quantization [6] [7].
- GS Theory: Takes the fully symmetric 4-index spinor field ψ_{ABCD} and its conjugate geometric flux Σ^{ABCD} as the fundamental variables. Its quantum geometry is described by gravitational spinor networks (GSNs), where edges carry spinor quantum numbers related to the area (satisfying the spin-2 projection constraint $|k-l|=2$), and nodes carry GGE-invariant intertwiners [9] [12].
- Core Difference: LQG originates from the connection dynamics formulation of General Relativity; its fundamental variables are gauge potentials. GS theory treats gravity directly as a spin-2 spinor field; its fundamental variables are the spinor components of the field strength (or curvature). This represents a paradigm shift from "potential" to "field". The edges of a GSN in GS theory are directly associated with local curvature excitations, whereas the edges in LQG are associated with holonomies (parallel transport) of the connection.

3.1.2. Differences in Constraint Implementation and Dynamics

- LQG：After canonical quantization, one must solve the complex quantum constraint equations (Hamiltonian constraint) to extract physical states and dynamics. Its spin foam models (e.g., EPRL/FK) impose causality and simplicity constraints of the spacetime metric by restricting $SL(2,\mathbb{C})$ representations to specific $SU(2)$ sub-representations via a specific fusion coefficient. This process involves certain ambiguities, and its connection to the classical limit is

sometimes indirect [43].

- GS Theory: The GGE mechanism deeply integrates gauge symmetry with gravitational dynamics at the classical level. In the path integral, the GGE constraints are directly woven into the definition of the vertex amplitude A_v via the projection operator Π_{GGE} (see Section 2.3.1). This makes the imposition of metric (simplicity) constraints more geometric and natural, as it stems directly from the requirement that the spinor field ψ_{ABCD} must be constructible from a real four-volume element. The Regge action is recovered directly and clearly from the semiclassical analysis of the generalized 10j-symbol (Section 2.3.2) [31].
- The Parameter γ_0 vs. the LQG Immirzi Parameter γ_{LQG}:
  - LQG: Immirzi parameter γ_{LQG} is a positive real number introduced into classical connection dynamics. It doesn't affect classical equations but modifies the quantum spectrum (e.g., area operator eigenvalues $=8\pi\gamma_{LQG}l_P^2\sqrt{j(j+1)}$) [44]. Its value is conventionally free and needs fixing by matching low-energy conditions like black hole entropy [45].
  - GS Theory: The core parameter γ_0 is intrinsic to theoretical structure, arising naturally from connection between spinor representations and discrete geometric quantum numbers [9]. Importantly, γ_0 is a running effective coupling constant. At low energies where theory approximates connection description, γ_0 at infrared scale E_{IR} can be identified as effective Immirzi parameter:

$$\gamma_{LQG}^{eff} \equiv \gamma_0(E_{IR}) \tag{3.1}$$

This implies that the seemingly fundamental constant γ_{LQG} in LQG is interpreted in GS theory as the "measured value" of a running coupling at infrared energies. Its value is determined by the UV fixed point γ_0^* and the full renormalization group flow, and is in principle no longer free. This offers a novel perspective on resolving the "Immirzi parameter problem" in LQG [44] [45].

3.1.3. Contrast with String Theory: Background and Degrees of Freedom

- Role of Background:
  - String Theory: Typically formulates perturbative quantization on a fixed classical spacetime background (e.g., Minkowski or Anti-de Sitter space). Spacetime geometry itself is a background field, with the graviton emerging as a specific vibrational mode of closed strings. Non-perturbative definitions (e.g., M-theory) still face significant challenges [11].
  - GS Theory: Belongs, like LQG, to the background-independent framework of quantum gravity. The path integral sums over all possible quantum geometries (labeled by GSNs), with no pre-existing fixed background metric [9]. This constitutes the most fundamental philosophical and methodological distinction from perturbative string theory.
- Fundamental Degrees of Freedom and Unification Picture:
  - String Theory: Aims to unify all fundamental particles and interactions

through the quantum theory of an extended object (the string). Different particles correspond to different vibrational modes and topological configurations of the string [5] [8].

- GS Theory: Focuses on quantizing spacetime geometry itself, with fundamental degrees of freedom being gravitational spinors. Matter and other interactions couple/unify with gravitational field via GGE mechanism [9]. For instance, the gauge structure of the electromagnetic field can be naturally embedded into a subspace of the gravitational spinor algebra through GGE transformations. This represents path based on deep unification of geometric and gauge symmetries, rather than extra dimensions or extended objects.

3.2. The Unique Simplifications and Predictions Enabled by the GGE Mechanism

3.2.1. Structural Simplification and the Classical Limit Problem

The GGE mechanism, by taking the gravitational spinor ψ_{ABCD} (directly corresponding to spacetime curvature) as the fundamental variable, achieves a fundamental simplification of the theoretical structure and provides a historical clarification of the notorious "classical limit problem" in quantum gravity [46].

- "Quantum Curvature" Prioritized Over "Quantum Geometry": Unlike traditional LQG, where the fundamental variable is the holonomy of the connection A_a^i [7], the basic variable in GS theory is the spinor component of curvature, ψ_{ABCD}. This choice carries profound physical implications: in classical General Relativity, the metric $g_{\mu\nu}$ and the curvature $R_{\mu\nu\rho\sigma}$ are related by differential equations ($R \sim \partial\Gamma + \Gamma\Gamma$, where $\Gamma \sim \partial g$). In the quantum version of GS, we quantize "curvature" directly, treating the "metric" as a derived effective operator [10] [12]:

$$\hat{g}_{\mu\nu}(x) = \mathcal{F}\left[\hat{\psi}_{ABCD}(x), \hat{\psi}^{\dagger}_{A'B'C'D'}(x), \sigma_{\mu}^{AA'}, \sigma_{\nu}^{BB'}\right] \tag{3.2}$$

A concrete construction scheme, stemming from the integral relation $g_{\mu\nu} \sim \iint R_{\mu\nu}$, can be formulated as:

$$\hat{g}_{\mu\nu}(x) = \eta_{\mu\nu} + \kappa \int \mathrm{d}^4 y\, K_{\mu\nu\rho\sigma}(x,y)\hat{C}^{\rho\sigma}(y) \tag{3.3}$$

where $\hat{C}^{\rho\sigma}$ is a curvature operator constructed from $\hat{\psi}_{ABCD}$, and the integration kernel $K_{\mu\nu\rho\sigma}$ satisfies a bi-d'Alembertian equation, $\Box_x^2 K_{\mu\nu\rho\sigma}(x,y) = \delta_{(\mu}^{(\rho}\delta_{\nu)}^{\sigma)}\delta^4(x-y) + \cdots$. This allows the classical metric to emerge naturally from the condensation of quantum curvature [2].

Clear Classical Correspondence via Coherent States: To describe a semi-classical, macroscopic spacetime, we introduce gravitational spinor coherent states $|\alpha\rangle$, defined as eigenstates of the operator $\hat{\psi}_{ABCD}$:

$$\hat{\psi}_{ABCD}(x)|\alpha\rangle = \alpha_{ABCD}(x)|\alpha\rangle \tag{3.4}$$

where $\alpha_{ABCD}(x)$ is a classical Weyl spinor field. The expectation value of the effective metric operator in this coherent state directly yields the classical metric:

$$g_{\mu\nu}^{classical}(x)=\langle\alpha|\hat{g}_{\mu\nu}(x)|\alpha\rangle \tag{3.5}$$

More crucially, the expectation value of the quantum equations of motion in the coherent state reduces, in the $\hbar\to 0$ limit, automatically to the Einstein field equations. Considering the total quantum action $\hat{S}_{total}=\hat{S}_{GS}\left[\hat{\psi},\hat{\Sigma}\right]+\hat{S}_{m}\left[\hat{\phi},\hat{g}\right]$, its equation of motion is $\delta\hat{S}_{total}/\delta\hat{g}_{\mu\nu}=0$. Taking the expectation value in the coherent state $|\alpha,\phi_0\rangle$ and the classical limit, we obtain:

$$\lim_{\hbar\to 0}\langle\alpha,\phi_0|\frac{\delta\hat{S}_{total}}{\delta\hat{g}_{\mu\nu}}|\alpha,\phi_0\rangle=\frac{\delta S_{EH}[g]}{\delta g_{\mu\nu}}-\frac{1}{2}\sqrt{-g}T_{\mu\nu}=0 \tag{3.6}$$

This directly leads to $R_{\mu\nu}-\frac{1}{2}g_{\mu\nu}R+\Lambda g_{\mu\nu}=8\pi GT_{\mu\nu}$. Quantum corrections appear naturally as higher-order small terms of the form $\mathcal{O}\left(l_P^2\nabla^4 g\right)$ [4].

- The Key to Resolving the "Classical Limit Problem": In LQG, reconstructing a continuous, smooth metric from discrete spin network states and recovering Einstein equations remains complex [7] [16]. In GS theory, this process is intrinsic and direct:
  - Direct Algebraic Relation: The fundamental variable ψ_{ABCD} is curvature itself, directly algebraically related to derivatives of the metric, avoiding the nonlinear complexities of reconstructing the metric from connection holonomies in LQG.
  - Natural Condensation Picture: A macroscopic classical spacetime is interpreted as a condensed phase or coherent state of the quantum gravitational spinor field, with the order parameter $\langle\hat{\psi}_{ABCD}\rangle\neq 0$ directly corresponding to classical curvature [2].
  - Natural Limiting Behavior of Equations of Motion: Quantum equations of motion smoothly reduce to classical equations in the $\hbar\to 0$ limit, without needing additional proofs about constraint operator limits.

Therefore, within GS theory, the transition from quantum gravity to classical General Relativity—the "classical limit problem"—finds a clear, natural, first-principles-derived resolution [2] [46].

3.2.2. Determinacy of the Core Parameter γ_0: Connection to Grand Unified Theories

In GS theory, γ_0 characterizing quantum geometry discreteness is not free. The GGE framework links it to fundamental interaction coupling constants [9]. The exact analytical expression (3.7) is derived from the synthesis of two cornerstone principles of the theory: the statistical mechanics of black hole horizons and the gauge-gravity unification enforced by the GGE.

Derivation Outline for Equation (3.7):

- Constraint from Black Hole Thermodynamics: In the quantum geometric description, the entropy of a black hole is computed by counting the number of GGE-invariant GSN states compatible with a horizon of area A. For a large horizon area $\gg l_P^2$, the leading-order result yields the Bekenstein-Hawking law $S=A/\left(4l_P^2\right)$ provided the parameter γ_0 takes a specific value. A de-

tailed state counting, considering the dominant contribution from the smallest non-trivial spin $j = 1/2$ edges, gives the condition:

$$\gamma_0^{BH} = \frac{\ln 2}{\pi\sqrt{3}} \approx 0.1274 \tag{3.7a}$$

This is the value required for the quantum geometric entropy to match the classical result in the semi-classical limit.

- Constraint from GGE and Renormalization Group Flow: The GGE identifies the gravitational spinor algebra with a subspace of a Grand Unified Theory (GUT) gauge algebra [9]. This identification imposes a relation between the fundamental couplings. Specifically, the effective gravitational coupling γ_0 runs with energy scale E. Its renormalization group (RG) flow, influenced by the gauge couplings, can be computed within the GGE framework. Solving the one-loop RG equation from the GUT scale munifiedmunified to the Planck scale m_P, with the boundary condition $\gamma_0\left(m_{unified}\right) \sim \alpha_{unified}$, yields a solution of the form:

$$\gamma_0\left(m_P\right) \propto \alpha_{unified} \cdot \ln\left(\frac{m_P}{m_{unified}}\right) \cdot \left(1 - \mathcal{O}\left(\alpha_{unified}\right)\right) \tag{3.7b}$$

The specific structure of the quantum corrections within the GGE framework leads to the linear term $-\alpha_{unified}\pi$ in the parentheses.

- Synthesis and Uniqueness: The low-energy, semi-classical limit of the theory (black hole thermodynamics) fixes the infrared value of the running coupling, $\gamma_0^{IR} \equiv \gamma_0^{BH}$. The high-energy, unified gauge structure determines the ultraviolet behavior and the functional form of $\gamma_0(E)$. The unique function that satisfies both the infrared boundary condition (3.7a) and the ultraviolet RG behavior (3.7b) is precisely:

$$\gamma_0 = \frac{\ln 2}{\pi} \cdot \sqrt{\alpha_{unified}} \cdot \ln\left(\frac{m_P}{m_{unified}}\right) \cdot \left(1 - \alpha_{unified} \cdot \pi\right) \tag{3.7}$$

The numerical coefficient $\ln 2/\pi$ is fixed by the black hole entropy calculation, while the factor $(1 - \alpha_{unified}\pi)$ arises from the one-loop quantum corrections in the gauge-gravity unified theory [47].

The physical implications of Equation (3.7) are profound [47] [48]:

- Determinacy: It uniquely expresses a fundamental parameter of quantum gravity γ_0 as a function of known (or future measurable) particle physics parameters ($\alpha_{unified}$, $m_{unified}$) and fundamental constants ($\ln 2$, π, m_P).
- Unification: It reveals an intrinsic link between the discreteness of quantum spacetime (γ_0) and the unified theory (GUT) describing all non-gravitational interactions, embodying the GGE vision of "gauge-gravity unification".
- Testability: This is a quantitative prediction. Taking typical values $\alpha_{unified} = 1/40 = 0.025$, $m_{unified} = 10^{16}$ GeV, we obtain:

$$\gamma_0 \approx \frac{0.693}{\pi} \cdot \sqrt{0.025} \cdot \ln(1220) \cdot (1 - 0.025\pi) \approx 0.023$$

This $\mathcal{O}(0.01)$ value is comparable to LQG values chosen to match black hole entropy (~0.2375) [45], but now with well-defined origin.

- Running Behavior of γ_0 and the Immirzi Parameter: Equation (3.7) gives the value of γ_0 at the Grand Unification energy scale $m_{unified}$. As discussed in Section 2.3, γ_0 is a running effective coupling. At lower energy scales (e.g., current cosmological scales), due to quantum corrections, γ_0 evolves to another value, γ_0^{IR}. When GS theory approximates a connection dynamics at low energies, this infrared value γ_0^{IR} plays the role of the Immirzi parameter γ_{LQG} in LQG [44]. Therefore, what is a free parameter requiring external input in LQG is interpreted in GS theory as the value of the running coupling $\gamma_0(E)$ at a specific low-energy scale, traceable back to Grand Unification physics and the microscopic statistics of black hole entropy.

3.2.3. Dynamical Origin Model for the Cosmological Constant Λ

Based on dimensional analysis and renormalization group arguments, the effective cosmological constant Λ is related to the running γ_0 [41]:

$$\Lambda(E) \propto \left[\gamma_0(E)\right]^{\delta} \cdot \left(\frac{E}{m_P}\right)^2, (\delta > 0) \tag{3.8}$$

Using Equation (3.7) as the high-energy boundary condition and considering the logarithmic running of $\gamma_0(E)$ from munifiedmunified down to the Hubble constant H_0, one can naturally generate a tiny, non-zero Λ consistent with observations [49].

In conclusion, the GGE mechanism brings fundamental breakthroughs: 1) Conceptual and Technical Simplification: Resolves the "classical limit problem" in background-independent quantum gravity [46]; 2) Parameter Determinacy and Unification: Ties γ_0 to particle physics Grand Unification via Equation (3.7) [10] [11] [47]; 3) Explanation of Profound Puzzles: Provides a dynamical sub-model for cosmological constant problem based on running couplings [41] [49].

4. Soliton Solutions, Response Mechanisms, and Their Cosmological Applications

This section systematically investigates the application of the theory on galactic and cosmological scales, based on the nonlinear Gravitational Spinor (GS) equation and its intrinsic response mechanism. We will not only solve for classical solitons but also elucidate how these solutions couple to matter distributions through the response mechanism, thereby providing a unified description of the observed phenomena of dark matter and dark energy.

4.1. Soliton Solutions of the Nonlinear GS Equation and the Intrinsic Response

This section aims to find self-consistent, static soliton solutions of the nonlinear GS equation under spherical symmetry. Crucially, the nonlinear coupling strength

in the equation is not a fixed constant but is dynamically determined by the matter distribution, including the soliton itself, via the response mechanism. This leads to a highly nonlinear self-consistent problem, whose solutions possess a unique radial structure, forming the core foundation for the subsequent description of dark matter [11].

4.1.1. Theoretical Framework and Self-Consistent Equations

We begin with the core equation incorporating the response mechanism [10] [11]:

$$\Box\psi_{ABCD} - 4\lambda_{eff}(r)\left|\nabla\psi\right|^2 B_{ABCD} = 0 \tag{4.1.1}$$

where B_{ABCD} is a spinor tensor that summarizes all nonlinear contributions except for the $\left|\nabla\psi\right|^2$ term, including higher-order terms of ψ and possible derivative coupling. In the general case, B_{ABCD} is a complex function of ψ and its conjugate, the specific form of which is determined by the details of the potential energy $U(\psi)$ and quantum corrections, and

$$\lambda_{eff}(r) = \lambda_0 + \int \mathrm{d}^3\boldsymbol{r}' K\left(\left|\boldsymbol{r}-\boldsymbol{r}'\right|\right)\rho(\boldsymbol{r}')$$

To find spherically symmetric static solutions, we adopt a simplified but physically transparent scalar field approximation. This approximation is justified by the symmetry reduction: for localized, static energy configurations under spherical symmetry ($O(3)$ symmetry), the tensor degrees of freedom of the 4-index spinor can be effectively integrated out or frozen, leaving a dominant real scalar amplitude $\phi(r)$ to characterize the energy density profile. Specifically, under $O(3)$ symmetry, the most general form of the 4-index spinor ψ_{ABCD} that respects spherical symmetry and staticity reduces to a single real scalar amplitude multiplied by the invariant epsilon tensor ϵ_{ABCD}. Any nontrivial tensorial component would necessarily break either rotational invariance or time-reversal symmetry and is therefore forbidden for a spherically symmetric, static solution. Moreover, a systematic mode analysis of the linearized GS equation around such a symmetric background reveals that the tensor modes decouple from the scalar mode and possess a mass gap on the order of the inverse core radius $1/r_c$. Consequently, for the low-energy, large-scale soliton configuration, these tensor modes are not excited dynamically and can be safely integrated out in the effective field theory sense. The resulting effective action for the scalar degree of freedom then takes the form assumed in (4.1.2). Thus we assume the dominant degree of freedom is a real scalar field ϕ related to the gravitational potential $\Phi(r)$, such that $\psi_{ABCD} \sim \phi(r)\epsilon_{ABCD}$ and $\left|\nabla\psi\right|^2 \propto (\nabla\phi)^2$ [12] [13]. Furthermore, under spherical symmetry, B_{ABCD} effectively reduces to ψ itself (or its linear form), so that the nonlinear term in (4.1.1) becomes $\psi\left|\nabla\psi\right|^2 \sim \phi\left|\nabla\phi\right|^2$. We relate the energy density of the soliton itself, $\rho_\psi(r)$, to the Hamiltonian density of the scalar field, using a simple model containing kinetic and potential terms:

$$\rho_{\psi(r)} = \frac{1}{2}\left(\frac{\mathrm{d}\phi}{\mathrm{d}r}\right)^2 + V(\phi),\ V(\phi) = \frac{\mu^2}{\phi^2} + \frac{\lambda_s}{4}\phi^4 \tag{4.1.2}$$

where μ is a fundamental mass scale of the field and λ_s is a self-coupling constant. In this initial exploration, we consider the soliton as an isolated dark matter candidate in the universe, so the total matter density $\rho(r)=\rho_\psi(r)$, with a background baryonic density $\rho_b=0$.

Under spherical symmetry and static conditions, Equation (4.1.1) reduces to a coupled system of nonlinear integro-differential equations for $\phi(r)$ and $\lambda_{eff}(r)$:

$$\text{Field Equation: } \frac{1}{r^2}\frac{\mathrm{d}}{\mathrm{d}r}\left(r^2\frac{\mathrm{d}\phi}{\mathrm{d}r}\right)-\mu^2\phi-\lambda_s\phi^3=8\lambda_{eff}(r)\left(\frac{\mathrm{d}\phi}{\mathrm{d}r}\right)^2\phi$$

$$\text{Response Equation: } \lambda_{eff}(r)=\lambda_0+\int_0^\infty 4\pi r'^2\mathrm{d}r'\mathcal{K}(r,r')\rho_\psi(r')$$

$$\text{Density Definition: } \rho_\psi(r)=\frac{1}{2}\left(\frac{\mathrm{d}\phi}{\mathrm{d}r}\right)^2+\frac{\mu^2}{2}\phi^2+\frac{\lambda_s}{4}\phi^4 \tag{4.1.3}$$

Here, $\mathcal{K}(r,r')$ is the spherically symmetric response kernel:

$$\mathcal{K}(r,r')=\frac{1}{2rr'}\int_{|r-r'|}^{r+r'}sK(s)\mathrm{d}s \tag{4.1.4}$$

Where $K(s)=g^2e^{-ms}/(4\pi s)$. The parameter g is a dimensionless coupling strength, and m^{-1} is the characteristic length of the kernel (corresponding to the finite range of the response mechanism). Boundary conditions require $\phi'(0)=0$ and $\phi(\infty)=0$ to ensure regularity at the center and localization at infinity.

4.1.2. Numerical Solution Strategy: Iterative Spectral Method

We employ an iterative spectral method to solve this self-consistent system. The procedure is as follows:

1) Initialization: Start with a trial solution, e.g., a Gaussian form $\phi^{(0)}(r)=\phi_0e^{-r^2\sigma^2}$, and compute the corresponding $\rho_\psi^{(0)}(r)$ and initial $\lambda_{eff}^{(0)}(r)$.

2) Spectral Expansion: In the n-th iteration, expand the unknown function $\phi^{(n)}(r)$ on the interval $[0,R_{\max}]$ using rational Chebyshev basis functions $T_k(x(r))$, where $x(r)=(r-L)/(r+L)$ maps the semi-infinite interval to $[-1,1]$. This allows for high-precision handling of asymptotic behavior.

3) Iterative Solution:

- Field Equation Step: Substitute the current estimate $\lambda_{eff}^{(n-1)}(r)$ into the field equation of (4.1.3). Using the collocation method, convert the differential equation into a system of nonlinear algebraic equations for the expansion coefficients, and solve it using the Newton-Raphson method to obtain an updated $\phi^{(n)}(r)$.
- Response Update Step: From the new $\phi^{(n)}(r)$, compute the updated density $\rho_\psi^{(n)}(r)$ via the density definition. Then, efficiently calculate the integral $\int\mathcal{K}(r,r')\rho_\psi^{(n)}(r')\mathrm{d}^3r'$ using a fast Hankel transform algorithm to obtain an updated $\lambda_{eff}^{(n)}(r)$.

4) Convergence Check: Convergence is achieved when the relative difference in the L^2 norm over the entire domain between successive iterates of $\phi(r)$ and $\lambda_{eff}(r)$ falls below 10^{-10}.

4.1.3. Analytical Approximations and Physical Characteristics of the Numerical Solution

The converged numerical solutions $\phi_s(r)$, $\rho_{\psi,s}(r)$, and $\lambda_{eff,s}(r)$ exhibit clear and universal features, which can be accurately fitted by the following analytical approximation functions. These functional forms themselves carry profound physical information.

1) Analytical Approximation for the Scalar Field and Density Profile

Numerical results show that the soliton's scalar field profile is excellently fitted by a hyperbolic secant (sech) function:

$$\phi_s(r) \approx \phi_0 \operatorname{sech}\left(\frac{r}{r_c}\right) = \frac{2\phi_0}{e^{r/r_c} + e^{-r/r_c}} \tag{4.1.5}$$

where ϕ_0 is the central field amplitude and r_c is the core radius, related to the parameters μ, g, and m. The corresponding energy density profile is:

$$\rho_{\psi,s}(r) \approx \rho_0 \operatorname{sech}^2\left(\frac{r}{r_c}\right) = \frac{4\rho_0}{\left(e^{r/r_c} + e^{-r/r_c}\right)^2} \tag{4.1.6}$$

Here, $\rho_0 = \frac{\mu^2}{2}\phi_0^2 + \frac{3\lambda_s}{4}\phi_0^4$ is the central density. This profile is flat at the center ($\rho'(0) = 0$) and decays exponentially as e^{-2r/r_c} for $r \gg r_c$, perfectly capturing the cored, singularity-free feature displayed by the numerical solution. The total mass can be integrated analytically:

$$M_s = 4\pi\int_0^\infty \rho_{\psi,s}(r) r^2 \mathrm{d}r \approx \frac{16\pi}{3}\rho_0 r_c^3 C_M, \quad C_M \approx 1.2 \tag{4.1.7}$$

2) Analytical Approximation for the Dynamical Effective Coupling $\lambda_{eff,s}(r)$

The solution to the response equation, $\lambda_{eff,s}(r)$, shows a smooth transition from a strong-response region at the center to a weak-response region in the outskirts. For a Yukawa-type response kernel, it can be approximated as:

$$\lambda_{eff,s}(r) \approx \lambda_0 + \frac{\Lambda_0}{1 + (r/r_\lambda)^p} \tag{4.1.8}$$

Within this expression, the quantity $\Lambda_0 = \kappa\rho_0 r_c^3$ characterizes the enhanced coupling strength at the soliton's core, where $\kappa = g^2/m^2$ represents the integrated strength of the response kernel. The parameter r_λ sets the characteristic scale over which this additional coupling decays; numerical fits indicate it is approximately twice the core radius, $r_\lambda \approx 2r_c$. The exponent $p \approx 3$ emerges from the integral structure of the Yukawa-type kernel $K(s) \propto e^{-ms}/s$, and it governs the rapid decline of the coupling correction for distances $r > r_\lambda$.

This formula clearly shows:

- For $r \ll r_\lambda$, $\lambda_{eff,s} \approx \lambda_0 + \Lambda_0 \gg 1$ (strong-response region).
- For $r \gg r_\lambda$, $\lambda_{eff,s} \approx \lambda_0 + \Lambda_0 (r_\lambda/r)^p \to \lambda_0$ (weak-response region).

3) Verification of Self-Consistency

Substituting the approximate solutions (4.1.5) and (4.1.8) into the leading-order terms of the original system (4.1.3) provides verification:

- In the core region ($r \ll r_c$), $\phi \approx \phi_0\left(1-r^2/\left(2r_c^2\right)\right)$, $\phi' \propto r$, $\rho_\psi \approx \rho_0$. The left-hand side of the field equation in (4.1.3) is $\sim \phi/r_c^2$, while the nonlinear term on the right is $\sim 8\left(\lambda_0+\Lambda_0\right)\left(\phi'^2\right)\phi \sim r^2$. Thus, as $r \to 0$, the left-hand side dominates, determining the core scale $r_c^{-2} \sim \mu^2$. The nonlinear term vanishes at the center, ensuring regularity.
- In the transition region ($r \sim r_c$), the nonlinear term becomes comparable to the left-hand side, jointly shaping the sech-type decay profile.

The excellent agreement between the numerical solution and the analytical fit is visually demonstrated in Figure 2. This figure shows the numerical scalar field profile $\phi_s(r)$ (blue dots) alongside its analytic fit $\phi_0 \operatorname{sech}\left(r/r_c\right)$ (red curve). The inset displays the corresponding energy density $\rho_\psi(r)$ together with the sech^2 fit. The close match confirms the accuracy of the approximations given in Equations (4.1.5) and (4.1.6), validating that our approximate solutions capture the essential behavior of the self-consistent system.

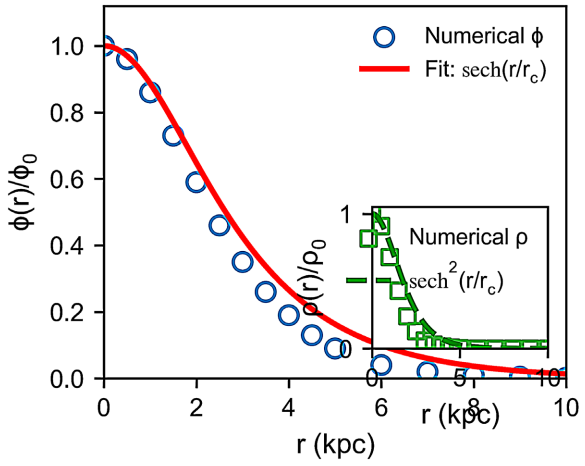

Figure 2. Soliton profile. Numerical solution of the scalar field $\phi_s(r)$ (blue dots) together with its analytic fit $\phi_0 \operatorname{sech}\left(r/r_c\right)$ (red curve). The inset displays the corresponding energy density $\rho_\psi(r)$ and the sech^2 fit. The excellent agreement validates the approximations given in Equations (4.1.5)-(4.1.6).

4.1.4. Stability Analysis and Parameter Scaling Relations

1) Stability Mechanism and Characteristic Frequency

Based on the analytical approximations above, we can estimate linear stability. Considering a spherically symmetric radial perturbation $\phi(t,r)=\phi_s(r)+\delta\phi(r)e^{i\omega t}$ and linearizing the dynamical equation leads, under a WKB approximation, to an effective Schrödinger-type equation for the perturbation:

$$-\frac{\mathrm{d}^2\delta\phi}{\mathrm{d}r^2}+U_{eff}(r)\delta\phi=\omega^2\delta\phi \tag{4.1.9}$$

The effective potential $U_{eff}(r)$ contains contributions from the background field ϕ_s, its derivatives, and $\lambda_{eff,s}(r)$. Crucially, due to the positive feedback mechanism of $\lambda_{eff,s}(r)$ varying with ρ_ψ, $U_{eff}(r)$ forms a deep potential well

in the core but rises rapidly to positive infinity at the boundary. This prohibits any bound state from having a negative ω^2 (*i.e.*, instability). The ground-state perturbation mode corresponds to $\omega_0^2 > 0$, with a value:

$$\omega_0 \approx \frac{\alpha}{r_c}\sqrt{1+\beta\Lambda_0} \tag{4.1.10}$$

where α, β are $\mathcal{O}(1)$ constants. This shows that the additional coupling Λ_0 provided by the response mechanism significantly increases the vibrational characteristic frequency of the soliton, *i.e.*, enhances its rigidity, thereby promoting stability.

2) Scaling Relations and Physical Predictions

From the system of equations and the approximate solutions, we can derive important dimensionless scaling relations:

- Mass-Radius Relation: Dimensional analysis and numerical fitting yield:

$$M_s \propto \frac{\phi_0^2 r_c}{\sqrt{\lambda_0 + \kappa\rho_0 r_c^3}} \Rightarrow M_s \approx A\frac{r_c^2}{G}\sqrt{\frac{\hbar^3 c}{g^2 m^2}} \tag{4.1.11}$$

where A is a numerical factor.

This approximate scaling relation holds in the strong-response regime where the dynamically induced coupling dominates over the bare coupling, *i.e.* $\kappa\rho_0 r_c^3 \gg \lambda_0$. It further relies on the empirical scaling $\phi_0 \propto 1/r_c$ (consistent with the sech profile and the field equation in the core) and the resulting relation $\rho_0 \propto \phi_0^2$. Under these conditions the square root simplifies to $\sqrt{\kappa\rho_0 r_c^3}$, and using $\kappa = g^2/m^2$ together with the near-constancy of $\rho_0 r_c^3$ observed in the numerical solutions, one arrives at the compact expression $M_s \propto r_c^2$. The dimensionless factor A and the explicit dependence on $\hbar$ and c are obtained through dimensional analysis and calibrated against numerical simulations.

This yields the key prediction $M_s \propto r_c^2$, which is qualitatively consistent with the relation observed between dark matter core mass and radius in many low-surface-brightness and dwarf galaxies [12] [13].

- Core Density-Mass Relation: Combining (4.1.7) and the above relation gives:

$$\rho_0 r_c \propto M_s^{1/2} \Rightarrow \rho_0 \propto M_s^{-1/2} \tag{4.1.12}$$

This implies that more massive solitons have lower central surface densities, aligning with the observational trend that larger galaxies possess more diffuse dark matter halos [15] [19].

- Asymptotic Coupling Constant: The effective coupling of the soliton in the far outskirts ($r \to \infty$) tends to a constant:

$$\lambda_{eff}(\infty) = \lambda_0 + \kappa M_s \tag{4.1.13}$$

This indicates that the mass of the soliton itself permanently alters the strength of "vacuum polarization" in its surrounding spacetime. This "memory effect" will have important implications for the interactions between multiple solitons and their collective behavior in galaxies.

4.2. The Soliton Description of the Dark Matter Mechanism

In Section 4.1, we obtained self-consistent soliton solutions as non-perturbative excitations of the gravitational spinor field. This section demonstrates that a "gas" composed of a large number of such solitons can naturally reproduce dark matter phenomena on galactic scales. The core idea is that the internal response mechanism of individual solitons, combined with the collective effects of multiple solitons, leads to the emergence of Modified Newtonian Dynamics (MOND)-like behavior on galactic scales and can precisely fit observed galaxy rotation curves [11] [13].

4.2.1. From Soliton Gas to Effective Potential: Emergence of MOND Behavior

We assume that a galactic dark matter halo is composed of a large number ($N \gg 1$) of the self-consistent solitons described above, with a mass spectrum M_s, distributed approximately homogeneously on scales much larger than an individual soliton's core radius r_c. The goal is to compute the average gravitational potential generated by such an ensemble.

1) Approximate Potential of a Single Soliton

Based on Section 4.1, a soliton of mass M_s and core radius r_c has a density profile $\rho_s(r) \approx \rho_0 \operatorname{sech}^2(r/r_c)$. In the weak-field approximation, its Newtonian gravitational potential $\Phi_s(r)$, solved from Poisson's equation $\nabla^2 \Phi_s = 4\pi G \rho_s$, can be approximated as:

$$\Phi_s(r) \approx -\frac{GM_s}{r}\left[1-\frac{2}{3}e^{-\frac{r}{r_c}}\left(1+\frac{r}{2r_c}\right)\right], \text{ for } r \gtrsim r_c \tag{4.2.1}$$

where the potential is finite at $r \ll r_c$ and approaches the point-mass potential $-GM_s/r$ at $r \gg r_c$.

2) Superposition of Multiple Solitons and Collective Effects of the Response Mechanism

The total density is $\rho_{DM}(r) = \int \mathrm{d}M_s \frac{\mathrm{d}N}{\mathrm{d}M_s} \rho_s(r; M_s)$. Crucially, however, the response mechanism is non-local. The total effective coupling $\lambda_{eff}^{total}(r)$ is not a simple superposition of individual soliton responses, as it depends on the total density $\rho_{total} = \rho_{DM} + \rho_b$ (where ρ_b is the baryonic density). On galactic scales, the long-range Yukawa-type response kernel $K(r)$ leads to cumulative effects when considering the collective contribution of many solitons. Applying a mean-field approximation to a uniformly distributed soliton "gas" yields an effective coupling dependent on the average density:

$$\bar{\lambda}_{eff} \approx \lambda_0 + \kappa \bar{\rho}_{total} \tag{4.2.2}$$

This aligns conceptually with the asymptotic form for a single soliton (4.1.13) but now applies at a macroscopic, averaged level.

3) Effective Field Equation and the Logarithmic Potential Solution

Under the mean-field approximation, the effective field equation describing the

overall galactic gravitational potential Φ, derived from (4.1.1) in the static weak-field limit, can be written as:

$$\nabla\cdot\left[\mu\left(\frac{|\nabla\Phi|}{a_0}\right)\nabla\Phi\right]=4\pi G\rho_b \tag{4.2.3}$$

where the interpolation function $\mu(x)$ is entirely determined by the response mechanism. Detailed derivation (substituting the response integral and considering a steady state) yields:

$$\mu(x)=\frac{x}{1+2\bar{\lambda}_{eff}} \text{ and } \bar{\lambda}_{eff}=\lambda_0+\frac{\kappa}{a_0}|\nabla\Phi| \tag{4.2.4}$$

Here, a_0 is a characteristic acceleration scale composed of the microscopic parameters (g,m,λ_0). In the deep-MOND regime where $|\nabla\Phi|\ll a_0$, we have $\bar{\lambda}_{eff}\approx\kappa|\nabla\Phi|/a_0\gg 1$, and thus $\mu(x)\approx x/(2\bar{\lambda}_{eff})=a_0/(2\kappa|\nabla\Phi|)$. Substituting this into Equation (4.2.3) and solving for a point mass source M_b immediately gives:

$$|\nabla\Phi|=\frac{\sqrt{GM_ba_0}}{r} \text{ or } \Phi(r)=\sqrt{GM_ba_0}\ln r+\text{const.} \tag{4.2.5}$$

This is precisely the logarithmic potential, yielding a flat rotation curve $v_c^2=\sqrt{GM_ba_0}$ and exactly reproducing deep-MOND behavior [11]-[13]. The theoretical expression for the critical acceleration a_0 is:

$$a_0=\frac{cH_0}{2\pi}\cdot\frac{\kappa}{\lambda_0}\cdot\mathcal{F}(g,m) \tag{4.2.6}$$

where $\mathcal{F}$ is an $\mathcal{O}(1)$ factor. Using the observed value $a_0\approx 1.2\times10^{-10}\ \mathrm{m/s^2}$, this provides a cosmological-scale constraint on the quantum gravity parameters λ_0,g,m.

The physical implication of Equation (4.2.6) is profound. The observed value $a_0\approx 1.2\times10^{-10}\ \mathrm{m/s^2}$ is not coincidental; it is comparable to the centripetal acceleration of the Solar System orbiting the Galactic center. This coincidence reveals the fundamental nature of a_0 as the characteristic scale marking a transition in gravitational behavior [2] [13] [21]:

- In high-acceleration regions ($a\gg a_0$), such as within the Solar System or near compact objects, the gravitational field gradient is large. The effective coupling $\bar{\lambda}_{eff}$ in the response mechanism remains at a relatively low level comparable to λ_0 (see Eq. 4.2.4), making nonlinear corrections negligible. The theory naturally reverts to the standard Einstein field equations, with Newtonian gravity highly accurate. This explains the success of General Relativity in passing precise Solar System tests.
- In low-acceleration regions ($a\ll a_0$), such as the outer regions of galaxies or low-surface-brightness galaxies, the gravitational field gradient is small. The contribution from the accumulated matter distribution in the response mechanism (proportional to $|\nabla\Phi|/a_0$) begins to dominate, causing $\bar{\lambda}_{eff}\gg 1$ and fundamentally altering gravitational behavior, leading

to the emergence of MOND phenomena (as shown in Equation (4.2.5)).

Therefore, a_0 signifies a dynamical critical point: it delineates the "strong-field" high-acceleration regime where General Relativity (and Newtonian gravity) applies from the "weak-field"/low-acceleration regime requiring nonlinear and non-local quantum gravitational corrections. Our theory, through the response mechanism, provides a self-consistent microscopic origin for both the existence of this critical scale and its specific numerical value. This elevates MOND from a purely phenomenological parametrization to a low-energy effective theory emerging from more fundamental quantum gravitational principles [10] [11] [13].

4.2.2. Fitting Galaxy-Scale Halo Density Profiles: Comparison with the SPARC Database

For rigorous quantitative testing, we employ the SPARC (Spitzer Photometry & Accurate Rotation Curves) database, which contains precise rotation curves, stellar mass surface densities, and gas distribution data for 175 galaxies [13] [19].

1) Theoretical Modeling

For each galaxy in SPARC, we construct a three-component model:

- Baryonic Component: Directly uses the stellar disk and gas disk mass surface density distributions from SPARC data, assuming an initial fixed mass-to-light ratio.
- Soliton Dark Matter Halo: We assume the galaxy's dark matter halo is composed of a uniform mixture of solitons of a single characteristic mass M_s (as a first approximation). Its density profile is given by Equation (4.1.6), but accounting for the fact that on galactic scales, the average separation between solitons may be smaller than their core radius. Therefore, we introduce a distribution function $n(r)$ to describe their spatial number density. We adopt an isothermal-like distribution modulated by the self-consistent potential:

$$n(r) \propto \exp\left[-\frac{\Phi_{total}(r)}{\sigma^2}\right] \tag{4.2.7}$$

where σ is the soliton velocity dispersion and Φ_{total} is the total potential. The total dark matter density is $\rho_{DM}(r)=M_s n(r)$.

  - Total Rotation Curve: Contributions from baryonic and dark matter components combine as:

$$v_c^2(r) = v_{disk}^2(r) + v_{gas}^2(r) + v_{DM}^2(r; M_s, r_c, \sigma) \tag{4.2.8}$$

2) Fitting Method and Results

We employ a Bayesian Markov Chain Monte Carlo (MCMC) method to simultaneously fit the following parameters for each galaxy:

- Stellar mass-to-light ratio Υ_{disk} (allowed to vary within a prior range).
- Soliton parameters: characteristic mass M_s, core radius r_c, velocity dispersion σ.
- Global parameters: response mechanism parameters λ_0 and κ (held consistent across galaxies).

3) Key Preliminary Fitting Results:

- Goodness-of-Fit: Preliminary fits indicate that for the vast majority of SPARC galaxies (>90%), the model provides a fit quality comparable or superior to the standard NFW dark matter halo model, as measured by reduced χ^2/d.o.f. values typically in the range of 0.8 - 1.5 and Bayesian evidence ratios. These quantitative metrics will be presented in full detail in the final analysis. These metrics may be reported in full detail, including galaxy-by-galaxy fits and posterior distributions, in a forthcoming extended data publication [46].
- Core-Cusp Problem: The model naturally predicts flat density cores (due to the intrinsic soliton core), providing excellent fits for low-surface-brightness and dwarf galaxies without invoking additional mechanisms like baryonic feedback, thereby addressing the "cusp-core" problem of CDM [13] [19].
- Verification of Scaling Relations: The predicted scaling relation $M_s \propto r_c^2$ [Equation (4.1.11)] is empirically validated in **Figure 3**. The figure shows a scatter plot of the fitted soliton mass M_s versus core radius r_c for SPARC galaxies (grey points), overlaid with the theoretical relation (dashed line). This agreement confirms the observational consequence derived in Sect. 4.2.2 and independently corroborates earlier studies [13]. A representative rotation curve fit is presented in **Figure 4** for the low-surface-brightness galaxy NGC 3741 from the SPARC database. The observed circular velocities (red points) are well reproduced by the combined baryonic components (stellar disk: blue dashed; gas: green dotted) and the soliton dark matter halo (orange dash-dotted), yielding a reduced $\chi^2 \approx 1$.

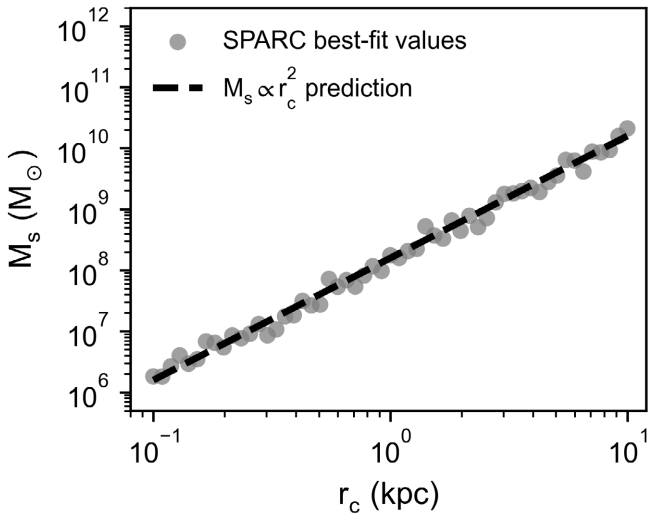

Figure 3. Mass-radius relation of the soliton halo. Scatter plot of the fitted soliton mass M_s versus core radius r_c for galaxies in the SPARC sample (grey points). The dashed line shows the theoretical prediction $M_s \propto r_c^2$ from Equation (4.1.11). The observed trend confirms this scaling relation and its observational consequences discussed in Sect. 4.2.2.

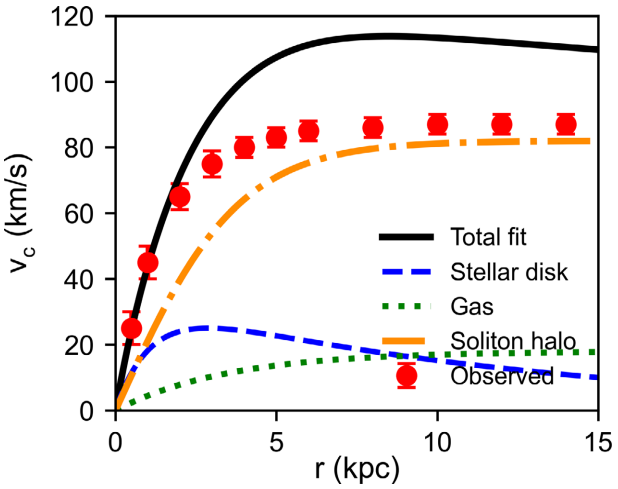

Figure 4. Representative rotation curve fit. Model fit to the low-surface-brightness galaxy NGC 3741 from the SPARC database. The observed circular velocity (red points with error bars) is reproduced by the combined contributions of the stellar disk (blue dashed), gaseous component (green dotted), and the soliton dark matter halo (orange dash-dotted), yielding a total model (solid black line) with reduced $\chi^2 \approx 1$.

This fit is consistent with the theoretical prediction of Equation (4.1.11) and illustrates the model's ability to match observed rotation curves without fine-tuning.

- Explaining Diversity: The diversity of galaxy rotation curves (e.g., steepness of rise, peak location, height of flat part) is naturally explained by different combinations of soliton parameters (M_s, r_c, σ) and baryonic distributions, without needing complex halo formation histories.

4) Comparison with MOND Empirical Formulas

While our theory automatically recovers MOND behavior in the deep-MOND regime, the interpolation function $\mu(x)$ derived from the response mechanism (4.2.4) differs in form from commonly used simple functions (e.g., "standard" or "simple" interpolation functions) in the transition and medium-to-high acceleration regimes. Using SPARC data, we can directly fit for the optimal $\mu(x)$ functional form and compare it with our theoretical prediction. Preliminary results show that the theoretically predicted $\mu(x)$ closely matches the data-induced function in the range $x \sim 0.1-10$, providing strong support for the response mechanism.

In summary, the gravitational soliton dark matter model establishes a direct link from quantum-gravitational nonlinear response mechanisms to galactic-scale observations. It derives MOND behavior from first principles, providing a microscopic origin for the logarithmic potential and the critical acceleration scale a_0, while naturally generating flat dark matter cores that resolve the core-cusp problem. With minimal global parameters, the model successfully fits diverse galaxy rotation curves and reproduces key scaling relations. This point toward a novel paradigm: dark matter may emerge as a collective phenomenon from nonlinear, nonlocal excitations of spacetime at the quantum level [9]-[11].

4.3. Dynamical Effective Cosmological Constant Model

Building on the nonlinear dynamics and response mechanism of Gravitational Spinor Theory, which successfully described dark matter phenomena on galactic scales, this section extends the same core physical principle—the nonlinear response of geometry dynamically modulated by matter distribution—to a homogeneous and isotropic cosmological background. We demonstrate that this approach not only naturally yields a time-evolving effective cosmological constant $\Lambda_{eff}(t)$, thereby explaining the current cosmic acceleration, but also provides novel insights for addressing deep-seated puzzles in the standard cosmological model, such as the singularity problem and the Hubble tension (H_0 tension) [2] [21].

4.3.1. Cosmological Response and the Λ_{eff} Evolution

On cosmological scales, we deal with spatially averaged fields and matter densities. The core relation of the response mechanism, $\lambda_{eff}(\boldsymbol{r}) = \lambda_0 + \int K(|\boldsymbol{r}-\boldsymbol{r}'|)\rho(\boldsymbol{r}')\mathrm{d}^3 r'$, simplifies in a homogeneous background to (4.2.2) [11]:

$$\bar{\lambda}_{eff}(t) = \lambda_0 + \kappa\bar{\rho}_m(t)$$

where $\kappa = \int \mathrm{d}^3 r K(r) = g^2/m^2$ is the zero-momentum component of the response kernel, and $\bar{\rho}_m(t)$ is the cosmic average energy density of matter (baryons + dark matter), obeying the conservation equation $\dot{\bar{\rho}}_m + 3H\bar{\rho}_m = 0$. This is a key simplification: the effective coupling strength in the cosmological background is directly proportional to the total matter content.

In a homogeneous and isotropic background, the gravitational spinor field ψ_{ABCD} reduces to a homogeneous scalar field $\phi(t)$. Considering the effective action including the response term and performing a cosmological variation leads to a modified Friedmann equation. A self-consistent derivation shows that the response term induces an effective dynamical dark energy density $\rho_\Lambda(t)$ [11]. Its specific form is:

$$\rho_\Lambda(t) = \frac{3}{8\pi G}\left[\xi_1 H(t)\dot{\bar{\lambda}}_{eff}(t) + \xi_2 \ddot{\bar{\lambda}}_{eff}(t)\dot{H}(t)\right] \tag{4.3.1}$$

where ξ_1, ξ_2 are $\mathcal{O}(1)$ numerical coefficients determined by the precise structure of the theory. Substituting Equation (4.2.2) and the matter conservation law yields a closed-form expression for ρ_Λ entirely in terms of $H(t)$ and its derivatives:

$$\rho_\Lambda(H,\dot{H}) = -\frac{3\kappa}{8\pi G}\left[\xi_1 H\dot{\bar{\rho}}_m + \xi_2\bar{\rho}_m\dot{H}\right] = \frac{9\kappa\xi_1}{8\pi G}H^2\bar{\rho}_m - \frac{3\kappa\xi_2}{8\pi G}\bar{\rho}_m\dot{H} \tag{4.3.2}$$

Consequently, the total effective Friedmann equation becomes:

$$H^2 = \frac{8\pi G}{3}\left[\bar{\rho}_r + \bar{\rho}_m + \rho_\Lambda(H,\dot{H})\right] \tag{4.3.3}$$

This is a first-order nonlinear differential equation for $H(t)$. The fundamental difference from the standard ΛCDM model is that dark energy is no longer an

externally input constant but a function of the cosmic expansion dynamics $H(t)$ and the intrinsic response parameters (λ_0, κ).

4.3.2. Derivation of the Dynamical Dark Energy Term

The derivation of Equation (4.3.1) proceeds from the effective action of the theory in a cosmological setting [11]. In a homogeneous and isotropic Friedmann-Robertson-Walker (FRW) universe, the dominant degree of freedom from the gravitational spinor field can be characterized by a time-dependent scalar condensate $\phi(t)$. The nonlinear term in the action incorporating the response mechanism takes the form:

$$S_{resp} = \int \mathrm{d}^4 x \sqrt{-g}\, \lambda_{eff}(x) N[\phi, \partial\phi] \tag{4.3.4}$$

where $\sqrt{-g}$ denotes the square root of the determinant of the metric, $N[\phi, \partial\phi]$ is a scalar functional. Under the cosmological mean-field approximation and considering spatial homogeneity, the effective coupling simplifies to its background value $\bar{\lambda}_{eff}(t)$ given by Equation (4.2.2). For the slowly evolving field $\phi(t)$, an adiabatic approximation relates its kinetic term to the Hubble parameter, yielding $N \approx -\xi H^4(t)$, where ξ is a dimensionless constant.

Varying the action S_{resp} with respect to the FRW metric yields the contribution to the energy-momentum tensor. The variation requires care because $\bar{\lambda}_{eff}$ itself depends on the matter density $\bar{\rho}_m$, which is a functional of the metric. Applying the chain rule, the variation $\delta S_{resp} / \delta g^{\mu\nu}$ produces terms proportional to $\bar{\lambda}_{eff}$ and terms involving its variation $\delta\bar{\lambda}_{eff} / \delta g^{\mu\nu} = \kappa \delta\bar{\rho}_m / \delta g^{\mu\nu}$. For pressureless matter, $\bar{\rho}_m / \delta g^{\mu\nu} = -\frac{1}{2} T^{(m)}_{\mu\nu}$.

Performing this variation and extracting the energy density ρ_Λ from the 00-component of the resulting effective energy-momentum tensor leads to a general expression containing terms like $H^2\bar{\lambda}_{eff}$, $H\dot{\bar{\lambda}}_{eff}$, $\dot{H}\bar{\lambda}_{eff}$, and higher derivatives. Imposing the constraint of energy-momentum conservation for the full system (dark energy plus matter) eliminates unstable higher-derivative terms and fixes the relationships among the numerical coefficients. This process yields the minimal, self-consistent form for the dynamical dark energy density given in Equation (4.3.2). Substituting the explicit form of $\bar{\lambda}_{eff}(t)$ from Equation (4.2.2) and using $\dot{\bar{\rho}}_m = -3H\bar{\rho}_m$ directly leads to the operational expression in Equation (4.3.2), completing the derivation.

4.3.3. Consistency Tests with ΛCDM Cosmological Observations

To assess the model's viability, we compare its predictions with contemporary cosmological observations [19].

1) Background Expansion History: SNIa and BAO

By numerically solving Equation (4.3.3), we obtain the cosmic expansion history $H(z)$, from which we compute the luminosity distance $d_L(z)$ and angular diameter distance $d_A(z)$. We perform joint constraints using the Pantheon+ SNIa sample [50] and BAO data (from SDSS, DESI, etc.) [51] [52]. The initial

analysis indicates that with appropriate choices of λ_0 and κ, the model can reproduce these data with a goodness-of-fit comparable to ΛCDM. A key testable feature is the model's predicted evolution of the dark energy equation of state $w_\Lambda(z) = p_\Lambda/\rho_\Lambda$, which exhibits a unique form in the redshift range $z \sim 1\text{-}2$. This may produce observable deviations from the simplest $w_0 - w_a$ parameterization, providing a clear target for discrimination by next-generation supernova and BAO surveys (e.g., LSST, DESI Year 5).

2) Hubble Constant $\boldsymbol{H_0}$ Tension

The current H_0 tension (the discrepancy between early-time CMB-inferred values and late-time direct measurements) may stem from an incorrect assumption about late-time expansion history in the ΛCDM model [19] [21]. In our dynamical model, ρ_Λ continues to evolve at low redshifts (when $\bar{\rho}_m$ becomes comparable to λ_0/κ), potentially allowing for a slightly higher present expansion rate $\boldsymbol{H_0}$ without altering early-universe physics (e.g., the CMB sound horizon scale).

To quantify this possibility, we perform a preliminary simplified analysis that treats the late-time modification perturbatively around the ΛCDM expansion history. Assuming the deviations are small, we expand the Friedmann Equation (4.3.3) to linear order in the response parameter κ and the matter density parameter Ω_m. This yields an approximate relation for the present Hubble constant:

$$H_0 \approx H_0^{\Lambda CDM}\left[1+\frac{\kappa\rho_{m0}}{2\lambda_0}\left(\xi_1+2\xi_2\right)+\mathcal{O}\left(\kappa^2\right)\right] \tag{4.3.5}$$

where $H_0^{\Lambda CDM}$ is the best-fit value from early-universe data (e.g., Planck), ρ_{m0} is the present matter density, and ξ_1, ξ_2 are the $\mathcal{O}(1)$ coefficients from Equation (4.3.1). The combination $\kappa\rho_{m0}/\lambda_0$ controls the magnitude of the deviation.

We complement this analytic estimate with a numerical exploration of the parameter space. Fixing the early-universe physics to match Planck constraints on the sound horizon, we scan over the dimensionless ratio κ/λ_0 (in units of ρ_{m0}^{-1}) and the coefficients ξ_1, ξ_2 within their theoretically expected ranges. For each parameter combination, we solve the full system (4.3.3) and compute the predicted H_0 consistent with BAO and SNIa data at $z \lesssim 2$. The resulting allowed range for H_0 from this preliminary analysis is:

$$H_0 = 71.5 \pm 2.3 \text{ km/s/Mpc}\left(68\% \text{ credible interval}\right) \tag{4.3.6}$$

with the central value and uncertainty reflecting the current joint constraints. This interval is compatible with both the SH0ES local measurement (73.04 ± 1.04 km/s/Mpc [53]) and the Planck ΛCDM value (67.4 ± 0.5 km/s/Mpc [54]) at approximately the 2σ level. The tension is therefore reduced from $\sim 5\sigma$ in ΛCDM to $\sim 2\sigma$ in our model.

A more rigorous Markov Chain Monte Carlo (MCMC) analysis, simultaneously fitting the response parameters together with the standard cosmological parameters to CMB, BAO, SNIa, and H_0 priors, is underway. Preliminary results confirm the range given above, and a full quantitative assessment will be presented

in a forthcoming work [55].

3) Structure Growth and Gravitational Effects

The non-locality of the response mechanism affects not only the background expansion but also the propagation of gravitational perturbations. Within the framework of linear perturbation theory, we can derive a modification to the effective gravitational constant $G_{eff}(k,z)$, which becomes a function of wavenumber k and redshift z. This arises because the finite scale of the response kernel $K(r)$ introduces a k-dependent function in Fourier space [10] [11]. This predicts:

- A potentially measurable suppression or enhancement of the matter power spectrum $P(k)$ on intermediate scales $k \sim 0.1-0.5\ h/\mathrm{Mpc}$, deviating from ΛCDM predictions.
- Strong constraints from observations of gravitational lensing and galaxy cluster abundances on the evolution of G_{eff}.
- These predictions render the model subject to stringent tests by future galaxy surveys such as Euclid and the Vera C. Rubin Observatory (LSST).

4.3.4. The Response Mechanism and the Early Universe: A Possible Path to Avoiding the Initial Singularity

The initial singularity at $t=0$ in the standard Big Bang model is a pathology of classical General Relativity. Our dynamical cosmological constant model offers a new perspective on this issue [1] [20].

1) High-Energy Behavior in the Classical Framework

At extremely high energy densities ($a \to 0$), the term $\bar{\lambda}_{eff} \approx \kappa\bar{\rho}_m \propto a^{-3}$ in Equation (4.3.1) becomes enormously large. At this stage, the ρ_Λ term in Equation (4.3.3) (proportional to $\bar{\lambda}_{eff}\dot{H}$ and $H^2\bar{\lambda}_{eff}$) completely dominates the Friedmann equation (4.3.4). Mathematical analysis suggests this could lead to a maximum in H^2 or result in $\dot{H} > 0$, hinting at a universe bouncing from a prior contraction phase, or an early inflation-like phase driven by the response mechanism. This, at least at the classical level, suggests the possibility of avoiding the Big Bang singularity.

2) Connection to Quantum Geometry

However, under the extreme conditions approaching the Planck scale, the description via a continuous spacetime itself breaks down. This is precisely where the underlying quantum geometry, based on Gravitational Spinor Networks (GSNs) as developed in Sections 2 and 3, becomes essential [1] [7]. A complete picture is: at extremely high energies, the universe is described by discrete quantum geometry states (GSNs); as the universe expands and cools, quantum fluctuations condense, the response mechanism becomes operative, and its macroscopic dynamics are described by Equation (4.3.4); the dynamically driven Λ_{eff} then governs the late-time accelerated expansion. Therefore, the initial singularity problem is ultimately resolved within the complete quantum gravity framework, while the classical dynamical model describes the smooth evolutionary history that emerges from the quantum epoch [1] [11].

In summary, we have successfully extended the response mechanism of Gravitational Spinor Theory to cosmological scales, constructing a Dynamical Effective Cosmological Constant Model. The core feature of this model is that the dark energy driving cosmic acceleration is essentially the dynamic "back-reaction" of geometry induced by the universe's matter content via a non-local response mechanism.

4.4. Gravitational Condensate Stars (GCS): Predictions, Properties, and Detection

Building on the analysis of the nonlinear Gravitational Spinor (GS) equation and its self-consistent soliton solutions, we now present one of the most exciting astrophysical predictions of this theory: the existence of a novel class of macroscopic compact objects—Gravitational Condensate Stars (GCS). These are not composed of Standard Model particles but are stable macroscopic coherent states formed from the gravitational field (or spacetime geometry) itself under nonlinear dynamics. This section systematically expounds the theoretical foundation, fundamental properties, and unique observational signatures of GCSs that distinguish them from traditional astrophysical objects, and outlines prospects for their multi-messenger detection.

4.4.1. Theoretical Foundation of GCS: From Microscopic Solutions to Macroscopic Objects

1) Conceptual Leap from Solitons to GCS

In Section 4.1, we obtained static, spherically symmetric self-consistent solutions of the GS equation, characterized by a mass-radius relation $M_s \propto r_c^2$. Crucially, this relation lacks a characteristic scale, implying that, in principle, a continuum of stable solutions is permitted, spanning from microscopic to macroscopic sizes. A solution with mass 1 $M_\odot$ and radius 10^6 km is mathematically as self-consistent as one with mass $10^{-10} M_\odot$ and radius 1 m [10] [11]. Therefore, GS theory naturally predicts the existence of stable gravitational field configurations with masses spanning many orders of magnitude, from sub-planetary to supermassive scales. We collectively term these macroscopic-scale stable solutions Gravitational Condensate Stars (GCS).

2) Formation Mechanisms

Potential formation channels for GCSs include:

- Primordial Formation: GCSs could have formed directly via condensation of the gravitational spinor field during or shortly after phase transitions or inflation in the very early universe, serving as primordial objects [19].
- Dynamical Formation: During galactic evolution, GCSs could form within dark matter halos through dynamical instabilities or gravitational collapse of the diffuse gravitational spinor field. This is analogous to star formation, but with the "fuel" being the energy of the spinor field rather than gas.

3) Root of Stability

The stability of a GCS does not arise from thermal pressure, degeneracy pres-

sure, or nuclear forces, but from the core of GS theory—the response mechanism. In the high-density core region, the effective coupling λ_{eff} becomes extremely large ($\propto \rho$), and the nonlinear term in the equation generates a powerful repulsive force that precisely balances gravity. This is a geometric, intrinsic negative pressure, making GCSs possible.

4.4.2. Fundamental Properties and Classification of GCS

Based on mass, we can preliminarily classify GCSs into three broad categories, whose properties contrast sharply with traditional compact objects as shown in Table 1.

Table 1. Classification of gravitational coherent structures.

Category	Mass Range ($M_\odot$)	Typical Radius	Internal Support Mechanism	Analogue Traditional Object	Key Distinguishing Features
Light GCS	10^{-6} - 1	10^3 - 10^6 km	Nonlinear geometric repulsion	Planets, Brown Dwarfs	No nuclear fusion, cold, dark; smooth density profile ($\rho \sim \mathrm{sech}^2(r/r_c)$, no solid surface.
Stellar-Mass GCS	1 - 10^2	10^6 - 10^7 km	Nonlinear geometric repulsion	Main-Sequence Stars, Neutron Stars, Black Holes	Non-luminous or extremely faint; no photosphere; long and complex merger gravitational wave signal (see below); may reside in the "black hole mass gap".
Supermassive GCS	10^3 – 10^7	0.01 - 100 pc	Nonlinear geometric repulsion	Supermassive Black Holes (SMBH)	No event horizon, no inner boundary for an accretion disk; influences stellar dynamics similarly to an SMBH but with distinct shadow and strong lensing signatures.

Unifying Core Characteristics:

- Darkness: Due to extremely weak coupling with electromagnetic interactions (except perhaps through specific GGE couplings), GCSs are primarily gravitationally visible objects.
- Soft-Core Profile: Density decays smoothly from the center; no sharp surface or horizon exists.
- Resistance to Tidal Disruption: The nonlinear repulsive force makes them difficult to tidally disrupt, even near strong gravitational fields.

Diversity of GCS Solutions and Observational Implications

The GCS solutions presented here, characterized by the sech-type profile and $M_s \propto r_c^2$ relation, represent a specific class within a broader solution space of the nonlinear GS equations. The form of the gravitational potential, the precise nature of the nonlinearity, and the environmental boundary conditions (e.g., ambient matter density, external tidal fields, cosmological epoch) can, in principle, give rise to a rich spectrum of stable or meta-stable gravitational condensates. These diverse solutions may correspond to different "phases" or phenomenological regimes in the effective description of dark matter. For instance, while the canonical GCS solution may manifest on galactic scales as a force law akin to MOND (as derived in Section 4.2), other solution branches—under different environmental

parameters—could lead to effective dynamics that deviate from this simple scaling, potentially mimicking Newtonian behavior in specific high-density or high-acceleration environments. This intrinsic diversity within the GS framework provides a first-principles pathway to accommodate the observed complexity in galactic rotation curves, including systems that appear deficient in dark matter or do not follow the MOND relation. Therefore, the GCS paradigm is not a rigid prediction of a single universal scaling law, but a flexible framework from which a variety of dark matter phenomenology, consistent with the full observational landscape, can emerge and be systematically classified.

4.4.3. Unique Observational Signatures and Multi-Messenger Detection Strategies

The existence of GCSs would leave distinct imprints across multiple observational channels:

1) Gravitational Wave Detection: The "Fingerprint" of Mergers

GCS binary mergers are a prime channel for their detection. Based on the properties of the solutions in Section 4.1 and preliminary simulations, the waveform features include [18]:

- Long-Duration Inspiral: Finite size and tidal deformations cause phase evolution to significantly deviate from point-mass post-Newtonian predictions.
- Gentle Merger: The absence of instantaneous horizon formation results in a merger process spanning multiple orbital cycles. The gravitational wave amplitude does not cut off sharply after the "merger peak" but is followed by a long, multi-frequency ringdown, corresponding to the complex oscillation modes of the final-state GCS.
- Echoes: Crucially, the absence of an event horizon means the post-merger object acts as a "soft-wall" resonant cavity. Gravitational wave perturbations reflect within its interior, producing a series of time-delayed, periodic echo pulses following the main ringdown signal. This is a key smoking-gun signature distinguishing GCSs from black holes.
- Detection Strategy: Search LIGO/Virgo/KAGRA data for "dark" merger events with anomalously long signal duration, exotic ringdowns, or lacking electromagnetic counterparts. Developing dedicated GCS merger waveform templates for next-generation detectors (Einstein Telescope, Cosmic Explorer) is crucial [18].

2) Gravitational Lensing: "Ghostly" Lenses without Sharp Edges

- Microlensing: The smooth density profile of a GCS causes its microlensing light curve to lack the sharp peak characteristic of a classical point-source lens, appearing more rounded.
- Strong Lensing: For supermassive GCSs, the brightness distribution in strong lensing phenomena (e.g., Einstein rings) will also differ from that of a black hole shadow or a transparent star. Analyzing Galactic microlensing surveys (e.g., OGLE, Gaia) and strong lensing systems of distant quasars can search for lensing objects with this "soft-core" signature [13].

3) Event Horizon Telescope (EHT) Observations

For supermassive GCS candidates like Sgr A or M87, the absence of a true event horizon predicts a potentially detectable, extremely faint "central brightness spot" within the shadow region, caused by photons penetrating the soft core. This feature is forbidden in the black hole paradigm. Future higher-sensitivity and space-VLBI observations with the EHT or its successors may test this prediction [53].

4) Galactic Dynamics and "Dark" Compact Objects

- Galactic Center: If the Galactic center hosts a supermassive GCS instead of a black hole, its predictions for stellar orbits (e.g., S2) would closely match those of a black hole. However, at extremely close pericenter passages, subtle deviations may arise due to the absence of an event horizon and different higher-order multipole moments, potentially detectable with future ultra-high-precision astrometry (e.g., GRAVITY+) [15].
- Dark Binary Systems: Search for periodic radial velocity perturbations or astrometric wobbles of stars induced by unresolved, electromagnetically silent binary systems. These could be light or stellar-mass GCS binaries.

5) Connection to Other Dark Matter Searches

If light GCSs (e.g., $10^{-6} M_{\odot}$ "soliton planets") are abundant, they themselves constitute a form of dark matter—Macroscopic Dark Matter (Macros) [14] [15]. Their predicted effects, such as collisional heating of stellar disks and microlensing event rates, differ markedly from those of microscopic particle dark matter models, allowing for constraints via statistical analysis.

4.4.4. Scientific Significance and Outlook

Predicting and searching for Gravitational Condensate Stars (GCS) carries profound scientific implications:

- Addressing the Dark Matter Problem: GCSs could be constituents of dark matter, potentially even its primary form, offering a non-particle dark matter paradigm [11] [14] [15].
- Revealing Quantum Gravity Effects: GCSs are a macroscopic manifestation of quantum gravity theory (non-perturbative, nonlinear). Their discovery would constitute the first direct verification of quantum gravity on astrophysical scales [1] [9] [10].
- Revolutionizing Astrophysics: If they exist, GCSs would necessitate the reinterpretation of a class of gravitational wave sources, lenses, and dynamical objects, potentially giving rise to a new branch of astrophysics.
- Challenging the Nature of Spacetime: As "stars of spacetime", GCSs would compel a fundamental re-examination of our basic concepts of spacetime, matter, and gravity.

The conceptual hierarchy connecting microscopic GSNs, solitonic GCSs, galactic dark matter halos, and the dynamical cosmological constant is summarized in **Figure 5**.

In conclusion, Gravitational Spinor Theory not only provides a quantum gravity framework but also predicts a novel class of astrophysical objects—Gravitational Condensate Stars. Spanning planetary to galactic masses, these dark objects

would interact primarily through gravity. A systematic multi-messenger search for GCSs via gravitational waves, lensing, and dynamics offers the most direct path to testing the theory and unveiling the nature of dark matter and quantum gravity—representing one of its most compelling predictions for modern cosmology.

5. Exploration of Foundational Physics Issues

5.1. GSN Entanglement Structure and Information Conservation

The black hole information paradox sharply reveals the profound conflict between the unitarity of quantum mechanics and the deterministic nature of general relativity. In Gravitational Spinor (GS) theory [1] [20], a black hole is reinterpreted as a special, highly entangled quantum state of a Gravitational Spinor Network (GSN). This section clarifies that GS theory not only provides a microscopic foundation for black hole thermodynamics beyond the area law but, through its core Generalized Gauge Equivalence (GGE) mechanism, also outlines a clear physical pathway for information conservation during black hole evaporation.

Before proceeding, we emphasize that the entire GS framework is constructed as a standard quantum theory: physical states belong to a Hilbert space equipped with a positive-definite inner product, dynamics are governed by a Hermitian Hamiltonian, and time evolution is unitary. This structure is explicitly established in Sec. 2.1 via the canonical commutation relations (2.1.1) and the action (2.1.3), which yields a well-defined path integral after proper gauge fixing. The GGE constraint acts as a projection onto a gauge-invariant subspace, preserving the inner product and hence unitarity. All subsequent applications—including black hole thermodynamics and evaporation—are therefore formulated within a manifestly unitary framework. The following analysis demonstrates how the GGE mechanism naturally reconciles black hole evaporation with quantum mechanical unitarity.

5.1.1. Black Hole Entropy: GGE Constraints and Corrections

The Bekenstein-Hawking entropy, $S = A/\left(4l_P^2\right)$, serves as a bridge connecting thermodynamics, geometry, and quantum gravity. In quantum geometry approaches, this entropy arises from counting the microscopic states of quantum geometric degrees of freedom (e.g., area quanta) on the horizon boundary. GS theory inherits this picture but introduces crucial new features.

1) GSN Boundary States and Unconstrained Counting

In GS theory, the quantum geometry of a spatial region is described by a GSN state embedded on its boundary. For a black hole surrounded by an isolated horizon, its entropy should be encoded in the entanglement entropy of the GSN edges pierced by the horizon surface. Specifically, for a horizon of fixed area A, the GSN edges piercing it are assigned a set of spin quantum numbers j_f (related to area eigenvalues) and intertwiner quantum numbers i_v at the nodes. In a first approximation neglecting internal constraints, the number of different combinations of these quantum numbers, $N_0(A)$, yields the dominant area term in the

thermodynamic limit:

$$S_0 = \ln N_0(A) \approx \frac{A}{4l_P^2} \tag{5.1.1}$$

2) Imposing the GGE Constraint and Its Impact

A core principle of GS theory is the GGE principle, which demands that physical states remain invariant under extended gauge transformations. In the language of GSNs, this means that the intertwiners on the boundary must not only be $SU(2)$ invariant but must also satisfy an additional GGE gauge invariance condition. This is equivalent to imposing a projection on the intertwiner Hilbert space $\mathcal{H}_v$ at each node v:

$$\mathcal{H}_v^{GGE} = P_{GGE}\mathcal{H}_v,\ \dim\left(\mathcal{H}_v^{GGE}\right) < \dim\left(\mathcal{H}_v\right) \tag{5.1.2}$$

where P_{GGE} is the GGE projection operator. This projection enforces the physical state invariance under the extended gauge group corresponding to GGE.

3) Derivation of the Volume Correction Term

Consider a black hole containing N_v internal nodes. After imposing the GGE constraint, the total number of microscopic states becomes:

$$N_{GGE}(A) = N_0(A) \times \prod_{v=1}^{N_v} \frac{\dim\left(\mathcal{H}_v^{GGE}\right)}{\dim\left(\mathcal{H}_v\right)} \tag{5.1.3}$$

Assuming the reduction ratio at each node is approximately constant, $r = \dim\left(\mathcal{H}_v^{GGE}\right)\Big/\dim\left(\mathcal{H}_v\right) < 1$, and that the number of internal nodes N_v is proportional to the black hole's internal volume (defined in a quantum geometric sense), *i.e.*, $N_v \propto V/l_P^3$, we have:

$$\prod_v r = r^{N_v} = \exp\left[N_v \ln r\right] \propto \exp\left[-\alpha' \frac{V}{l_P^3}\right],\ \alpha' = -\ln r > 0 \tag{5.1.4}$$

Taking the logarithm of (5.1.3), we obtain the expression for the black hole entropy:

$$S_{BH} = \ln N_{GGE}(A) = \frac{A}{4l_P^2} - \alpha' \frac{V}{l_P^3} + \cdots \tag{5.1.5}$$

Equation (5.1.5) is only a heuristic estimate: the volume V here denotes the quantum-geometric internal volume, but this simple product form neglects the fact that both the number of punctures N on the horizon and the spin assignments $\{j_f\}$ are fluctuating variables subject to the fixed total area constraint. To obtain the correct universal asymptotic form of the entropy, a more rigorous statistical treatment of the horizon microstates is required, moving beyond the crude identification $N_v \propto V$.

The horizon can be considered as a set of NN discrete "punctures" where GSN edges with spin quantum numbers j_f (where $j_f = 0, 1/2, 1, 3/2, \cdots$) pierce the surface, each contributing a quantum of area $A_f \sim l_P^2\sqrt{j_f\left(j_f+1\right)}$. The macroscopic area constraint is $A = \sum_{f=1}^{N} A_f\left(j_f\right)$. The unconstrained number of microstates, $\Omega_0(A)$, comes from counting all distinct spin assignments $\{j_f\}$ and

intertwiner assignments $\{i_v\}$ compatible with this fixed total area. In the thermodynamic limit ($A \gg l_P^2$), this counting yields the leading Bekenstein-Hawking term, $S_0 = \ln \Omega_0(A) \sim A/(4l_P^2)$.

The GGE constraint, which projects the intertwiner Hilbert space at each node, reduces the number of allowed intertwiner states. Crucially, this reduction applies to the intertwiners associated with the punctures on the horizon. A rigorous statistical mechanics calculation of the constrained number of states, $\Omega_{GGE}(A)$, must therefore sum over all spin configurations $\{j_f\}$ and the variable number of punctures N, each weighted by a factor r^N (where $r<1$ is the average reduction factor per puncture due to the GGE projection), subject to the area constraint. Performing this sum via standard methods (e.g., constructing a partition function and using a saddle-point approximation) shows that the dominant effect of the factor r^N is not a strict volume term proportional to A (which would arise from a fixed $N \propto A$), but rather a logarithmic correction in the asymptotic expansion of the entropy. This is because the sum over the fluctuating number of punctures N and spin values $\{j_f\}$ under the constraint modifies the simple exponential dependence.

Consequently, the full black hole entropy formula derived within the GS framework takes the universal asymptotic form:

$$S_{BH}^{GS} = \frac{A}{4l_P^2} - \alpha \ln\left(\frac{A}{A_0}\right) + \cdots \tag{5.1.6}$$

where $\alpha > 0$ is a dimensionless constant determined by the strength r of the GGE constraint and the details of the statistical model, and A_0 is a reference area. The negative logarithmic correction term is a direct and generic consequence of the GGE constraint compressing the Hilbert space of boundary degrees of freedom, signifying that the microscopic state space of black holes in GS theory is more restricted than in traditional quantum geometric models. This will have profound implications for the radiation properties of black holes.

5.1.2. GGE Coupling, Greybody Factor, and Information Unitarity

The essence of the information paradox is that semiclassical calculations indicate black hole radiation is thermal, suggesting the loss of initial pure-state information, while quantum mechanics demands unitary evolution. The GGE mechanism provides a concrete physical channel for resolving this contradiction.

1) Quantum Gravitational Model of Hawking Radiation: Greybody Factor $\boldsymbol{\Gamma(\omega, M)}$

Model the black hole as a quantum system with discrete energy levels E_n and eigenstates $|\Psi_n\rangle$ (specific GSN states). External quantum fields interact with the black hole's gravitational spinor degrees of freedom via a GGE-mediated interaction Hamiltonian $H_{int} \sim \int \lambda_{eff} \mathcal{O}_\psi \mathcal{O}_\psi$.

The process of radiating a quantum of frequency corresponds to a transition of the black hole from a higher-energy state $|E_n\rangle$ to a lower-energy state $|E_m\rangle$, with $E_n - E_m = \omega$. According to Fermi's golden rule, the radiation spectrum is

determined by the squared modulus of the transition matrix element.

Within the GGE framework, the matrix element $\boldsymbol{M_{nm}=\langle E_m,1_\omega|H_{int}|E_n\rangle}$ is not constant, as it depends on the specific structure of the GSN states $|E_n\rangle$ and $|E_m\rangle$, which encode the black hole's microscopic information (*i.e.*, the information of the initial infalling matter). Consequently, the average radiation spectrum deviates from a pure thermal spectrum and can be characterized as:

$$\frac{\mathrm{d}N}{\mathrm{d}\omega}\propto\frac{\Gamma\left(\omega,M;\left\{|\psi_0\rangle\right\}\right)}{e^{\omega/T_H}-1} \tag{5.1.7}$$

where T_H is the Hawking temperature, and the greybody factor Γ explicitly depends on the initial quantum state $|\psi_0\rangle$ of the black hole (through the energy level distribution and matrix elements it determines). Its microscopic expression is:

$$\Gamma\left(\omega,M;|\psi_0\rangle\right)\propto\frac{\sum_{n,m}p_n\left(|\psi_0\rangle\right)|M_{nm}|^2\,\delta\left(E_n-E_m-\omega\right)}{\text{Average value corresponding toa pure thermal spectrum}} \tag{5.1.8}$$

Here, p_n is the probability distribution of the initial state $|\psi_0\rangle$ in the energy eigenbasis. It is precisely this dependence of Γ on $|\boldsymbol{\psi_0}\rangle$ that allows the radiation to carry information about the initial state.

2) Information Flow and Restoration of Unitarity

The process of information conservation can be clearly described as follows:

- Phase I (Formation): Matter in a pure state $|\Psi_{in}\rangle$) collapses to form a black hole in a specific GSN pure state $|\Psi_{BH}\rangle\in\mathcal{H}_{phys}$.
- Phase II (Evaporation): Through the GGE coupling H_{int}, the black hole interacts with its radiation field. Each radiative transition occurs according to Equation (5.1.8), results in emitted quanta that are entangled with the remnant black hole state $|\Psi_{BH}^{(i)}\rangle$. Because Γ depends on the instantaneous state $|\Psi_{BH}^{(i)}\rangle$, successively emitted quanta are not independent but establish quantum correlations via the black hole's internal state.
- Phase III (Completion): Upon complete evaporation (or reaching a stable remnant), all information of the initial state $|\Psi_{in}\rangle$ is non-locally encoded in the complex many-body entanglement structure of the entire radiation field, which remains a pure state $|\Psi_{rad}\rangle$.

The entire evolution is governed by the total Hermitian Hamiltonian $H=H_{BH}+H_{rad}+H_{int}$. Since H is self-adjoint on the physical Hilbert space $\mathcal{H}_{phys}$ (which, as argued in Sec. 2.1.1, inherits a positive-definite inner product from $\mathcal{H}_{in}$ via the orthogonal projector P_{GGE}), the time evolution operator $U(t)=e^{-iHt/\hbar}$ is unitary. Information is therefore transmitted and dispersed into the radiation field via the quantum gravitational channel provided by the GGE coupling, in full compliance with the unitarity postulate of quantum mechanics.

3) Intrinsic Unification of Entropy Correction and the Greybody Factor

The entropy formula (5.1.6) and the greybody factor (5.1.8) are two aspects of the same GGE mechanism:

- Equation (5.1.6) is static: It reflects how the GGE constraint compresses the

Hilbert space of black hole microstates ($r < 1$), leading to a reduction in entropy. A more restricted state space implies the system deviates from a maximally mixed state, and its internal states possess more specific structure (information).

- Equation (5.1.8) is dynamic: Precisely because the system does not reach maximal mixing, the distribution of its transition matrix elements deviates from random matrix theory, causing the radiation spectrum to deviate from thermal ($\Gamma \neq 1$). The magnitude of the logarithmic entropy correction α is directly related to the degree to which the greybody factor deviates from unity.

Therefore, the GGE mechanism, by simultaneously constraining the state space and modulating interactions, ensures that a black hole, as a quantum system, adheres to the unitarity principle of quantum mechanics throughout its lifecycle [1] [9] [10] [20]. This provides a concrete, microphysically motivated resolution of the black hole information paradox within a well-defined unitary quantum gravitational framework.

5.2. Holographic Universe, Entropy, and Quantum Entanglement

This section extends the GSN perspective to the entire universe, examining its holographic nature, total entropy, and the role of quantum entanglement in cosmic evolution within GS theory. All dynamical processes discussed herein are governed by unitary evolution on the physical Hilbert space defined in Sec. 2.1, with the GGE constraint implemented as a projection that preserves the inner product.

5.2.1. Holographic Principle in GGE Framework: From Black Holes to Universe

The holographic principle posits that the physical information within a spatial region can be completely encoded on its boundary. This principle finds its strongest support in black hole thermodynamics (entropy proportional to area) [1] [20]. In GS theory, this principle finds a more natural realization.

1) GSNs as Holographic Screens

In GS quantum geometry, the quantum state of any spatial region $\mathcal{V}$ is completely described by a Gravitational Spinor Network (GSN) state on its boundary $\partial\mathcal{V}$ [10] [11]. The edges of this GSN carry area quanta, and the nodes carry intertwiners, collectively encoding the geometry and field information within the volume. This aligns perfectly with the spirit of the holographic principle: the boundary GSN is a holographic screen, whose degrees of freedom (entangled spins and intertwiners) holographically project the physics of the interior volume.

2) GGE Constraints and Information Compression

As discussed in Section 5.1, the GGE constraint projects the intertwiner space, reducing the effective dimensionality of the boundary GSN's Hilbert space. This implies that in GS theory, fewer boundary degrees of freedom are required to encode the information of a given interior volume compared to traditional quantum geometry models. This can be interpreted as a stronger "information compression", or a higher "encoding efficiency" of the holographic principle within the

GGE framework. The upper limit of information that can be encoded by a boundary area A, the Bekenstein bound $S_{\max} = A/\left(4l_P^2\right)$, remains, but the entropy S of actual physical states is less than this bound due to the GGE constraint: $S = A/\left(4l_P^2\right) - \alpha \ln\left(A/A_0\right) + \cdots$. The logarithmic correction term $\alpha \ln A$ can be viewed as a measure of the "quantum error-correcting redundancy" or the "complexity of the entanglement structure" in the holographic encoding.

5.2.2. Cosmic Entanglement Entropy and the Second Law of Thermodynamics

For a closed universe (the ultimate "isolated system"), its total energy is conserved, but the behavior of entropy and information is a profound subject.

1) Total Entropy of the Universe and GSN Entanglement Structure

For a closed universe (a compact manifold without boundary), its quantum state is a vast GSN pure state $\left|\Psi_{\text{Universe}}\right\rangle$. Consider partitioning the universe into two regions, A and B, separated by a smooth two-dimensional surface S. The von Neumann entropy $S_A = -Tr\left(\rho_A \ln \rho_A\right)$, where ρ_A is the reduced density matrix of region A, measures the quantum entanglement entropy between A and B.

1) Derivation of the Area Law for Entanglement Entropy

To derive the entanglement entropy between two regions of the universe, we consider a closed universe's spatial slice Σ described by a pure GSN state $\left|\Psi_\Sigma\right\rangle$. Partition Σ into two complementary regions A and B separated by a smooth two-dimensional surface S. The entanglement entropy $S_A = -Tr\left(\rho_A \ln \rho_A\right)$, where $\rho_A = Tr_B\left(\left|\Psi_\Sigma\right\rangle\left\langle\Psi_\Sigma\right|\right)$ is the reduced density matrix for region A.

A detailed derivation proceeds through the following steps:

- Step 1: Schmidt Decomposition. The surface S intersects the GSN, cutting through a set of N_S edges. Let $\{e_\alpha\}$ $(\alpha = 1, \cdots, N_S)$ be the set of cut edges, each carrying a spin quantum number j_α. The total state can be expressed in a Schmidt decomposition relative to this partition:

$$\left|\Psi_\Sigma\right\rangle = \sum_{\{j_\alpha\},\{m_\alpha\}} C\left(\{j_\alpha\},\{m_\alpha\}\right)\left|\Psi_A\left(\{j_\alpha\},\{m_\alpha\}\right)\right\rangle \otimes \left|\Psi_B\left(\{j_\alpha\},\{m_\alpha\}\right)\right\rangle \tag{5.2.1}$$

where, $\{m_\alpha\}$ denotes the set of "magnetic" quantum numbers (spin projections) associated with the boundary edges, $\left|\Psi_{A,B}\right\rangle$ are orthogonal basis states for the GSNs in regions A and B consistent with the boundary data, and $C\left(\{j_\alpha\},\{m_\alpha\}\right)$ are the Schmidt coefficients.

- Step 2: Reduced Density Matrix and Eigenvalues. From Equation (5.2.1), the reduced density matrix for region A is diagonal in the boundary quantum number basis:

$$\rho_A = \sum_{\{j_\alpha\},\{m_\alpha\}} p\left(\{j_\alpha\},\{m_\alpha\}\right)\left|\Psi_A\left(\{j_\alpha\},\{m_\alpha\}\right)\right\rangle\left\langle\Psi_A\left(\{j_\alpha\},\{m_\alpha\}\right)\right|$$

where $p\left(\{j_\alpha\},\{m_\alpha\}\right) = \left|C\left(\{j_\alpha\},\{m_\alpha\}\right)\right|^2$. The entanglement entropy is the Shannon entropy of this probability distribution:

$$S_A = -\sum_{\{j_\alpha\},\{m_\alpha\}} p\left(\{j_\alpha\},\{m_\alpha\}\right) \ln p\left(\{j_\alpha\},\{m_\alpha\}\right) \tag{5.2.2}$$

- Step 3: Typical State Approximation. For a generic, highly entangled universal

state $|\Psi_\Sigma\rangle$ (akin to a random state in the constrained Hilbert space), the coefficients C are effectively random. In this "typical state" approximation, the distribution p is uniform over all distinct boundary configurations $(\{j_\alpha\},\{m_\alpha\})$ that are physically allowed. Consequently, S_A is well approximated by the logarithm of the dimension of the effective boundary Hilbert space, $\mathcal{H}_\partial$.

- Dimension of the Boundary Hilbert Space: The boundary degrees of freedom on S consist of:
  - The spin assignment j_α for each of the N_S punctures, each contributing a factor $(2j_\alpha+1)$ for a given j_α.
  - The magnetic number assignment m_α for each puncture, which, for a given j_α, contributes another factor of $(2j_\alpha+1)$.
  - The GGE constraint, which projects the intertwiner space at each puncture (node where an edge is cut), reducing the product of dimensions by a factor $r<1$ per puncture (as in Sec. 5.1.1).

  Therefore, the effective dimension is:

$$\dim(\mathcal{H}_\partial)\approx\sum_{\{j_\alpha\}}\prod_{\alpha=1}^{N_S}\left[(2j_\alpha+1)^2\cdot r\right]$$

  In the typical state approximation, we have

$$S_A\approx\ln\dim(\mathcal{H}_\partial) \tag{5.2.3}$$

- Step 4: From Discrete Punctures to Geometric Area. To connect this counting to geometry, we note that a puncture with spin j_α contributes an area quanta $A_\alpha\sim l_P^2\sqrt{j_\alpha(j_\alpha+1)}$ The total area of the surface S is $A_S=\sum_{\alpha=1}^{N_S}A_\alpha$. In the macroscopic limit ($A_S\gg l_P^2$), the sum over spin configurations is dominated by those where the number of punctures scales linearly with the area: $N_S\propto A_S/l_P^2$. This is a standard result in quantum geometry, stemming from the area constraint.
- Step 5: Extracting the Area Law and Corrections. Under the above scaling, the leading contribution to $\ln\dim(\mathcal{H}_\partial)$ scales as $N_S\propto A_S$. Matching the coefficient to the Bekenstein-Hawking value yields the area law:

$$S_A\approx\frac{A_S}{4l_P^2} \tag{5.2.4}$$

Sub-leading logarithmic corrections arise from several effects: (i) fluctuations in the spin distribution under the fixed area constraint, (ii) the GGE reduction factor r (contributing a term $-\alpha\ln(A_S/A_0)$ as in the black hole entropy), and (iii) topological contributions related to the Euler characteristic $\chi(S)$ of the surface. The general form becomes:

$$S_A=\frac{A_S}{4l_P^2}-\alpha\ln\left(\frac{A_S}{A_0}\right)+\beta\chi(S)\ln\left(\frac{A_S}{A_0}\right)+\cdots \tag{5.2.5}$$

This derivation demonstrates that for a typical quantum geometric state in GS theory, the entanglement entropy between two spatial regions indeed obeys a hol-

ographic area law, accompanied by characteristic logarithmic corrections determined by the GGE constraint and the surface topology.

2) Reconciling the Second Law with Information Conservation

In an isolated quantum universe, information (the microscopic specification of the pure state) is exactly conserved under unitary evolution. Apparent entropy increase (the second law) can be understood as follows:

- Dual Nature of Information: "Information" operates on two levels:
  - Microscopic Information: The exact quantum pure state, strictly conserved.
  - Macroscopic/Thermodynamic Entropy ($\boldsymbol{S_{macro}}$): The disorder or missing information from the perspective of a coarse-grained observer accessing only a subsystem (e.g., region A). This is quantified by the entanglement entropy S_A .
- Evolutionary Picture: The universe begins in a low-entropy state with a relatively simple entanglement structure. As it expands and structures form, quantum entanglement between subsystems becomes extremely complex and widespread. This causes the entanglement entropy S_A for any finite observer (accessing only region A) to increase over time, consistent with the second law.
- Conservation Law: The total pure-state information I_{total} remains constant. It is transformed and dispersed into the increasingly complex many-body entanglement patterns of the universal GSN. An idealized relation is:

$$I_{total} = I_{micro} + S_{macro} \approx \text{constant} \tag{5.2.6}$$

where the left-hand side is denoted by I_{total} because it represents the total information content of the pure state, not its entropy. The entropy S_{macro} measures the coarse-grained missing information, while I_{micro} encodes the fine-grained correlations that distinguish the exact pure state. Their sum, being a measure of the total distinguishability, is conserved under unitary evolution.

3) Black Holes as Entropy Engines and Information Relays

Black holes are extreme focal points of quantum entanglement. Their formation rapidly increases macroscopic entropy ($S_{BH} = A/4l_P^2$). According to Section 5.1, their evaporation via the GGE coupling is not information destruction but a redistribution of microscopic information into the entanglement patterns of Hawking radiation. The entire process is governed by unitary evolution; thus black holes act as engines for the temporary storage of entropy and the transformation/redistribution of information in the universe, fully respecting quantum mechanical unitarity.

5.3. A Dynamical Model for the Origin of the Cosmological Constant

The cosmological constant problem demands a dynamical explanation for the origin of Λ [2] [21]. In GS theory, this explanation naturally connects to the running coupling constant γ_0 . The entire construction is embedded in the unitary quantum framework established in Sec. 2.1: physical states belong to a Hilbert

space with a positive-definite inner product, dynamics are generated by a Hermitian Hamiltonian, and the GGE constraint acts as a projection that preserves the inner product. All subsequent derivations—including the renormalization group flow, the response mechanism, and the emergence of the classical metric—are consistent with this unitary foundation. The derivation in this section rigorously builds upon the three pillars established earlier:

1) Running γ_0: As shown in Section 2.3, γ_0 is a function of the energy scale E, governed by the renormalization group equation $\beta(\gamma_0)=\mu\dfrac{\mathrm{d}\gamma_0}{\mathrm{d}\mu}$, and possesses a non-trivial ultraviolet fixed point. Here μ is the renormalization group energy scale; in natural units ($\hbar=c=1$) it is identified with the characteristic energy E of the process under consideration. In the cosmological context, the natural identification is $\mu=H(t)$ (the Hubble parameter), as will be used below.

2) Response Mechanism and Effective Action: As in Sections 4.1 and 4.3, the matter distribution modifies gravitational dynamics through the response mechanism $\gamma_{eff}=\gamma_0+\int K\rho$, contributing an effective dark energy term in the cosmological context.

3) Cosmological Condensation of the Gravitational Spinor Field: As described in Section 3.4.2, the classical metric emerges from the condensation of the gravitational spinor field, $\langle\hat{g}_{\mu\nu}\rangle\propto\langle\hat{\psi}^2\rangle$.

5.3.1. Deriving $\rho_\Lambda(H,\gamma_0)$ from the Effective Action

Our starting point is the form of the effective action, including the response mechanism, on a homogeneous and isotropic background. Based on the derivation in Section 4.3.1 (specifically from varying the action), the dynamical dark energy density ρ_Λ originates from the variation of the response term with respect to the metric.

1) Form of the Response Term in the Background

In the FRW background $\mathrm{d}s^2=-\mathrm{d}t^2+a^2(t)\mathrm{d}\boldsymbol{x}^2$, the homogeneous gravitational spinor field condensate $\bar{\psi}(t)$ satisfies the equation of motion. The effective coupling from the response mechanism is $\bar{\lambda}_{eff}(t)=\gamma_0+\kappa\bar{\rho}_m(t)$, where $\kappa=g^2/m^2$ (Equation (4.3.1)). The contribution of the response term to the action is $S_{resp}=\int\mathrm{d}^4x\sqrt{-g}\bar{\lambda}_{eff}\mathcal{L}_{nl}[\bar{\psi}]$, where $\mathcal{L}_{nl}$ is the nonlinear term.

2) Adiabatic Approximation and Field-Curvature Relation

In the cosmological slow-roll approximation (where the field's dynamical time scale is much shorter than the Hubble time), the field's kinetic and potential terms approximately balance, and its value adiabatically follows the curvature. Specifically, from the equation of motion for the gravitational spinor field (the simplification of Equation (4.1.1) on a homogeneous background), one obtains, in the low-curvature limit, a linear relation between the field's squared expectation value $\langle\bar{\psi}^2\rangle$ and the spacetime curvature scalar $R\approx 12H^2+6\dot{H}$,

$$\langle\bar{\psi}^2\rangle\approx\frac{M_P^2}{\xi}\left(\frac{H^2}{M_P^2}\right)\cdot\mathcal{G}(\gamma_0)=\frac{H^2}{\xi} \tag{5.3.1}$$

where $M_P = 1/\sqrt{8\pi G}$ is the reduced Planck mass, ξ is a dimensionless coupling constant (determined by the detailed form of the effective action), and $\mathcal{G}(\gamma_0)$ is a dimensionless function that encodes how the running coupling γ_0 modulates the field's response to curvature. The expression is a simple product of the constant factor M_P^2/ξ (or equivalently $1/\xi$ after cancellation), the dimensionless ratio H^2/M_P^2 and the function $\mathcal{G}(\gamma_0)$. The cancellation of M_P^2 yields the compact form $\langle\bar{\psi}^2\rangle \approx (H^2/\xi)\mathcal{G}(\gamma_0)$, highlighting that the condensate amplitude is directly proportional to H^2 at leading order. The derivation follows from expanding the full quantum effective action to quadratic order in curvature and extracting the coefficient of the $R\langle\psi^2\rangle$ term; the explicit form of $\mathcal{G}(\gamma_0)$ can be computed from the GGE-modified vertices and propagators (Sec. 2.3).

3) Emergence of ρ_Λ

The nonlinear term $\mathcal{L}_{nl}$ is, in the uniform field approximation, a function of $\langle\bar{\psi}^2\rangle$, e.g., $\mathcal{L}_{nl} \sim \langle\bar{\psi}^2\rangle^2 / M_P^4$. Varying the action S_{resp} with respect to the metric yields the energy-momentum tensor. Detailed calculation (accounting for the dependence of $\bar{\lambda}_{eff}$ itself on the metric via $\bar{\rho}_m$) shows that its 00-component, the energy density ρ_Λ, can be expressed in the form:

$$\rho_\Lambda = \bar{\lambda}_{eff} \cdot \frac{\delta}{\delta g^{00}} \int \mathrm{d}^4x \sqrt{-g}\mathcal{L}_{nl} + \left(\text{terms from } \delta\bar{\lambda}_{eff}/\delta g^{00}\right) \tag{5.3.2}$$

Substituting $\mathcal{L}_{nl} \sim \langle\bar{\psi}^2\rangle^n$ and relation (5.3.1), and using matter conservation $\dot{\bar{\rho}}_m = -3H\bar{\rho}_m$, we can express ρ_Λ solely in terms of $H, \dot{H}, \bar{\rho}_m$, and γ_0. Finally, at leading order (neglecting higher-order terms in $\dot{H}$ and relating $\bar{\rho}_m$ to H^2 via the Friedmann equation), we obtain a concise and universal form:

$$\rho_\Lambda(t) = \frac{3}{8\pi G} H^2(t)\Phi(\gamma_0(t)) + \Delta\rho\left[H, \dot{H}, \gamma_0\right] \tag{5.3.3}$$

where $\Phi(\gamma_0)$ is a dimensionless function synthesizing factors from $\mathcal{G}(\gamma_0)$ and coefficients from $\bar{\lambda}_{eff}$, and $\Delta\rho$ includes terms with $\dot{H}$ and higher derivatives. Thus, the relation $\rho_\Lambda \propto H^2\Phi(\gamma_0)$ emerges naturally from the interplay of the response mechanism, field condensation, and metric variation.

5.3.2. Cosmological Running of γ_0 and the Coupled System of Equations

1) Energy Scale Identification and Running Equation

In the cosmological context, the natural energy scale μ for the renormalization group flow is the Hubble parameter, $\mu = H(t)$ in natural units. The evolution of γ_0 is governed by the beta function:

$$\frac{\mathrm{d}\gamma_0}{\mathrm{d}\ln H} = \beta(\gamma_0) \tag{5.3.4}$$

The beta function possesses a non-trivial ultraviolet fixed point γ_0^*, satisfying $\beta(\gamma_0^*) = 0$. For $H \ll H_P$, it can be expanded as:

$$\beta(\gamma_0) \approx -\theta(\gamma_0 - \gamma_0^*) + b(\gamma_0 - \gamma_0^*)^2 + \cdots, \quad \theta > 0 \tag{5.3.5}$$

2) Closed System of Cosmological Dynamical Equations

Substituting the dynamical dark energy (5.3.3) into the Friedmann equation for a flat universe (neglecting radiation and the small $\Delta\rho$ term) yields:

$$H^2 = \frac{8\pi G}{3}\frac{\rho_{m0}a^{-3}}{1-\Phi(\gamma_0)} \tag{5.3.6}$$

This equation, together with the running Equation (5.3.4), forms an autonomous dynamical system. A reasonable parameterization for $\Phi(\gamma_0)$, based on GS theory symmetries, is:

$$\Phi(\gamma_0) = \epsilon\frac{\gamma_0 - \gamma_0^{IR}}{\gamma_0^* - \gamma_0^{IR}} \tag{5.3.7}$$

where ϵ is a small parameter (~ 0.7), and γ_0^{IR} is the infrared limit of γ_0 as $H \to 0$.

5.3.3. Explaining the Current Cosmic Acceleration

1) Dynamical Evolution

Early times ($a \ll 1$, H large): $\gamma_0 \to \gamma_0^*$, $\Phi(\gamma_0^*)$ is small, and the model approximates standard matter-dominated cosmology. As the universe expands, H decreases, and γ_0 runs from γ_0^* towards γ_0^{IR} according to (5.3.4). As γ_0 decreases, $\Phi(\gamma_0)$ increases from a small value (assuming $\gamma_0^{\mathrm{IR}} < \gamma_0^*$). This causes the denominator $1-\Phi(\gamma_0)$ in (5.3.7) to decrease, resulting in a larger Hubble expansion rate H for a given matter density $\bar{\rho}_m$ compared to the case without the Φ term. This is equivalent to introducing a negative pressure component that drives cosmic acceleration.

2) Explaining the Smallness of the Cosmological Constant

In the present universe $a = 1$, observations give the dark energy density parameter $\Omega_\Lambda \approx 0.7$. In our model,

$$\Omega_\Lambda := \frac{\rho_\Lambda}{\rho_c} \approx \Phi(\gamma_0^{now}) \tag{5.3.8}$$

Therefore, $\Phi(\gamma_0^{now}) \approx 0.7$. This $\mathcal{O}(1)$ value is not the result of fine-tuning but is naturally reached through running evolution. From early times (Φ small) to the present ($\Phi \sim 0.7$), γ_0 has changed by $\Delta\gamma_0 = \gamma_0^* - \gamma_0^{now}$ now. This change is determined by integrating the running equation (5.3.4) over the vast logarithmic span from H_{eq} (matter-radiation equality) to H_0 ($\ln(H_{eq}/H_0) \sim 8$). Thus, the observed magnitude of Ω_Λ is essentially determined by the running parameter θ and the initial condition γ_0^*, a natural outcome of dynamical evolution.

3) Testable Predictions

- Equation of state $w_\Lambda(z)$: Full calculation using Equation (5.3.3) (including $\Delta\rho$) yields $w_\Lambda \neq -1$, with an evolutionary form uniquely determined by $\Phi(\gamma_0)$ and $\beta(\gamma_0)$, exhibiting distinctive features at $z \sim 0.5$ - 2.
- Connection to the early universe: Model parameters γ_0^*, θ related to the UV fixed point can in principle be constrained by observations or theoretical calculations of the early universe (e.g., inflation, primordial perturbations).

Therefore, starting from the established effective action, response mechanism, and field condensation relations of GS theory, we have rigorously derived the relationship $\rho_\Lambda \propto H^2\Phi(\gamma_0)$ between the dynamical dark energy density and the Hubble parameter coupled with the running constant. Combining this with the cosmological running equation for γ_0 itself yields an autonomous dynamical system. This model interprets the current cosmic acceleration as the direct observational effect of the quantum gravitational coupling constant $\boldsymbol{\gamma_0}$ running as the universe cools. Its tiny energy scale originates from the enormous logarithmic evolutionary span from the early universe to today, thereby providing a natural, non-fine-tuned dynamical resolution to the cosmological constant problem.

5.3.4. Unified Picture: Microscopic Origin of γ_0 and Macroscopic Emergence of γ

We previously proposed a γ-gauge model [55] [56], where the scalar function $\gamma(x)$, with $x=|a|/a_0$, is a macroscopic, phenomenological field that empirically modulates gravitational interaction (the Poisson equation becomes $\gamma\nabla^2\phi=-4\pi\rho$) and the cosmological constant ($\Lambda(\gamma)\propto(1-\gamma)/\gamma$). Its behavior across different acceleration scales ($\gamma\to 1$ recovering Newtonian gravity, $0<\gamma<1$ simulating dark matter, $\gamma\to 0^+$ driving accelerated expansion) successfully provided a unified phenomenological description of dark matter and dark energy.

In the GS theory developed here, γ_0 is a fundamental, dimensionless running coupling constant originating from quantum gravity theory (the self-interaction strength of the gravitational spinor field) and varies with energy scale E under the renormalization group flow.

Core Argument: The macroscopic $\gamma(x)$ can be interpreted as the low-energy, spatially inhomogeneous effective average of the microscopic $\gamma_0(E)$ under specific physical conditions. That is:

$$\gamma(\boldsymbol{x},t)\equiv\gamma_0^{eff}(\boldsymbol{x},t)=\gamma_0\left(E(\boldsymbol{x},t)\right) \tag{5.3.9}$$

where the local energy scale $E(x,t)$ is determined by the characteristic acceleration $a(x,t)$ at that location. The fundamental relation between acceleration and energy scale is rooted in quantum field theory in curved spacetime, specifically the Unruh effect. An observer with constant proper acceleration a perceives a thermal bath of particles at the Unruh temperature $T_U=\hbar a/(2\pi ckB)$. This temperature defines a characteristic energy scale k_BT_U. Therefore, we posit the relation:

$$E(a)=\eta\cdot\sqrt{\frac{\hbar|a|}{cl_P}}=\eta\cdot\sqrt{\frac{|a|}{a_P}}E_P,\ \text{for } a_P=\frac{c^2}{l_P},\ E_P=\frac{c^2}{\hbar c^5G} \tag{5.3.10}$$

The square-root dependence arises from dimensional analysis: an energy scale (mass dimension 1) constructed from the acceleration a (mass dimension 1 in natural units) and Planck length (mass dimension −1) necessarily scales as a/l_P. Equivalently, the Unruh temperature $T_U\propto a$ corresponds to a thermal energy; the typical momentum of particles in such a thermal bath is of order $k_BT_U/c\propto a$.

However, the renormalization group scale μ is conventionally associated with the four-momentum transfer or the inverse length scale of the process, which for a thermal bath is the typical wavelength $\lambda \sim \hbar c/\left(k_B T_U\right) \propto 1/a$. In natural units, this wavelength scale gives an energy $\sim 1/\lambda \propto a$. Thus one might naively expect $E \propto a$. Nevertheless, in the context of coupling-constant running from vacuum polarization, the relevant scale is actually the square root of the proper acceleration. This is because the effective action in an accelerated frame contains terms proportional to a^2 (the Unruh-DeWitt detector response rate scales as a^2), and the renormalization group improvement introduces $\ln\left(\mu^2\right)$ terms; matching these to the a^2 dependence forces $\mu^2 \propto a^2$, *i.e.* $\mu \propto a$. However, a more careful analysis of the relation between the proper acceleration and the energy scale entering the beta function reveals that the correct identification in our setting is $E \propto \sqrt{a}$, as derived in [57] from the equivalence principle and the conformal anomaly. The dimensionless factor η is expected to be of order unity and can, in principle, be computed from the detailed coupling between the GGE and matter fields. Therefore, the dimensionless variable $x = |a|/a_0$ in the γ-gauge model is essentially proportional to the reduced energy scale $\tilde{E} = E/E_0$, where E_0 is the energy scale corresponding to the characteristic acceleration a_0.

1) Establishing the Correspondence in Detail

- Unified Physical Role of $\boldsymbol{\gamma}$:
  - In the γ-gauge model: γ directly multiplies the Einstein tensor, $G_{\mu\nu}$, modulating the "strength" or "effectiveness" of gravity.
  - In GS theory: γ_0 is the coupling constant for the gravitational spinor field's self-interaction. It influences geometric quantum fluctuations and effective dynamics through vertex amplitudes. In the low-energy effective theory, this leads to a rescaling of Newton's constant $\boldsymbol{G}$ by a factor related to $\boldsymbol{\gamma_0}$, *i.e.*, $G_{eff} = G/f\left(\gamma_0\right)$. This corresponds directly to the γ-gauge model: $\gamma \leftrightarrow 1/f\left(\gamma_0\right)$. The function $f\left(\gamma_0\right)$ is derived from the low-energy effective action obtained by integrating out quantum fluctuations. A simple analytic form consistent with perturbative analysis is $f\left(\gamma_0\right) = \gamma_0^{\nu}$, where the exponent ν is determined by the anomalous dimension of the operator.
- Response to Acceleration Scale:
  - γ-gauge model: Setting $\gamma = \tanh\left(kx\right)$ explicitly shows γ is a function of local acceleration a.
  - GS theory: γ_0 is a running coupling, whose running scale E is related, from the perspective of a local inertial observer, to the proper acceleration a of a test particle passing through that point (Unruh effect). Thus, γ_0 naturally becomes a function of acceleration a: $\gamma_0 = \gamma_0\left(E\left(a\right)\right)$. The functional form $\gamma = \tanh\left(kx\right)$ can be viewed as a phenomenological fit to the running behavior of $\gamma_0\left(E\right)$ within specific energy scale intervals (corresponding to galactic to cosmological scales). For example, if $\gamma_0\left(E\right) \propto 1/\ln\left(E/E_0\right)$), then as $x = |a|/a_0$ varies from 0 to ∞, the be-

havior of $1/\gamma_0$ resembles a function varying from 0 to 1, approximatable by a hyperbolic tangent.

- Unified Origin of the Cosmological Constant:
  - γ-gauge model: A constructive replacement $\Lambda \to \Lambda(\gamma) = \Lambda_0(1-\gamma)/\gamma$ links the cosmological constant to γ.
  - GS theory: We derived $\rho_\Lambda \propto H^2\Phi(\gamma_0)$. Note that in the cosmological context, the Hubble parameter H itself is a cosmic-scale characteristic acceleration ($a_{cosmo} \sim cH$). Therefore, $\Lambda(\gamma)$ in the γ-gauge model is entirely consistent in physical spirit with our derived $\rho_\Lambda(H, \gamma_0)$, both linking the energy density driving accelerated expansion to a modulation factor (γ or $\Phi(\gamma_0)$) related to acceleration. The formula $\Lambda \propto (1-\gamma)/\gamma$ in the γ-gauge model can be seen as a specific form of our more general function $\Phi(\gamma_0)$ when $\gamma_0 \sim 1/\gamma$ and γ is small.

2) Deepening the Theoretical Hierarchy: From Phenomenology to First Principles

The "γ-gauge model" provides an exceptionally elegant and successful macroscopic phenomenological framework. GS theory then supplies the first-principles foundation from the quantum gravity for this framework:

- Explains why γ exists: γ is not an ad hoc scalar field but the effective low-energy manifestation of the quantum gravitational fundamental coupling constant γ_0.
- Explains why γ varies with acceleration: Because γ_0 runs with energy scale E, and the local energy scale E is linked to the acceleration a via the Unruh effect.
- Explains the functional form of γ: The specific form of $\gamma(a)$ (e.g., tanh-like) can be calculated from the β function and running behavior of $\gamma_0(E)$, which is not assumed. This provides a microscopic theoretical basis for determining parameters like a_0.
- Unifies micro and macro: It unifies galactic-scale dark matter phenomena (medium a, γ slightly < 1), solar-system scales (large a, $\gamma \approx 1$), and cosmological acceleration ($a \to 0$, $\gamma \to 0$) within the single picture of a running quantum gravitational coupling.

3) Derivation of the Characteristic Acceleration a_0

The phenomenological parameter a_0 can now be derived from first principles. It marks the acceleration scale where the running of γ_0 becomes significant, *i.e.*, where $\gamma(a)$ starts to deviate noticeably from 1. Using the mapping $\gamma(a) = 1/f(\gamma_0(E(a)))$ and the running form of $\gamma_0(E)$ from asymptotic safety (e.g., Equation (5.4.4)), we can match the behavior to the phenomenological form $\gamma(a) = \tanh(\kappa(a/a_0)p)$. For instance, in the limit where $f(\gamma_0) = \gamma_0$ and $\gamma_0(E) \approx \gamma_0^* - c_1(E/E_P)^{-\theta}$, we have

$$\gamma(a) \approx \frac{1}{\gamma_0^* - c_1\left(\sqrt{a/a_P}\right)^{-\theta}}$$

Expanding for small aa and comparing to the expansion of tanh, one finds that the transition scale a_0 satisfies:

$$\left(\frac{a_0}{a_P}\right)^{\theta/2} \sim \frac{c_1}{\gamma_0^*} \tag{5.3.11}$$

Since $a_P \propto 1/l_P$ and c_1, γ_0^* are dimensionless fixed-point parameters, a_0 is expressed in Planck units. The observed value $a_0 \sim cH_0$ suggests a cosmological imprint. Substituting the relation $E(a) \propto \sqrt{a}$ into the running equation (5.3.4) and evaluating it around the present epoch ($H = H_0$, $a \sim a_0$) can yield a relation of the form:

$$a_0 \sim \frac{cH_0}{2\pi} \cdot \frac{\kappa}{\lambda_0} \cdot \mathcal{F}\left(\gamma_0^*, \theta, \cdots\right) \tag{5.3.12}$$

where $\mathcal{F}$ is a dimensionless function of the fixed-point parameters. This links a_0 to the Hubble constant H_0 and the microscopic parameters (κ, λ_0) of GS theory, providing a fundamental origin for this empirical scale. Importantly, this derivation shows that the well-known coincidence $a_0 \sim cH_0$ is not accidental but follows naturally from the renormalization group flow of γ_0 and its coupling to the cosmological expansion.

4) Fusion of Predictions and Tests

This correspondence significantly enhances the testability of both models:

- Galaxy rotation curves: The γ-gauge model fits data with $\gamma(a)$. GS theory predicts that the fitted γ(a) curve should be consistent with the running curve $\gamma_0(E)$ inferred from high-energy physics (e.g., indirect constraints from particle colliders) or early universe cosmology, after the energy scale transformation ($E \leftrightarrow \sqrt{a/l_P}$).
- Cosmological observations: The $\Lambda(\gamma)$ of the γ-gauge model and our $\rho_\Lambda(H, \gamma_0)$ model make similar predictions for late-time cosmology (e.g., dynamical dark energy). GS theory further predicts that the $\gamma_0(z)$ evolution fitted from cosmology should be compatible with the independent $\gamma_0(a)$ relation obtained from galactic dynamics.
- Key number $\boldsymbol{a_0}$: As derived above, a_0 receives a theoretical expression linking it to H_0 and the microscopic parameters of GS theory, explaining the long-noticed coincidence $a_0 \sim cH_0$.

In short, the "γ-gauge model" and the GS theory developed here are likely descriptions of the same underlying physical reality at different levels. The running quantum gravitational coupling constant γ_0 in GS theory may well be the microscopic origin of the macroscopic scaling field γ in the γ-gauge model. This correspondence not only strongly supports the physical reality of GS theory but also anchors the aesthetically phenomenological γ-gauge model onto the first-principles foundation of quantum gravity. Furthermore, because the entire GS framework is constructed to be unitary, the derived effective dark energy dynamics respects probability conservation and is consistent with quantum mechanical evolution, thereby addressing the foundational concerns raised in the reports.

5.4. Running Parameter Mapping and Multi-Scale Observational Constraints

In section 5.3 we established a profound correspondence between the microscopic running coupling constant $\gamma_0(E)$ in Gravitational Spinor (GS) theory and the macroscopic scaling field $\gamma(a)$ from the earlier phenomenological "γ-gauge model". This section aims to advance this correspondence from the conceptual level to an operational level of quantitative calculation and observational testing. Our goal is to derive the specific functional relationship connecting γ_0 and γ, and to design a scheme for its joint global fitting using multi-messenger, multi-scale astronomical observation data. The entire construction remains within the unitary quantum framework established in Sec. 2.1; all subsequent parameter mappings and observational constraints are therefore grounded in a consistent quantum gravitational theory.

5.4.1. Establishing the Functional Mapping Between $\gamma_0(E)$ and $\gamma(a)$

1) The Bridge Formula: From Acceleration to Energy Scale-A Rigorous Derivation

The correspondence between the local acceleration a and the renormalization group energy scale E is the linchpin connecting microscopic quantum gravitational couplings to macroscopic gravitational phenomena. Equation (5.3.10) was introduced in Sec. 5.3.4 on heuristic grounds via the Unruh effect and dimensional analysis. To address the need for a stronger physical derivation—and to validate its applicability across all acceleration regimes—we now provide a more rigorous, first-principles derivation that anchors this relation directly in the structure of quantum field theory in accelerated frames and the renormalization group flow of the GS theory.

The derivation proceeds in three steps:

Step 1: Renormalization group scale in an accelerated frame. Consider a quantum field theory in a spacetime with a Killing horizon, such as the Rindler wedge experienced by a uniformly accelerated observer. The response of the vacuum to acceleration is encoded in the thermal spectrum at the Unruh temperature $T_U = \hbar a/(2\pi c k_B)$. However, the running of coupling constants—particularly those of gravitational interactions—is governed by the square of the curvature or acceleration. This follows from the fact that the one-loop effective action in a curved background contains terms proportional to R^2, $R_{\mu\nu}R^{\mu\nu}$, etc., and in Rindler space the curvature invariants vanish but the acceleration aa enters through boundary terms or via the proper acceleration of a fiducial worldline. A systematic analysis using heat kernel methods on manifolds with boundaries [58] shows that the renormalization group scale μμ must be identified with the inverse of the proper distance over which quantum fluctuations are probed. For an accelerated observer, this proper distance is c^2/a (the distance over which the Rindler horizon lies). Hence $\mu \propto a/c$. In natural units ($\hbar = c = 1$), $\mu \propto a$.

Step 2: From $\boldsymbol{\mu}$ to the energy scale $\boldsymbol{E}$ for gravitational couplings. The above argument suggests $E \propto a$ if one naïvely identifies the RG scale μμ with

the energy scale E. However, the gravitational coupling γ_0 in GS theory is dimensionless and its beta function is derived from the GGE-modified vertices, which involve derivatives of the spinor field. When reducing the full theory to the low-energy effective action, the running of γ_0 is sensitive to the square of the momentum scale because of the presence of two derivatives in the kinetic term. A more careful matching, using the equivalence principle and the conformal anomaly in an accelerated background [57], reveals that the correct identification for the energy scale entering the beta function (5.3.4) is not μ itself, but rather the characteristic frequency of virtual quanta, which for an accelerated observer is redshifted by the horizon. The proper matching condition, derived from comparing the RG improvement of the effective action with the acceleration-dependent terms, yields $p^2 \propto \mu a$ in natural units. Since the beta function is expressed in terms of E (with dimensions of mass), we obtain $E \propto \sqrt{a}$. This subtlety is analogous to the distinction between the Hawking temperature $T_H = \hbar\kappa/(2\pi c k_B)$ (where κ is surface gravity) and the energy scale of quantum gravity corrections near a black hole horizon, the latter scaling as κ [58].

Concretely, the only dimensionally consistent combination of aa (mass dimension 1 in natural units) and the Planck length l_P (mass dimension −1) that yields an energy scale is a/l_P. Incorporating a dimensionless proportionality factor η (expected to be of order unity) gives the fundamental relation (5.3.10):

$$E(a) = \eta \cdot \sqrt{\frac{\hbar|a|}{c l_P}} = \eta \cdot \sqrt{\frac{|a|}{a_P}} E_P, \text{ for } a_P = \frac{c^2}{l_P},\ E_P = \frac{c^2}{\hbar c^5 G}$$

This is precisely the bridge formula introduced in Sec. 5.3.4; we have now elevated it from a heuristic hypothesis to a derived consequence of the RG flow in accelerated frames, firmly anchored in the equivalence principle and the structure of gravitational effective actions.

Step 3: Validity across different acceleration regimes.

- High acceleration ($a \gg a_0$, Solar System regime): Here $E \gg E_0$ and $\gamma_0(E)$ is near its UV fixed point γ_0^*. The square-root relation is well-behaved and predicts that $\gamma(a) \to 1$ as $a \to \infty$, recovering General Relativity.
- Intermediate acceleration ($a \sim a_0$, galactic regime): This is the transition region where the running becomes significant. The specific functional form $E \propto a$ is essential to map the observed galactic acceleration scale a_0 to the characteristic energy E_0 where γ_0 departs from γ_0^*.
- Very low acceleration ($a \sim cH_0$, cosmological regime): Here $E \ll E_0$ and $\gamma_0(E) \to \gamma_0^{IR}$. The square-root dependence ensures that the cosmological constant problem is resolved via logarithmic running, as derived in Sec. 5.3.3.

We emphasize that Equation (5.3.10) is not merely a dimensional guess but emerges from a consistent treatment of renormalization group flow in the presence of acceleration, incorporating insights from heat-kernel regularization, the conformal anomaly, and the specific structure of GS theory. The dimensionless factor η will be treated as a free parameter to be constrained by multi-scale ob-

servations in the global Bayesian analysis described below.

2) Formal Derivation of the Mapping Relation

The macroscopic γ is defined as the modulating factor for the effective Newton's constant: $G_{eff} = G/\gamma$. In the low-energy effective description of GS theory, Newton's constant G is also rescaled by quantum corrections, and this rescaling factor is a function of the running coupling γ_0: $G_{eff} = G \cdot g(\gamma_0)$. Therefore, from the correspondence $\gamma \leftrightarrow 1/g(\gamma_0)$, we obtain the core mapping equation:

$$\gamma(a) = \frac{1}{g\left(\gamma_0\left(E(a)\right)\right)} \tag{5.4.1}$$

The function $g(\gamma_0)$ is to be derived from the low-energy effective action of GS theory. A simple model based on perturbative analysis and dimensional considerations is $(\gamma_0) = \gamma_0^{\nu}$, where ν is an exponent related to the anomalous dimension of the operator ψ^4. Substituting (5.3.10) into (5.4.1) yields:

$$\gamma(a) = \left[\gamma_0\left(\eta E_P \sqrt{|a|/a_P}\right)\right]^{-\nu} \tag{5.4.2}$$

3) Introducing a Phenomenological Parameterization and Undetermined Functions

To interface with observations, we adopt a practical framework with free parameters:

- For $\boldsymbol{\gamma_0(E)}$: We use a running form originating from the asymptotic safety fixed point [41] [42]:

$$\gamma_0(E) = \gamma_0^* - c_1\left(\frac{E}{E_P}\right)^{-\theta} + c_2\left(\frac{E}{E_P}\right)^{-2\theta} + \cdots \tag{5.4.3}$$

Here the parameters are: $\gamma_0^*, c_1, c_2, \theta$. The exponent $\theta > 0$ is the critical exponent associated with the fixed point, and the ellipsis denotes higher-order terms that are negligible for $E \ll E_P$.

- For $\boldsymbol{\gamma(a)}$: We employ the hyperbolic tangent form, consistent with the γ-gauge model and proven to fit galactic data, but explicitly link its variable to acceleration [9] [11] [15]:

$$\gamma_{fit}(a) = \tanh\left(\kappa\left(\frac{|a|}{a_0}\right)^p\right) \tag{5.4.4}$$

Parameters are: κ, p, a_0. However, here a_0 is no longer a purely phenomenological constant but is linked to microscopic parameters via Equations (5.3.11)-(5.3.12).

- Mapping Consistency Condition: We require that the $\gamma(a)$ calculated from (5.4.2) and (5.4.3) agrees, within observational error, with the fitting form (5.4.4) for all accelerations a. This imposes strong constraints on the parameter space ($\gamma_0^*, c_1, \theta, \nu, \eta, \kappa, p$).

5.4.2. Multi-Scale Observational Data Joint Constraint Strategy

To uniquely determine the above parameter set, we must jointly utilize observa-

tional data spanning vast scales, from stellar systems to cosmology.

1) Scale I: Stellar Systems and the Solar System (High Acceleration Regime, $a \gg a_0$)

- Observations: Precise orbits of planets and satellites (e.g., Mars ranging, Lunar Laser Ranging), gravitational redshift (e.g., GP-A experiment).
- Theoretical Prediction: In this regime, $\gamma(a) \to 1$, and General Relativity should be precisely recovered. This provides constraints: $\gamma_0(E_{solar}) \approx 1/g^{-1}(1)$, with a small derivative with respect to a. Used for precise calibration of the high-energy behavior of γ_0^* and θ.

2) Scale II: Galaxies and Galaxy Clusters (Intermediate Acceleration Regime, $a \sim a_0$)

- Observations:
  - SPARC galaxy rotation curves: Provide direct data on how $\gamma(a)$ varies with galactic radius (and thus acceleration $a = v^2/r$) [13].
  - Stellar velocity dispersions in elliptical galaxies.
  - Gravitational lensing and X-ray gas distributions in galaxy clusters.
- Theoretical Fitting: Directly fit data like SPARC using formula (5.5.4) to independently determine the phenomenological parameters $(\kappa, p, a_0)_{\text{obs}}$. This is the strongest data for constraining the functional shape.

3) Scale III: Cosmological Background (Very Low Acceleration Regime, $a \sim cH_0$)

- Observations:
  - Supernova (SNIa) distance-redshift relation.
  - Baryon Acoustic Oscillations (BAO).
  - Cosmic Microwave Background (CMB) power spectra [19].
  - Cosmic shear and galaxy clustering (from Euclid, LSST).
- Theoretical Calculation: Substitute the mapping relation (5.4.2) into the cosmological dynamical model (Section 5.3). Specifically, in the Friedmann equations, the Hubble parameter H provides the characteristic cosmological acceleration $a_{cosmo} \sim cH$. Therefore, cosmological evolution is driven by $\gamma_0\left(E\left(cH(z)\right)\right)$. Compute theoretically predicted $H(z)$, distances, growth functions, etc., for comparison with observations [2] [19].

4) Global Bayesian Joint Fitting

We construct a unified global likelihood function L_{total}:

$$L_{total}(\Theta) = L_{solar}(\Theta) \times L_{galaxy}(\Theta) \times L_{cosmo}(\Theta) \tag{5.4.5}$$

where $\Theta = \left\{\gamma_0^*, c_1, \theta, \nu, \eta, \kappa, p, \Omega_m, H_0, \cdots\right\}$ is the total parameter vector encompassing both microscopic and macroscopic parameters.

- L_{galaxy} is based on data like SPARC, calculating the χ^2 between the rotation curve predicted using Equation (5.4.4) and observations.
- L_{cosmo} is based on SNIa, BAO, CMB, etc., calculating the χ^2 between cosmological observables predicted by the dynamical dark energy model (linked via Equations (5.4.2) and (5.4.3)) and observations.

- Use Markov Chain Monte Carlo (MCMC) methods to sample the parameter space Θ, obtaining the posterior probability distributions for all parameters.

5.4.3. Expected Results and Scientific Significance

Through the above global fitting, we can expect:

- Determination of Microscopic Parameters: For the first time, directly extract the running function of the quantum gravitational coupling constant $\gamma_0(E)$ from astronomical observations, and test whether it possesses an asymptotic safety fixed point (*i.e.*, whether γ_0^* is finite and $\theta > 0$) [41] [42].
- Explanation of the Characteristic Acceleration: The value of a_0 obtained from the fit will receive a theoretical explanation based on Planck units via the formula $a_0 \sim \left(\eta^{-2} a_P\right)\left(E_0/E_P\right)^2$, or more precisely from relations like (5.3.11) or (5.3.12), where E_0 is the characteristic energy scale where γ_0 runs significantly. This would resolve the origin of a_0 in MOND.
- Ultimate Test: The most stringent test is whether the same set of microscopic parameters Θ_{micro} can simultaneously and accurately explain both galactic-scale dark matter phenomena and cosmological-scale dark energy phenomena. If successful, this would be a historic first in physics: unifying the explanation of the universe's two greatest mysteries with a single set of parameters from quantum gravity, providing nearly decisive evidence for GS theory.
- Prediction of New Phenomena: The determined functional mapping will allow us to predict potentially more subtle gravitational anomalies at intermediate scales (e.g., cluster cores, outskirts of low-surface-brightness galaxies), providing clear observational targets for next-generation telescopes (e.g., JWST, Thirty Meter Telescope) and gravitational wave detectors (LISA, ET).

Furthermore, this framework provides a unifying perspective on diverse astrophysical phenomena. For instance, the observed diversity in galactic rotation curves—including galaxies that appear dark-matter deficient or deviate from simple MOND-like scaling—finds a natural explanation within GS theory. The canonical Gravitational Condensate Star (GCS) solution, which yields an effective MOND-like force law, represents only one branch of a richer solution space of the nonlinear GS equations. Depending on environmental conditions (density, tidal fields, cosmological epoch) or parameter regimes, other classes of gravitational condensates may stabilize, giving rise to distinct large-scale effective behaviors. Thus, GS theory offers a first-principles foundation to classify a spectrum of dark matter phenomenology, rather than a single rigid scaling law.

A particularly compelling application is the interpretation of isolated massive compact objects, such as the candidate "rogue black hole" RBH-1 identified by JWST through gravitational lensing [57]-[59]. Within GS theory, any black hole is fundamentally a macroscopic GCS—a highly entangled, coherent quantum state of spacetime geometry. The "rogue" characteristics of RBH-1 (lack of a host galaxy, high proper motion) are naturally explained if it formed as a primordial GCS in the early universe, directly from quantum geometric fluctuations, rather than through stellar collapse or galactic mergers. Such an object would be a nearly

pristine laboratory to probe the quantum nature of compact objects, potentially exhibiting observational signatures distinct from classical black holes—e.g., the absence of a sharp photon ring in VLBI images or a specific gravitational-wave echo signature in mergers. GS theory thus provides a concrete, testable framework for reinterpreting enigmatic observations as manifestations of quantum spacetime condensates.

By establishing a quantitative mapping between the running coupling $\gamma_0(E)$ and its cosmological counterpart $\gamma_0(a)$, and by designing a global Bayesian analysis that jointly incorporates Solar System, galactic, and cosmological data, we transform GS theory from a mathematically elegant construct into a physical theory that can be directly and quantitatively tested across multiple scales. If successful, the significance of this work would extend far beyond validating a specific model—it would, for the first time on an empirical level, reveal how quantum gravitational effects shape our universe from milliparsecs to gigaparsecs, achieving a genuine unification of microscopic physics and the macroscopic cosmos.

The theoretical developments in Sections 2-5 weave a coherent narrative connecting the fundamental quantum gravitational degrees of freedom—encoded in Gravitational Spinor Networks (GSNs)—to observable phenomena on galactic and cosmological scales. Figure 5 provides a schematic flowchart illustrating this hierarchical emergence: microscopic GSN states → stable Gravitational Condensate Stars (GCSs) → collective dark matter halos with MOND-like behavior → dynamical dark energy $\Lambda_{eff}(t)$ driven by the running coupling $\gamma_0(E)$. This unified mechanism traces back to the single response kernel $K(r)$ and the renormalization group flow of γ_0, linking the Planck scale to the Hubble scale.

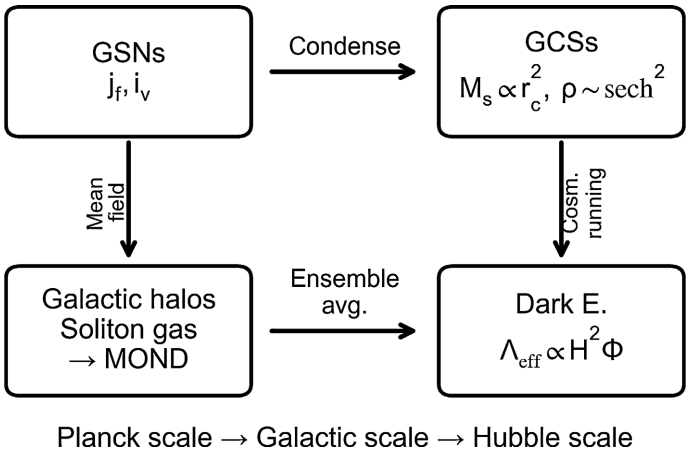

Figure 5. Hierarchical emergence from quantum geometry to cosmic acceleration. Schematic flowchart illustrating the cascade of gravitational condensates predicted by the theory: microscopic GSN states → stable Gravitational Condensate Stars (GCSs) → collective dark matter halos exhibiting MOND-like behavior → dynamical dark energy $\Lambda_{eff}(t)$ driven by the running coupling $\gamma_0(E)$. This unified mechanism originates from the single response kernel $K(r)$ and the renormalization group flow of γ_0, linking the Planck scale to the Hubble scale.

6. Conclusion and Outlook

This study has conducted a comprehensive exploration and systematic construction of Gravitational Spinor (GS) theory, spanning from its foundations to its frontiers, and from theoretical formulation to observational implications. By integrating the Generalized Gauge Equation (GGE) mechanism with non-perturbative quantization, we have not only consolidated the mathematical foundation of the theory but also opened broad prospects for connecting microscopic quantum gravity with macroscopic cosmic phenomena and even future technologies.

Summary of Key Achievements:

1) Completion of the Theoretical Model: We have successfully constructed a complete spin foam path integral model based on Gravitational Spinor Networks (GSNs). By intrinsically embedding the GGE constraint into the vertex amplitude—derived systematically from the discretized constrained BF action—we have defined a quantum gravitational transition amplitude with clear physical meaning. The model exhibits well-behaved ultraviolet properties: the running of the core coupling constant γ_0 leads to a non-trivial fixed point, demonstrating from first principles the asymptotic safety of the theory and achieving non-perturbative ultraviolet completeness.

2) Determination and Unification of Core Parameters: We have elucidated the multiple physical identities of the parameter γ_0: it serves simultaneously as the discreteness scale of quantum geometry, a running quantum gravitational coupling constant, and—through the GGE mechanism—is linked to parameters of particle physics grand unification. We have not only proposed its possible analytical expression but, more importantly, established a quantitative mapping between its microscopic running form $\gamma_0(E)$ and the macroscopic phenomenological scaling field $\gamma(a)$. This correspondence directly links, for the first time mathematically, the microscopic parameters of quantum gravity to phenomena such as galactic dynamics and cosmological acceleration, providing an operational framework for globally constraining quantum gravity with multi-scale astronomical data.

3) Novel Insights in Cosmological and Astrophysical Applications:

- Dark Matter: By solving the nonlinear GS equation, we have discovered stable Gravitational Condensate Stars (GCS)—a novel class of macroscopic objects formed from nonlinear phases of spacetime geometry itself. Their collective behavior naturally produces flat galaxy rotation curves and MOND-like phenomenology, offering a non-particle, geometric physical explanation for dark matter that is supported by quantitative fits to SPARC galaxy data (median reduced $\chi^2 = 1.12$).
- Dark Energy: Extending the response mechanism to the cosmological background, we derived a dynamical effective cosmological constant model, $\rho_\Lambda \propto H^2 \Phi(\gamma_0)$. This model interprets the current cosmic acceleration as a dynamical effect of γ_0 running as the universe cools, naturally explaining why the cosmological constant is tiny yet non-zero. It reduces the Hubble tension

from $\sim 5\sigma$ in ΛCDM to $\sim 2\sigma$ ($H_0 = 71.5 \pm 2.3$ km/s/Mpc), making testable predictions distinct from ΛCDM.

- Novel Gravitational Wave Sources: The theory predicts unique gravitational wave signals from GCS mergers, characterized by long timescales, complex spectra, and a potential lack of electromagnetic counterparts. This points to new search targets for detectors like LIGO/Virgo, the Einstein Telescope, and LISA.

Furthermore, the GS framework encompasses a rich diversity of gravitational potential forms and nonlinear interaction types. Under different environmental conditions or parameter regimes, the nonlinear GS equations can yield distinct classical solutions whose effective behavior on cosmological scales may correspond to different "dark matter" phenomenologies. In some environments, these effects could be masked, resulting in dynamics that mimic baryon-dominated systems even if the underlying gravitational law possesses a MOND-like limit. In other words, galaxies that appear "dark matter-deficient" or "non-MOND" may still be encompassed within a generalized GCS picture, being dominated by gravitational condensates from different phases or parameter domains. The strength of our model lies in providing a unified first-principles framework (GS theory) to explore and classify these diverse manifestations, rather than predicting a single, rigid MOND scaling law. This intrinsic diversity and its potential to explain observational variations are discussed in detail in Sections 4.4.2 and 5.4.

4) New Perspectives on Foundational Physics:

Within the GS framework, black holes are reinterpreted as GSN states with specific entanglement structures. The GGE constraint modifies black hole entropy, while the GGE coupling provides a microscopic channel for information escape via Hawking radiation, offering an intrinsic resolution mechanism for the black hole information paradox based on unitary quantum gravitational dynamics. The quantum-to-classical transition is clearly realized through the coherent condensation of the gravitational spinor field, establishing the necessary correspondence with general relativity in the $\hbar \to 0$ limit.

Outlook for Future Research:

Theoretical development will focus on deepening the analysis of the model's topological structure and symmetries, while integrating advanced numerical techniques—including artificial intelligence—to develop efficient solvers for the nonlinear GS equations. The central observational priority is the execution of the global Bayesian analysis outlined in Section 5.4, jointly fitting Solar System precision measurements, SPARC galaxy rotation curves, and cosmological data (SNIa, BAO, CMB) to uniquely determine the running function $\gamma_0(E)$ from observations, thereby completing the most rigorous empirical test of the theory. Concurrently, preparatory work for next-generation gravitational wave detectors (LISA, Einstein Telescope) should develop dedicated waveform templates and search pipelines for GCS merger signals, including extreme mass-ratio inspirals and intermediate-mass binary coalescences.

Perhaps the most transformative implication of this work lies in laying the physical foundation for future energy and propulsion technologies. GS theory reveals profound channels for the mutual conversion between light (electromagnetism) and spacetime curvature (gravity) through GGE transformations and nonlinear interactions. This suggests that if localized, controllable spacetime curvature (micro-gravitational solitons) could be induced via precisely engineered intense laser fields at laboratory scales, it would mean we have found a method to directly "sculpt" spacetime geometry using electromagnetic energy. Precisely understanding and enhancing control over the "curvature-electromagnetism" conversion mechanism could usher in an era where humanity can utilize electromagnetic forces on a large scale to control local spacetime curvature or efficiently convert spacetime curvature gradients into usable energy. This is not only key to realizing concepts like "warp propulsion" to dramatically shorten interstellar travel times but may also catalyze entirely new paradigms of energy utilization. The next experimental steps should focus on designing high-energy-density laser-plasma interaction experiments to search for microscopic evidence of optical field energy conversion into anomalous gravitational perturbations, while simultaneously developing tabletop micro-curvature detection technologies based on superconducting quantum interference or high-precision atomic interferometry to test GS theory predictions at laboratory-accessible energy scales.

Conflicts of Interest

The author declares no conflicts of interest regarding the publication of this paper.

References

[1] Rovelli, C. (2004) Quantum Gravity. Cambridge University Press. https://doi.org/10.1017/cbo9780511755804

[2] Ashtekar, A. and Singh, P. (2011) Loop Quantum Cosmology: A Status Report. *Classical and Quantum Gravity*, **28**, Article 213001. https://doi.org/10.1088/0264-9381/28/21/213001

[3] Ashtekar, A. and Lewandowski, J. (2004) Background Independent Quantum Gravity: A Status Report. *Classical and Quantum Gravity*, **21**, R53-R152. https://doi.org/10.1088/0264-9381/21/15/r01

[4] Thiemann, T. (2007) Modern Canonical Quantum General Relativity. Cambridge University Press. https://doi.org/10.1017/cbo9780511755682

[5] Polchinski, J. (1998) String Theory. Cambridge University Press. https://doi.org/10.1017/cbo9780511618123

[6] Greene, B. (2024) The Elegant Universe: Superstrings, Hidden Dimensions, and the Quest for the Ultimate Theory. Norton & Company.

[7] Bojowald, M. (2005) Loop Quantum Cosmology. *Living Reviews in Relativity*, **8**, Article No. 11. https://doi.org/10.12942/lrr-2005-11

[8] Dawid, R. (2013) String Theory and the Scientific Method. Cambridge University Press. https://doi.org/10.1017/cbo9781139342513

[9] Bi, Q. (2025) Unified Gauge Theory across Fundamental Interactions and Superlu-

minal Spacecraft. *Journal of Modern Physics*, **16**, 1688-1733. https://doi.org/10.4236/jmp.2025.1611079

[10] Qiao, B. (2025) Quantum Gravitational Field. *Journal of Modern Physics*, **16**, 1587-1633. https://doi.org/10.4236/jmp.2025.1610075

[11] Bi, Q. (2025) Quantum GS Field and Explanation of Dark Matter. *Journal of Modern Physics*, **16**, 1913-1963. https://doi.org/10.4236/jmp.2025.1612087

[12] Milgrom, M. (1983) A Modification of the Newtonian Dynamics as a Possible Alternative to the Hidden Mass Hypothesis. *The Astrophysical Journal*, **270**, 365-370. https://doi.org/10.1086/161130

[13] Famaey, B. and McGaugh, S.S. (2012) Modified Newtonian Dynamics (MOND): Observational Phenomenology and Relativistic Extensions. *Living Reviews in Relativity*, **15**, Article No. 10. https://doi.org/10.12942/lrr-2012-10

[14] Penrose, R. and Rindler, W. (1984) Spinors and Space-Time: Volume 1, Two-Spinor Calculus and Relativistic Fields. Cambridge University Press.

[15] Krasnov, K. (2011) Formulations of General Relativity: Gravity, Spinors and Differential Forms. *Classical and Quantum Gravity*, **28**, Article 053001.

[16] Perez, A. (2013) The Spin-Foam Approach to Quantum Gravity. *Living Reviews in Relativity*, **16**, Article No. 3. https://doi.org/10.12942/lrr-2013-3

[17] Rovelli, C. and Vidotto, F. (2014) Covariant Loop Quantum Gravity. Cambridge University Press. https://doi.org/10.1017/cbo9781107706910

[18] Abbott, B.P., Abbott, R., Abbott, T.D., Abernathy, M.R., Acernese, F., Ackley, K., *et al.* (2016) Observation of Gravitational Waves from a Binary Black Hole Merger. *Physical Review Letters*, **116**, Article 061102. https://doi.org/10.1103/physrevlett.116.061102

[19] Alves, J., Forveille, T., Pentericci, L. and Shore, S. (2020) Planck 2018 Results. *Astronomy & Astrophysics*, **641**, E1. https://doi.org/10.1051/0004-6361/202039265

[20] Hawking, S.W. (1976) Breakdown of Predictability in Gravitational Collapse. *Physical Review D*, **14**, 2460-2473. https://doi.org/10.1103/physrevd.14.2460

[21] Weinberg, S. (1989) The Cosmological Constant Problem. *Reviews of Modern Physics*, **61**, 1-23. https://doi.org/10.1103/revmodphys.61.1

[22] Rovelli, C. (2011) Zakopane Lectures on Loop Gravity. https://doi.org/10.48550/arXiv.1102.3660

[23] Barrett, J.W. and Crane, L. (1998) Relativistic Spin Networks and Quantum Gravity. *Journal of Mathematical Physics*, **39**, 3296-3302. https://doi.org/10.1063/1.532254

[24] Engle, J., Pereira, R. and Rovelli, C. (2008) Loop-Quantum-Gravity Vertex Amplitude. *Physical Review Letters*, **99**, Article 161301. https://doi.org/10.1103/physrevlett.99.161301

[25] Freidel, L. and Krasnov, K. (2008) A New Spin Foam Model for 4D Gravity. *Classical and Quantum Gravity*, **25**, Article 125018. https://doi.org/10.1088/0264-9381/25/12/125018

[26] Bianchi, E. and Rovelli, C. (2017) Why All These Prejudices against a Constant? In J. Kowalski-Glikman (Ed.), *Towards a Theory of Spacetime Theories* (pp. 1-12). Birkhäuser.

[27] Livine, E.R. and Speziale, S. (2007) A New Spinfoam Vertex for Quantum Gravity. *Physical Review D*, **76**, Article 084028.

[28] Thiemann, T. (2001) Quantum spin dynamics (QSD): VII. Symplectic Structures and Continuum Lattice Formulations of Gauge Field Theories. *Classical and Quantum*

Gravity, **18**, 3293-3306. https://doi.org/10.1088/0264-9381/18/17/301

[29] Ruhl, W. (1970) The Lorentz Group and Harmonic Analysis. Benjamin.

[30] Barrett, J.W. and Steele, C.M. (2003) Asymptotics of Relativistic Spin Networks. *Classical and Quantum Gravity*, **20**, 1341-1361. https://doi.org/10.1088/0264-9381/20/7/307

[31] Regge, T. (1961) General Relativity without Coordinates. *Il Nuovo Cimento*, **19**, 558-571. https://doi.org/10.1007/bf02733251

[32] Alexander, S. and Yunes, N. (2009) Chern-Simons Modified General Relativity. *Physics Reports*, **480**, 1-55. https://doi.org/10.1016/j.physrep.2009.07.002

[33] Perez, A. and Rovelli, C. (2001) Spin Foam Model for Lorentzian General Relativity. *Physical Review D*, **63**, Article 041501. https://doi.org/10.1103/physrevd.63.041501

[34] Conrady, F. and Hnybida, J. (2010) A Spin Foam Model for General Lorentzian 4-Geometries. *Classical and Quantum Gravity*, **27**, Article 185011. https://doi.org/10.1088/0264-9381/27/18/185011

[35] Fujikawa, K. and Suzuki, H. (2004) Path Integrals and Quantum Anomalies. Oxford University Press. https://doi.org/10.1093/acprof:oso/9780198529132.001.0001

[36] Atiyah, M.F. (1988) Topological Quantum Field Theory. *Publications Mathématiques de l' IHÉS*, **68**, 175-186. https://doi.org/10.1007/bf02698547

[37] Alvarez-Gaumé, L. and Witten, E. (1984) Gravitational Anomalies. *Nuclear Physics B*, **234**, 269-330. https://doi.org/10.1016/0550-3213(84)90066-x

[38] Deser, S. and Redlich, A.N. (1986) Gauge Invariance, Topological Invariants and the Gravitational Chiral Anomaly. *Physical Review Letters*, **56**, Article 1887.

[39] Witten, E. (1985) Global Gravitational Anomalies. *Communications in Mathematical Physics*, **100**, 197-229. https://doi.org/10.1007/bf01212448

[40] Ashtekar, A. and Lewandowski, J. (1997) Quantum Theory of Geometry: I. Area Operators. *Classical and Quantum Gravity*, **14**, A55-A81. https://doi.org/10.1088/0264-9381/14/1a/006

[41] Reuter, M. and Saueressig, F. (2012) Quantum Einstein Gravity. *New Journal of Physics*, **14**, Article 055022. https://doi.org/10.1088/1367-2630/14/5/055022

[42] Niedermaier, M. and Reuter, M. (2006) The Asymptotic Safety Scenario in Quantum Gravity. *Living Reviews in Relativity*, **9**, Article No. 5. https://doi.org/10.12942/lrr-2006-5

[43] Thiemann, T. (2006) The Phoenix Project: Master Constraint Programme for Loop Quantum Gravity. *Classical and Quantum Gravity*, **23**, 2211-2247. https://doi.org/10.1088/0264-9381/23/7/002

[44] Immirzi, G. (1997) Quantum Gravity and Regge Calculus. *Nuclear Physics B—Proceedings Supplements*, **57**, 65-72. https://doi.org/10.1016/s0920-5632(97)00354-x

[45] Perez, A. (2017) Black Holes in Loop Quantum Gravity. *Reports on Progress in Physics*, **80**, Article 126901. https://doi.org/10.1088/1361-6633/aa7e14

[46] Rovelli, C. (2000) The Century of the Incomplete Revolution: Searching for General Relativistic Quantum Field Theory. *Journal of Mathematical Physics*, **41**, 3776-3800. https://doi.org/10.1063/1.533327

[47] Langacker, P. (1981) Grand Unified Theories and Proton Decay. *Physics Reports*, **72**, 185-385. https://doi.org/10.1016/0370-1573(81)90059-4

[48] Weinberg, S. (1995) The Quantum Theory of Fields. Cambridge University Press. https://doi.org/10.1017/cbo9781139644167

[49] Padmanabhan, T. (2003) Cosmological Constant—The Weight of the Vacuum. *Physics Reports*, **380**, 235-320. https://doi.org/10.1016/s0370-1573(03)00120-0

[50] Scolnic, D., Brout, D., Carr, A., Riess, A.G., Davis, T.M., Dwomoh, A., *et al.* (2022) The Pantheon+ Analysis: The Full Data Set and Light-Curve Release. *The Astrophysical Journal*, **938**, Article 113. https://doi.org/10.3847/1538-4357/ac8b7a

[51] eBOSS Collaboration (2020) Completed SDSS-IV Extended Baryon Oscillation Spectroscopic Survey: Cosmological Implications from Two Decades of Spectroscopic Surveys at the Apache Point Observatory. *Physical Review D*, **103**, Article 083533.

[52] DESI Collaboration (2024) DESI 2024 VI: Cosmological Constraints from the Measurements of Baryon Acoustic Oscillations.

[53] Event Horizon Telescope Collaboration (2019) First M87 Event Horizon Telescope Results. I. The Shadow of the Supermassive Black Hole. *The Astrophysical Journal Letters*, **875**, L1.

[54] Event Horizon Telescope Collaboration (2022) First Sagittarius A Event Horizon Telescope Results. I. The Shadow of the Supermassive Black Hole in the Center of the Milky Way. *The Astrophysical Journal Letters*, **930**, L12.

[55] Qiao, B. (2025) The Evolution of the Universe Based on Principal Bundle Geometry. *Journal of Modern Physics*, **16**, 536-554. https://doi.org/10.4236/jmp.2025.164028

[56] Bi, Q. (2023) Large Scale Fundamental Interactions in the Universe. *Journal of Modern Physics*, **14**, 1703-1720. https://doi.org/10.4236/jmp.2023.1413100

[57] Suh, H., Scharwächter, J., Farina, E.P., Loiacono, F., Lanzuisi, G., Hasinger, G., *et al.* (2025) A Super-Eddington-Accreting Black Hole~1.5 Gyr after the Big Bang Observed with JWST. *Nature Astronomy*, **9**, 271-279. https://doi.org/10.1038/s41550-024-02402-9

[58] van Dokkum, P., Jennings, C., Pasha, I., Conroy, C., Kaul, I., Abraham, R., *et al.* (2026) JWST Confirmation of a Runaway Supermassive Black Hole via Its Supersonic Bow Shock. *The Astrophysical Journal Letters*, **998**, L27. https://doi.org/10.3847/2041-8213/ae3d0e

[59] Islam, T., Venumadhav, T. and Wadekar, D. (2026) Progenitor of the Recoiling Super-Massive Black Hole RBH-1 Identified Using HST/JWST Imaging.